NAVAL POSTGRADUATE SCHOOL

MONTEREY, CALIFORNIA

THESIS

THERMOMECHANICAL ANALYSIS OF GROUND-BASED DIRECTED ENERGY WEAPONS ON SATELLITES AND INTERCONTINENTAL BALLISTIC MISSILES

by

Georgios Mantzouris

September 2006

Thesis Advisor:	Ramesh Kolar
Co-Advisor:	Brij Agrawal
Second Reader:	Phillip E. Pace

THIS PAGE INTENTIONALLY LEFT BLANK

REPORT DOCUMENTATION PAGE			Form Approved OMB No. 0704-0188
Public reporting burden for this collection of information is estimated to average 1 hour per response, including the time for reviewing instruction, searching existing data sources, gathering and maintaining the data needed, and completing and reviewing the collection of information. Send comments regarding this burden estimate or any other aspect of this collection of information, including suggestions for reducing this burden, to Washington headquarters Services, Directorate for Information Operations and Reports, 1215 Jefferson Davis Highway, Suite 1204, Arlington, VA 22202-4302, and to the Office of Management and Budget, Paperwork Reduction Project (0704-0188) Washington DC 20503.			
1. AGENCY USE ONLY ***(Leave blank)***	**2. REPORT DATE** September 2006	**3. REPORT TYPE AND DATES COVERED** Master's Thesis	
4. TITLE AND SUBTITLE: Thermo-mechanical Analysis of Ground-based Directed Energy Weapons on Satellites and Intercontinental Ballistic Missiles			**5. FUNDING NUMBERS**
6. AUTHOR(S) Georgios Mantzouris			
7. PERFORMING ORGANIZATION NAME(S) AND ADDRESS(ES) Naval Postgraduate School Monterey, CA 93943-5000			**8. PERFORMING ORGANIZATION REPORT NUMBER**
9. SPONSORING /MONITORING AGENCY NAME(S) AND ADDRESS(ES) N/A			**10. SPONSORING/MONITORING AGENCY REPORT NUMBER**
11. SUPPLEMENTARY NOTES The views expressed in this thesis are those of the author and do not reflect the official policy or position of the Department of Defense or the U.S. Government.			
12a. DISTRIBUTION / AVAILABILITY STATEMENT Approved for public release; distribution is unlimited			**12b. DISTRIBUTION CODE** A

13. ABSTRACT

Thermo mechanical modeling and simulation of a satellite and intercontinental ballistic missile assumes importance due to the increased interest in assessing the potential of such attacks. Effective and innovative methods are sought in assessing the structural integrity of such structural components. In this study, we present modeling and simulation aspects of two generic models loaded by high energy laser beam. We present an application of MSC software in modeling thermo-mechanical behavior, both steady state and transient behavior of satellite and missile structures. Thermal energies used for simulation correspond to high energy laser flux available at low earth orbits as reported in literature. A brief review of the concepts involved is outlined. The analysis is performed under several scenarios that include thermal failures due to steady state as well as transient thermal exposures. The thermal exposure times and locations are varied to assess typical failure modes of the structure. Analysis is done in order to define suitable material thicknesses that will make a satellite or a ballistic missile hardened enough to withstand these specific amounts of energy. Other parameters of interest pertaining to this study are the pulse width, and resulting transient phenomena affecting the behavior. Temperature gradients as well as resulting thermal stresses and thermal deformations are reported in this study.

14. SUBJECT TERMS Thermo-mechanical analysis, Satellites, Intercontinental Ballistic Missiles, Transient analysis, Steady state analysis, Thermal Analysis, Ground-based Lasers, Orbits, Laser Weapons, Quickbird, Taepondong, Failure Modes, Patran, Nastran, Pulse width, Material Properties.			**15. NUMBER OF PAGES** 122
			16. PRICE CODE
17. SECURITY CLASSIFICATION OF REPORT Unclassified	**18. SECURITY CLASSIFICATION OF THIS PAGE** Unclassified	**19. SECURITY CLASSIFICATION OF ABSTRACT** Unclassified	**20. LIMITATION OF ABSTRACT** UL

NSN 7540-01-280-5500 Standard Form 298 (Rev. 2-89)
Prescribed by ANSI Std. 239-18

THIS PAGE INTENTIONALLY LEFT BLANK

Approved for public release; distribution is unlimited

THERMOMECHANICAL EFFECTS OF GROUND-BASED DIRECTED ENERGY WEAPONS ON SATELLITES AND INTERCONTINENTAL BALLISTIC MISSILES

Georgios Mantzouris
Lieutenant Junior Grade, Hellenic Navy
B.S., Hellenic Naval Academy, 1998

Submitted in partial fulfillment of the
requirements for the degrees of

MASTER OF SCIENCE IN ASTRONAUTICAL ENGINEERING

and

MASTER OF SCIENCE IN SYSTEMS ENGINEERING

from the

NAVAL POSTGRADUATE SCHOOL
September 2006

Author: Georgios Mantzouris

Approved by: Ramesh Kolar
Thesis Advisor

Brij Agrawal
Co-Advisor

Phillip E. Pace
Second Reader

Dan Boger
Chairman, Information Warfare Department

Anthony Healey
Chairman, Mechanical and Astronautical Engineering Department

THIS PAGE INTENTIONALLY LEFT BLANK

ABSTRACT

Thermo mechanical modeling and simulation of a satellite and intercontinental ballistic missile assumes importance due to the increased interest in assessing the potential of such attacks. Effective and innovative methods are sought in assessing the structural integrity of such structural components. In this study, we present modeling and simulation aspects of two generic models loaded by high energy laser beam. We present an application of MSC software in modeling thermo-mechanical behavior, both steady state and transient behavior of satellite and missile structures. Thermal energies used for simulation correspond to high energy laser flux available at low earth orbits as reported in literature. A brief review of the concepts involved is outlined. The analysis is performed under several scenarios that include thermal failures due to steady state as well as transient thermal exposures. The thermal exposure times and locations are varied to assess typical failure modes of the structure. Analysis is done in order to define suitable material thicknesses that will make a satellite or a ballistic missile hardened enough to withstand these specific amounts of energy. Other parameters of interest pertaining to this study are the pulse width and resulting transient phenomena affecting the behavior. Temperature gradients as well as resulting thermal stresses and thermal deformations are reported in this study. Results presented allow survivability and vulnerability analysis of space assets and lead their risk assessment and mitigation.

THIS PAGE INTENTIONALLY LEFT BLANK

TABLE OF CONTENTS

LIST OF FIGURES

LIST OF TABLES

THIS PAGE INTENTIONALLY LEFT BLANK

ACKNOWLEDGMENTS

I would like to thank my thesis advisor, Professor Ramesh Kolar, who was always by my side throughout this project. Only with his experience, assistance and immense patience, have I been able to publish the results of this thesis and accredit my work among the scientific communities. Also, it is my desire to thank the Departments of Mechanical and Astronautical Engineering and Information Sciences, along with each of my instructors who gave me the knowledge and courage to produce this study.

I would like to thank the Hellenic Navy for sending me in United States to study and cultivate my academic experience, and for always supporting my professional and personal ambitions.

Moreover, a huge acknowledgement is dedicated to my wife, Renia, who supported me throughout this effort and helped me when it was necessary, in order to fulfill my personal goals. She was patient and alone at my long hours of work and absence from home, giving me always the sign that she is by my side in good and bad times.

Last, but not least, I would like here to remember, respect and thank my parents, Ioannis and Christina Mantzouris, who instilled on me the confidence to pursue my dreams — from my early years of childhood up to now, they are trying to teach, help and protect me during the long journey of life.

THIS PAGE INTENTIONALLY LEFT BLANK

EXECUTIVE SUMMARY

There are numerous unhardened satellites on orbit and intercontinental ballistic missiles, which may be affected by ground-based laser energy weapons. In a worst case scenario, in which an opponent sends laser directed energy, towards an unhardened space asset on orbit, it can cause major damages and/or total destruction of it. This thesis investigates how this energy affects the survivability and vulnerability of satellites and ballistic missiles, and associated risk assessment and mitigation.

A goal to keep space assets (satellite, intercontinental ballistic missile in mid-course) operational, active and on the desired orbit, performing specified operations over its life-span, is a demand for every mission. To achieve this, we have to harden satellites and intercontinental ballistic missiles and make them withstand effects that may be caused by directed energy laser weapon's energy. An investigation into the thermo-mechanical behavior and damage assessment of satellite and intercontinental ballistic missile structures, exposed to ground-based directed energy weapons, has been done.

The problems addressed include the amount of laser energy required to damage a satellite in different orbits (LEO – MEO – HEO) – according to specified damage criteria and damage to a model of an intercontinental ballistic missile during the boost phase. Furthermore, a methodology based on multi-discipline physics is developed, on the effects of laser energy on the space assets. The temperature distributions resulting from thermal loads are calculated. These temperature gradients are used to reveal the corresponding thermal deformations — damages that are produced. Moreover, the corresponding thermal stresses, due to these deformations, have been computed. This analysis has led us into developing parameter design curves that show the variation of laser energy input and corresponding satellite design variables such as weight, thickness, material strength and thermal properties.

The various results of this incoming energy, from ground-based directed laser energy weapons, onto satellites and ballistic missiles have been investigated thoroughly. This incoming energy has been transformed into thermal energy flux, and it is coupled with structural components. A simulation on thermal analysis results in critical

temperature distributions on structures and on external surfaces, as well. Also, resulting thermal deformations and stresses are studied and finally, conclusions deduced that lead us to set survivability criteria.

To illustrate the methodology, models of a satellite bus and an intercontinental ballistic missile have been built, based on QUICKBIRD and Taepondong characteristics from open literature, using MSC/Patran and MSC/NASTRAN engineering analysis tools. Overall dimensions match the selected actual structures, and suitable materials and other dimensions are assumed so that the total weight is comparable to actual targets. We define suitable material thicknesses that make a satellite/ ballistic missile strong enough to withstand these specific amounts of energy. Other parameters of interest, pertaining to this analysis, are the pulse width, and resulting transient phenomena affecting the behavior.

The vulnerabilities and survivability of these model space assets are pointed out in the context of the available laser energies. The analysis presented provides tools for risk reduction and mitigation in the assessment of the potential dangers of such targets.

I. INTRODUCTION[1]

The era of directed energy weapons is almost upon us. As of today, many directed energy weapon projects are under development among different countries in the world. There are myriad of problems though, that needs to be resolved, but with the evolution of scientific researches, we will see magnificent results, in the coming years.

By using the beams of laser energy focused on specific areas, these types of weapons can travel at 300 million meters per second (speed of light) and potentially destroy targets in less than seconds. Its use is effective for both strategic and tactical purposes and this is one of the driving factors that make these modern weapons wanted so much in the current battlefields. Also, the capability of "burning holes through materials" has naturally led to speculation that the laser is not only the dominant future weapon but is the tool that every country wants in order to defend and secure its borders and serves some of its military purposes.

New warfare concepts have been established and the potential for a speed of light response has set new dimensions in military operations and engagement scenarios. Lasers that are used extensively in a number of different military applications and serving various needs can be divided into three main categories, in accordance with the area of application. First, we define ground-based laser energy weapons as those that have been placed on ground stations or on sea level platforms. Second, we have the Airborne directed energy lasers which are placed on aircrafts or other platforms that operate in the lower atmosphere. Finally, beyond earth's atmosphere, laser weapons located on satellites or on other platforms in space, make up the last category of space based laser energy weapons.

---

[1] Parts of the thesis were presented at the following conferences:

- Mantzouris, G., and Kolar, R., "Thermo-mechanical Analysis of Ground Based Directed Energy Weapons on a Ballistic Missile Model," MSC Virtual Product Development Conference 2006, July 17–19, Huntington Beach, CA
- Mantzouris, G., and Kolar, R., "Thermo-mechanical Analysis of Ground Based Directed Energy Weapons on A Satellite Model," Presented at the 5th Directed Energy Test and Evaluation Conference, 2006, Aug 1–3, Albuquerque. This paper is also submitted for publication in The Journal of Directed Energy.

In this thesis, we consider only the capability of ground-based laser energy weapons to deliver adequate amounts of laser energy on different orbits (LEO-MEO-GEO) and produce significant destructive results to a satellite or an intercontinental ballistic missile. Laser energy travels through the atmosphere, as a beam of light, and undergoes various propagation losses, and deposits in a certain amount of thermal energy available to damage the space asset external surfaces. This beam delivers its energy either in a continuous wave mode (CW) or in a pulse mode to a small area on target. The intensity has to be fairly big in order for the satellite surface material to melt and produce the desired catastrophic results. There are numerous satellites/ ballistic missiles in service that are unhardened and therefore are vulnerable to any external source of laser energy coming from ground-based laser energy weapons. It may be noted that the modeling and simulation of the thermo-mechanical behavior of satellites and ICBM is applicable for other modes of laser weapons as well.

II. THESIS OUTLINE

In the following chapters, we analyze the thermo-mechanical behavior and observe damage assessment of a satellite and ballistic missile structures under directed energy weapons. In Chapter II, we set the required background knowledge in order to make a good estimation for the amount of laser energy that is required to affect a satellite on different orbits. Also, we present historical evolution of directed energy weapons, in past decades, in conjunction with space warfare. Another field that is addressed is the different possible ways that this amount of energy affects a space asset on orbit. An overview of existing satellite orbits and most commonly used ballistic missiles flight paths is given in order to understand the different amounts of laser energy required for different altitudes in space.

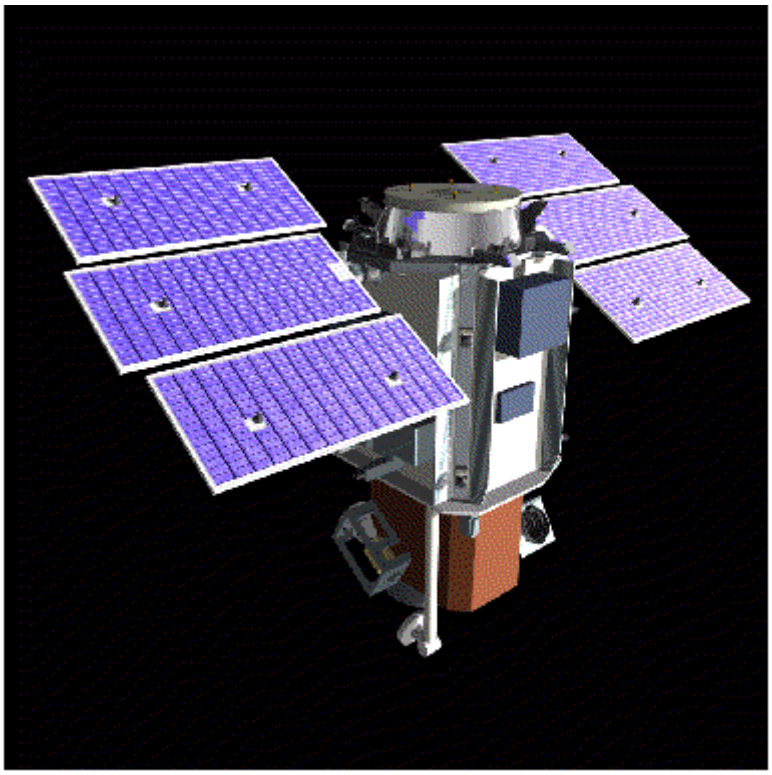

Figure 1. Illustration of the Quickbird Spacecraft (From [Ref. 1])

Chapter III gives the overview of both the satellite and ballistic missile models created using MS/Patran and NASTRAN software. The satellite is based on “Quickbird” spacecraft as shown above in Figure 1 and is currently in service. The ballistic missile is based on the North Korean Taepondong ballistic missile, which is currently reported to be in production. Simulation of a real satellite and ballistic missile provides solutions to real world problems with the new methodology developed.

Chapter IV outlines the theoretical background of the software. The steps involved in thermal analysis subjected to laser impact, both steady and transient analysis, is given. The resulting temperature distributions then are applied and resulting thermal deformations and thermal stresses are computed. The results are used to make suitable assessments.

Chapter V outlines the procedure and steps of thermo-mechanical analysis of incoming laser energy from ground-based directed energy weapons onto the models. The effects of laser energy are discussed on different orbits (LEO – MEO – GEO). This incoming energy is transformed into thermal energy and is coupled with the structural components of the satellite model. A thermal analysis results in critical temperature distributions, presented in Chapters VI and VII, on the model structures. The resulting thermal deformations and stresses are computed using nonlinear option in the NASTRAN software. Figure 2 shows simulation of a prototype satellite bus model using modal analysis. Results similar to those shown in Figures 2 and 3, are presented after the thermo-mechanical analysis has been done. Thermal deformations that are induced by the laser thermal energy onto satellite and ballistic missiles structures and their effects are described.

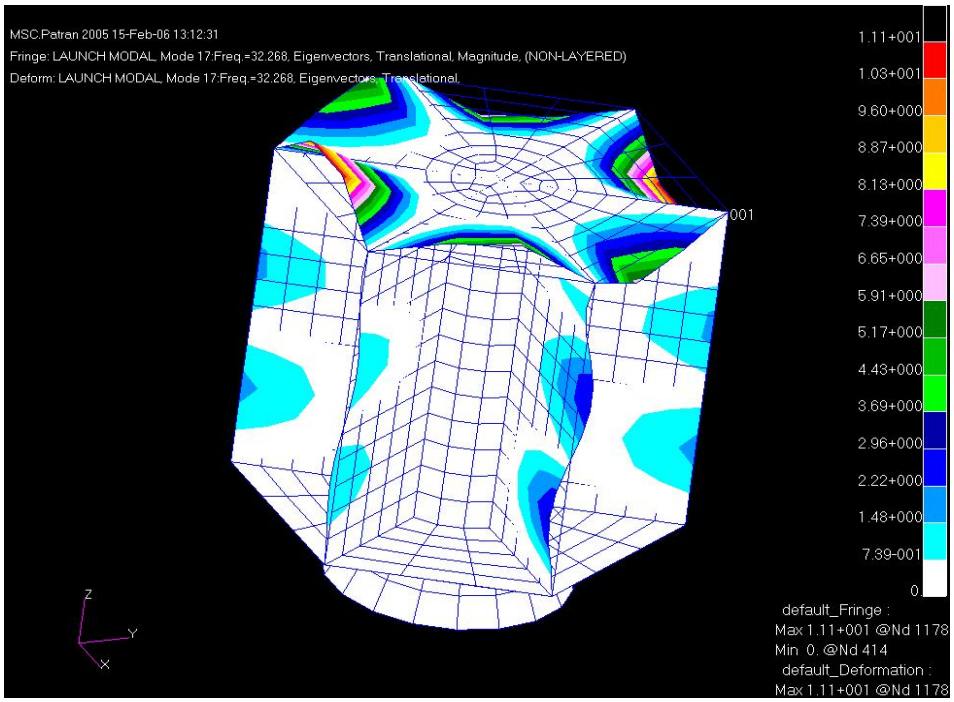

Figure 2. Satellite Bus Modal Analysis for Frequency: 32.268 Hz

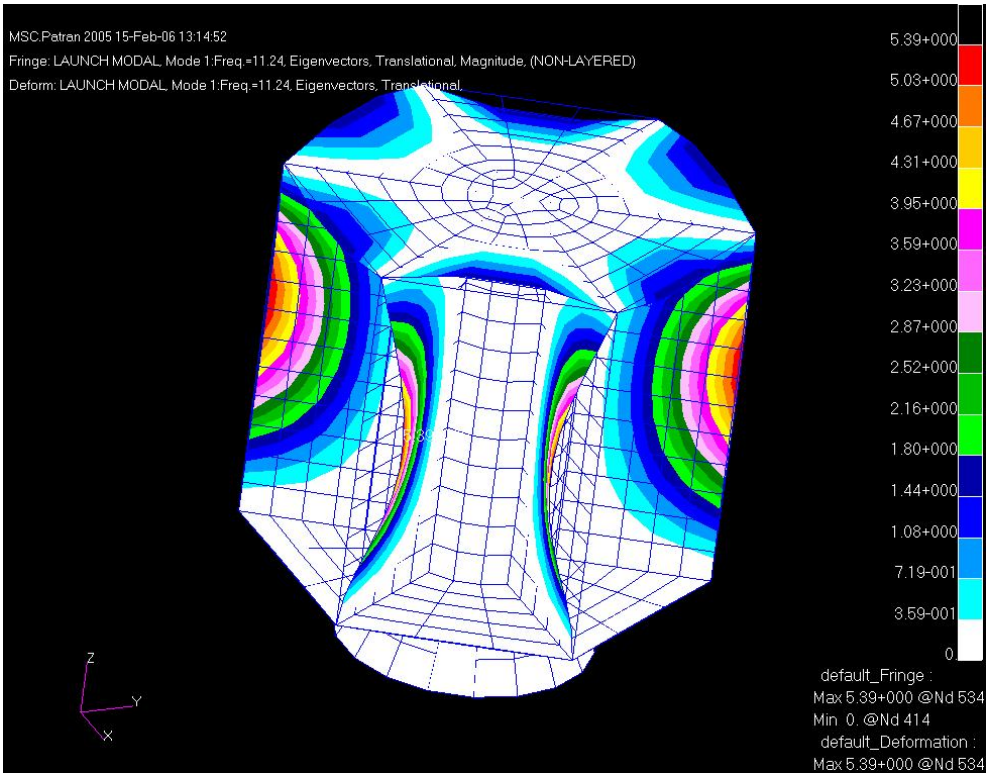

Figure 3. Satellite Bus Model Modal Analysis for Frequency 11.24 Hz

Finally, in Chapter VIII, conclusions, recommendations and future applications of the present study are presented. The information is useful for contractors, manufacturers, space and defense agencies in their vulnerability and survivability studies and ensuing risk reduction and mitigation. The results also help in assessment of safe and reliable operations of space assets during their designed life cycle.

III. LITERATURE REVIEW

As is generally accepted in laser research communities, Albert Einstein was the first to describe the procedure that atoms could emit and absorb radiation. He later referred to this innovative thought as the stimulated emission of radiation and led to the foundation for the development of lasers. The first laser (**L**ight **A**mplification by the **S**timulated **E**mission of **R**adiation) was first developed by Theodore H. Maiman in 1960 at the Hughes Aircraft Corporation research Laboratory [Ref. 2]. From that point on and for the following decades, several efforts were made for the development, and innumerable laser applications have taken place in our world. From civilian to military environments, there is a widely accepted opinion that lasers today dominate our life, from simple to very complex applications.

Federal agencies in the United States and throughout the world are using lasers for military operations, inventing new technologies and enhancing the already existing capabilities of lasers. Space warfare is one of the fields where lasers have various applications. Remote sensing, environmental protection, weather forecasting, and military defensive purposes are some of the many applications that one can find in space. Treaties among countries have been signed in the past to provide for the safe and beneficial use of lasers in space.

One of the areas that have attracted a lot of attention from research communities is the notion of the use of ground-based lasers as the mean of transferring energy into space. Many research centers in United States, such as NASA Glenn Research Center [Ref. 3], are trying to invent methods of transmitting laser energy through the atmosphere and give adequate power to orbiting satellites on eclipse, or even provide power to future moon stationed bases by ground-based laser illumination [Ref. 3]. Other than that, various studies and also extensive experiments have already been made in order to create a laser that will be capable of transmitting amounts of energy through the atmosphere for defensive and strategic purposes. The Unites States Air Force doctrine for the latest planned space weapons program states that the Ground-based Laser would propagate

laser beams through the atmosphere to Low Earth Orbit satellites to provide robust defensive and offensive space control capability [Ref. 4].

Reviewing the published literature, the United States and Russia are the leaders in constructing laser machines that have capability to deliver thermal energy needed to damage satellites, temporarily or even permanently, in different orbits. They have already tested anti-satellite weapons but have not deployed them [Ref. 5]. An attempt was made with a laser ASAT test in 1997, in which a low power chemical laser (30 Watts) was able to temporarily blind a United States Air Force satellite orbiting at an altitude of 425 kilometers. Another attempt was reported by the United States Army using ground-based mid infrared advanced chemical laser (MIRACL) against an orbiting U.S. satellite. To investigate the effects on the imaging satellite's sensors, the laser fired beams of varying durations (1 second and 10 seconds), simulating both an inadvertent lasing and a hostile attack on a satellite. The Army called the attempt a "partial success" because the satellite failed to download data during the lasing period [Ref. 17]. So, the question that arises is that, if one can temporarily disable a satellite using a simple 30 watt laser on the ground, what are the potential consequences using a megawatt class laser [Ref. 6]. As we see from the above-mentioned examples, there exists a capability of low and high power lasers, with simple acquisition and tracking illumination techniques, to saturate the optical sensors or telemetry of a low earth orbit satellites. Therefore, high-power lasers have a potential to cause damage to satellites at different levels of vulnerability. It may be mentioned that there are several issues that need to be addressed, such as atmospheric propagation, mobility, and other tactical matters.

A. DAMAGE CRITERION

1. Satellites

Energy is needed to be delivered to the target, such as a space asset. A weapon must therefore produce adequate energy to damage a target, including energy associated with atmospheric propagation losses. The anticipated target and also the engagement range are the two main factors for the design of a weapon to reach the target. The above mentioned factors determine the necessary amount of laser energy for damaging a target.

Typically, a military system classifies two types of attacks as possibilities. Firstly, the so-called “soft kill” attack is considered to be the one that can blur satellite cameras, destroy electronic systems or even degrade the solar arrays performance. With this type of attack, a satellite continues to stay on orbit but is no longer able to provide any useful information. In contrast, “hard kill” attack occurs when total destruction of the target is expected. The type of attack selected each time depends upon the mission requirements. In the absence of specific requirements, we can assume that the attack with the best effectiveness on the target is the “hard kill” attack, as it gives us immediate feedback of the damage of the targeted satellite.

In order to vaporize a material, a sufficient amount of heat has to be deposited on it and for specific time duration. Figure 4 summarizes the general thermal properties of the common metals that are used in the analysis and design of satellites. It may be observed from the last column, that an amount of 10,000 joules of energy would be adequate to vaporize most common materials. This is a good all purpose damage criterion, useful as a measure of the amount of energy a ground-based laser (GBL) weapon needs to deliver in order to damage a satellite.

MATERIAL	DENSITY (gm/cm^3)	MELTING POINT, T_m (^0C)	VAPORIZATION POINT, T_v (^0C)	HEAT CAPACITY (J/gm^0C)	HEAT OF FUSION (J/gm)	HEAT OF VAPORIZATION (J/gm)
ALUMINUM	2.7	660	2500	0.9	400	11000
COPPER	8.96	1100	2600	0.38	210	4700
MAGNESIUM	1.74	650	1100	1.0	370	5300
IRON	7.9	1500	3000	0.46	250	6300
TITANIUM	4.5	1700	3700	0.52	320	8800

Figure 4. Thermal Properties of Common Metals (From [Ref. 7])

The table presents a generic data for the energies. The laser energy also needs to be delivered on a small region and in a short time. If energy is delivered over a long period of time the metal will have sufficient time to dissipate away the incoming energy as fast as it is being deposited and it may not heat up to the melting point (conduction – convection – radiation mechanisms). Thus, if energy is deposited more rapidly than the material can dissipate, positive damage of the satellite may be ensured.

Following the above criteria, we define heat flux (Joules/cm^2) as the energy in Joules that has to be deposited on a satellite surface per unit area (cm^2) This is almost constant for short pulse widths and increases rapidly as the pulse width increases.. Therefore, it is advantageous to keep the pulse duration short in order to have the lowest possible amount of heat flux to be delivered on target [Ref. 6].

A generic and "all purpose damage criterion" for GBL weapons would serve as the failure criteria and lead to the analytical study conducted. Figure 5 shows the depth of any material that is being vaporized if we have a heat flux of 10^4 Joules with respect to the area of engagement. We can easily observe that in order to vaporize a 1 cm of satellite's surface material, it is required to deposit 10^4 Joules on an area of 1 cm^2. Consequently, we can take 10^4 Joules/cm^2 as our all purpose damage criterion and state that making a hole in a satellite to a depth of about 1 centimeter is sufficient to damage almost anything on it. Taking into account that 1 cm is a very thick target, and the thickness of a satellite external surface is in the order of millimeters, then we can conclude that the fluence necessary to damage a satellite would be in the order of 100 Joules/cm^2, a value which is also consistent with published estimates [Ref. 7].

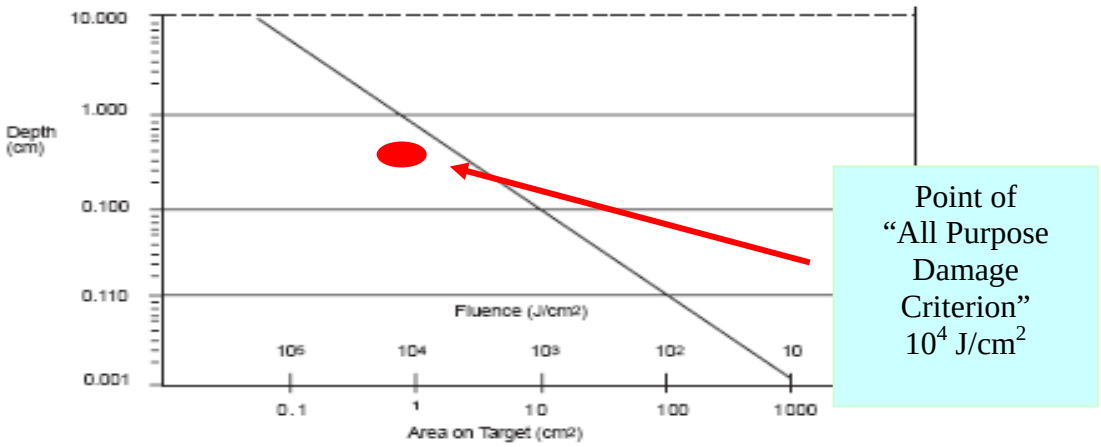

Figure 5. Depth Vaporized by 10e4 Joules versus Area Engaged and Flux (From [Ref. 7])

2. Intercontinental Ballistic Missiles (ICBMs)

Similar, to satellites, ICBMs is another field where the ground-based laser weapon technology may be applied. We will make a brief overview of the damage criterion and also we will pinpoint some of the main characteristics that are needed to be taken into account in order for a ground-based laser energy weapon to damage the ICBM in the boost phase (middle phase). ICBMs are considered as space assets and the present methodology is applied to study survivability and vulnerability as well as associated risk and risk mitigation.

The view in DoD is that high energy laser weapons represent the most promising response to the increased threat posed by ballistic missiles. In fact, the laser beam is probably the ideal instrument for destroying a ballistic missile [Ref 9]. One failure mode is for the laser to destroy the ballistic missile through the skin heated to melting temperatures or high temperatures for the fuel tanks to explode. It may be noted that the ICBM construction is very robust, with usage of large thickness and high strength materials..

There are various ways to destroy a ballistic missile or make it inactive for the rest of its course. One approach is for the laser to specifically target the electronic circuits, which are used for guidance control, and render the missile incapable of staying on course [Ref. 9]. Another kill mechanism is to melt a section of material surrounding the missile's fuel tank and detonate the fuel. A third, and more realistic kill mechanism is

to heat missile's skin until internal stresses cause a catastrophic failure of the skin around the fuel tank. This type of failure requires the least amount of laser energy to destroy the missile [Ref. 9], but acquisition of the specific area on missile surface is extremely difficult.

ICBM's damage criterion is similar to the satellite's case in terms of the material physical properties [Ref. 9]. If we set, again, as an "all purpose damage criterion" the heat flux of 10^4 Joules/ cm^2 (Figure 5) [Ref. 9], then our approach may be used in the ICBM survivability and vulnerability studies. It has been shown in the literature that a missile's material can be destroyed in a few seconds with only 1 MW of laser power. One liter corresponds to a hole with the dimension of 10cm x 10cm x 10cm which is generally enough to structurally disable most threat missiles [Ref. 11]. In Table 1 missile vulnerability parameters are given for some of the most common ballistic missile threats.

Name/Country of Missile	Range (km)	Missile Burn Time (sec)	Material	Thickness (mm)
Scud B (Russia)	300	75	Steel	1
Al-Husayn (Iraq)	650	90	Steel	1
No-Dong 1 (Korea)	1000	70	Steel	3
SS-18 (Russia)	10000	324	Aluminum	2

Table 1. Missile Vulnerability Parameters [Ref. 9]

Although theoretically we can infer that ballistic missiles can be easily compared with satellite's case and so destroyed accordingly, it is generally accepted that ballistic missile threats are very difficult targets for laser weapons because of the very little time a defensive laser weapon system has to react. In Table 1 is shown that reaction times vary

approximately from 1 to 5 minutes if the missile has to fly distances up to 10,000 kilometers. Moreover, acquisition and tracking issues are of great concern and that is what it makes the destruction of a ballistic missile a cumbersome procedure.

In this thesis, along with the satellite model, a basic prototype ballistic missile model is created using the same software tools. Missile skin is constructed from different materials and thicknesses for the sake of the study of thermo-mechanical effects on missile's external surfaces. Incoming laser energy hits the missile normally on pre-selected area and analysis proceeds to compute steady and transient temperature distributions, thermal deformations and subsequent thermal stresses.

B. ATMOSPHERIC PROPAGATION LOSSES

The study of the propagation of laser radiation through atmosphere is important as certain wavelengths, and therefore, certain lasers may be eliminated on the basis that their beam cannot reach the target with sufficient energy. We focus in this report on space assets and in particular in Low – Medium and Geosynchronous Earth orbits. A ground-based laser passes through the atmosphere in order to reach the target and a detailed knowledge of the propagation losses is needed to calculate the total energy required at the generation as well as in the design of the weapon system itself. Interaction of laser energy with atmospheric matter influences the available energies at different orbits. The major atmospheric propagation issues that arise are:

- Absorption
- Scattering
- Turbulence
- Thermal Blooming and
- Diffraction

1. Absorption

Absorption is the process by which incident radiation is absorbed by the medium. For this to occur, the substance must be opaque to the incident radiation. A portion of the absorbed radiation is converted into internal heat energy, which is subsequently emitted or reradiated at longer thermal infrared wavelengths [Ref. 8]. This interaction of energy

with the medium is explained through an exponential decay governed by the absorption coefficient, α. The irradiance incident upon a surface is described by the following equation:

$$I(z) = I_0 e^{-\alpha z}$$

Where, I is the irradiance at range z, and I_0 is the initial irradiance. The absorption coefficient is dependent upon the size of the particles suspended and the frequency of the light that is being considered. The primary atmospheric components that contribute to absorption are water, dioxide, diatomic oxygen and ozone. These molecules absorb the electromagnetic radiation and convert it to molecular vibration and rotation [Ref. 10]. It is not feasible to control the atmospheric absorption. A solution is to use specific atmospheric "windows" where the selected laser wavelength is not greatly affected by absorption. These windows are shown in Figure 6, with the available wavelengths are shown as blue regions. For example, the region approximately from 5-7 μ is dominated by water and carbon dioxide absorption. Therefore, laser wavelength inside this region is not used.

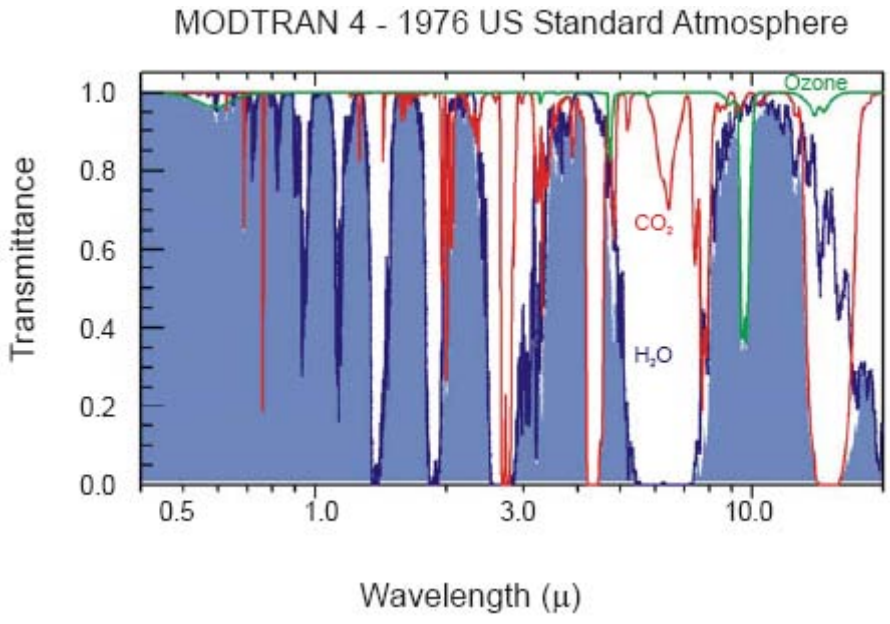

Figure 6. Atmospheric Absorption (From [Ref. 8])

2. Scattering

Another important propagation loss mechanism is atmospheric scattering. Here electromagnetic radiation (photons) is scattered by various particles in earth's atmosphere, such as aerosols and clouds (water droplets). There are three different kinds of scattering- Rayleigh scattering, Mie Scattering and Non selective scattering.

Rayleigh scattering (Figure 9) refers to the scattering of light off of molecules in the air, and from particles up to about a tenth of the wavelength of light. The strong wavelength dependence of Rayleigh scattering favors the short wavelength λ, since the scattered intensity *I* is proportional to λ^{-4} [Ref. 11].

The probability of Rayleigh scattering of scattering interactions is inversely proportional to the fourth power of wavelength. This is illustrated in Figure 8 and expressed by the equation below:

$$\text{Probability of scattering} = \frac{1}{\lambda^{-4}}$$

For particle sizes larger or comparable to light's wavelength, Mie scattering is dominating. This scattering produces a pattern like an antenna lobe, with a sharper more intense forward lobe, as shown in Figure 9. In Mie scattering the dependence of the scattering probability on wavelength decreases and the scattering directionality involves as well. Mie scattering produces the almost white glare around the sun when a lot of particulate material is present in the air [Ref. 8].

Finally, non selective scattering is the mechanism that results when the size of the scatterer is much larger than the wavelength. The term non selective, means that this type of scattering is independent of the wavelength.

Scattering

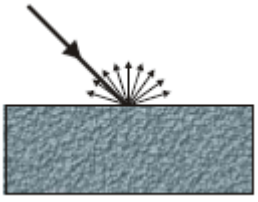

Figure 7. Energy Interaction with matter: Scattering (From Ref. [8])

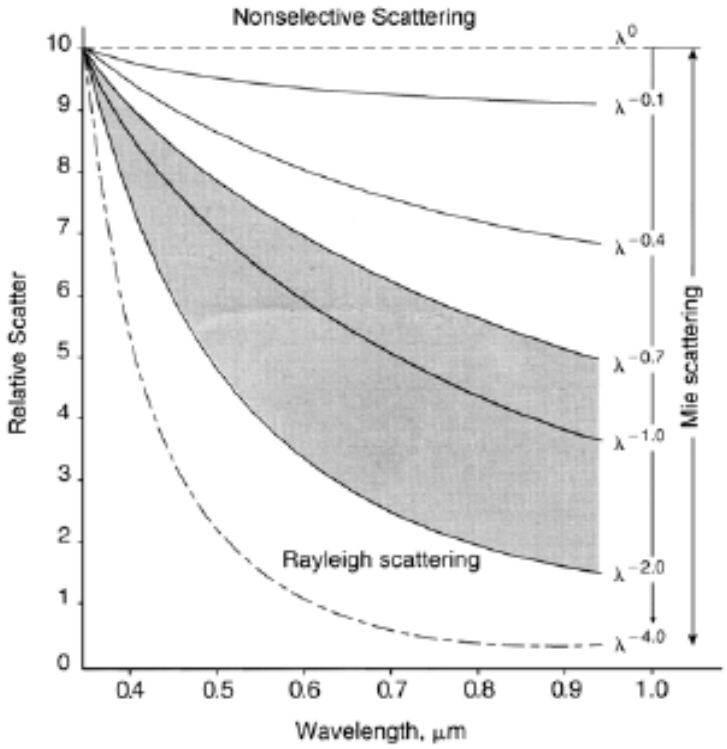

Figure 8. Atmospheric Scattering Diagram (From Ref. [8])

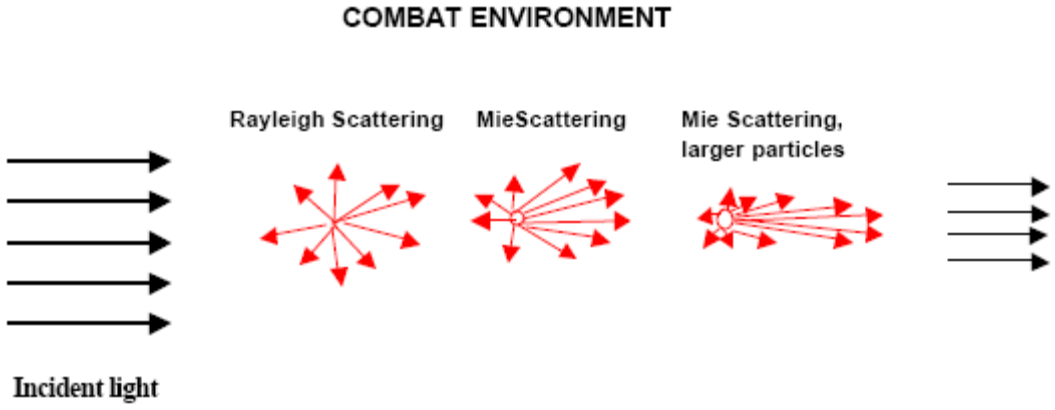

Figure 9. Rayleigh and Mie Scattering (From Ref. [11])

The combined effects of absorption and scattering are shown in Figure 10. It may be observed that the absorption due to ozone becomes very significant below 0.35 μ and the atmosphere is opaque to sunlight below 0.3 μ due to ozone layers at high altitudes. The overall atmosphere is more transparent in the long wave infrared (11-12 μ) than in

visible spectrum (0.4 - 0.7 μ) [Ref 8]. The grey regions indicate the atmospheric transparency due to absorption and scattering.

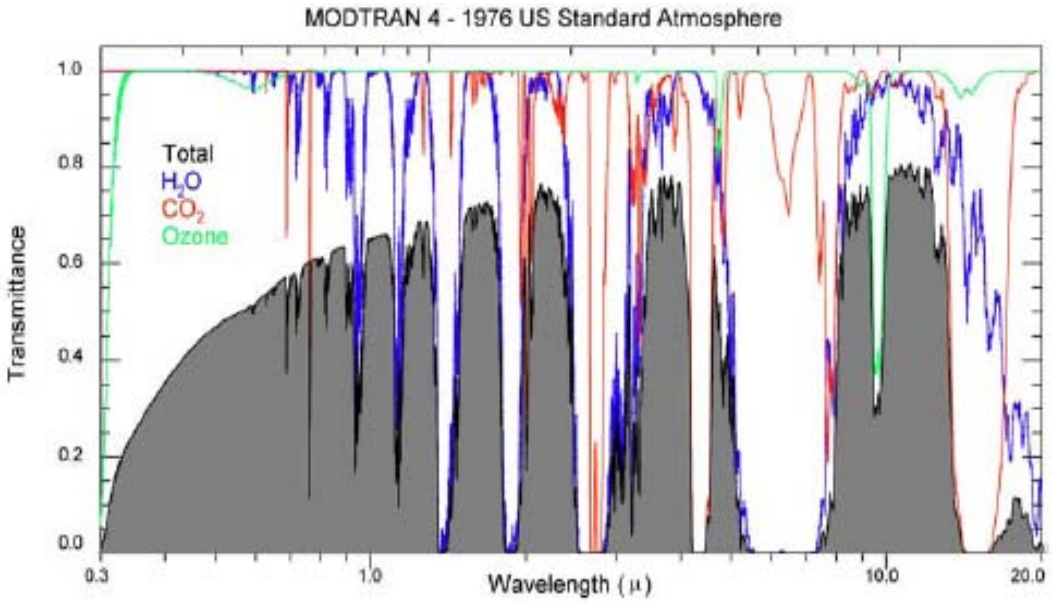

Figure 10. Atmospheric Absorption and Scattering (From Ref. [8])

3. Turbulence

The third factor that creates a serious problem in energy propagation is the atmospheric turbulence, as shown in Figure 11. It is caused by the temperature and density fluctuations in atmosphere. Small irregularities in density produce variations in the index of refraction which turns into small fluctuations in the direction in which light propagates (Snell's law), on the order of one part in a million.

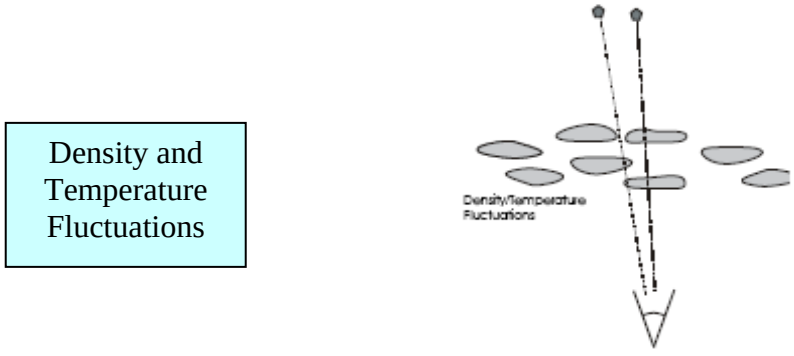

Figure 11. The apparent position of star will fluctuate as the rays pass through time varying light paths (From Ref. [8])

Density and temperature fluctuations have a profound effect on beam propagation through the variations they cause in the index of refraction of the air. Light ray is observed to bend as it passes through regions of differing refractive index. In principle, it is possible to know and account for fluctuations in the index of refraction if we know how the temperature and density vary along the beam path. In practice, of course, it is impossible to know these quantities everywhere, because they are constantly shifting. There is a defined parameter known as coherence length, r_0. This coherence length is depending on three factors [Ref. 7], the degree of turbulence along the path beam, the wavelength of light and the total path length from beam to target. Taking into account the above factors, we have [Ref. 7]:

$$r_0 = [0.423(2\pi/\lambda)^2 \int_0^Z C_N{}^2(z)dz]^{\frac{-3}{5}}$$

Where, $C_N(z)$ is the refractive index structure coefficient and characterizes the turbulence at a point z along the beam path. The total integrated effect of turbulence is taken into account by integrating the square of this quantity over the whole beam path.
Measurements of $C_N(z)$ has been obtained experimentally by probing the atmosphere with a laser and examining the effect of turbulence on its propagation [Ref 7]. Typical data are shown in Figure 9.

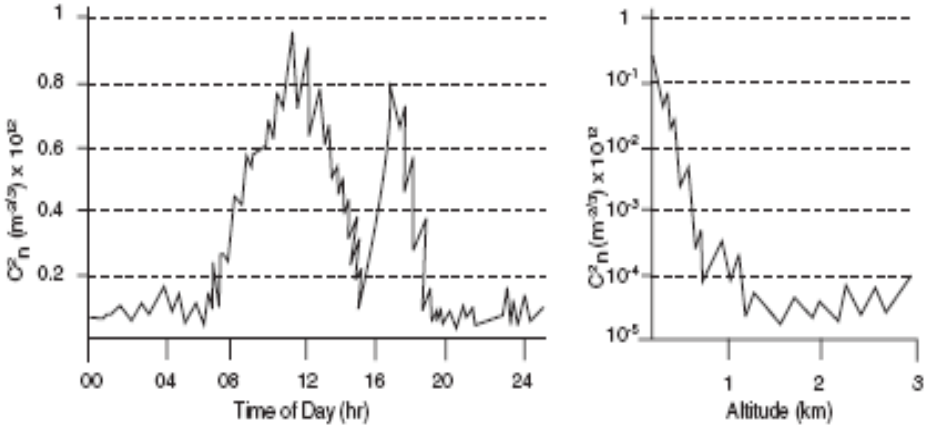

Figure 12. Atmospheric Structure Factor versus Time and Altitude (From Ref. [7])

As we can see from Figure 12, turbulence is least during the hours of darkness, when there is no solar heating to introduce temperature inhomogeneities. Also, as a function of altitude, $C_N(z)$ decreases, since solar heating is higher near the ground [Ref. 7]. These irregularities in the atmospheric boundary layer have characteristic scale sizes of tens of meters and fluctuate on timescales of milliseconds to seconds. The impact of atmospheric turbulence is much greater for telescopes looking through atmosphere than sensors looking down on earth from space [Ref. 8]. In order to reduce the atmospheric turbulence effects, adaptive optics technology may be used.

4. Thermal Blooming

When a high power optical beam travels through atmosphere, random temperature variations caused by turbulence take place. This is a nonlinear phenomenon and the beam loses its energy as a result of absorption. This energy is deposited into the air resulting in increased air temperatures. The rise produces an increase in air density and also increases the index of refraction. This lead to a phenomenon called thermal blooming and the sequence of events are illustrated in Figure 13.

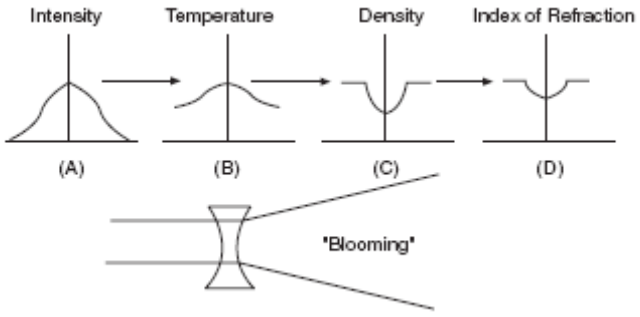

Figure 13. The Physics of Thermal Blooming (From Ref. [7])

As we observe from Figure 10, blooming has an effect of defocusing the beam of light that propagates through the atmosphere. Thermal blooming can be controlled by reducing the intensity of the beam and also by using adaptive optics technology so as to increase the intensity of the beam near focus. Figure 14 shows the effect of thermal blooming on a beam of light. We clearly see how adverse is the spreading of the beam if thermal blooming occurs.

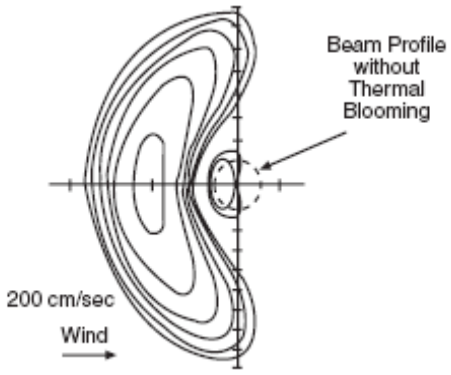

Figure 14. Beam Profile with and without Thermal Blooming (From Ref. [7])

We consider a uniform beam with velocity *v*, having an intensity profile which varies with radius as [Ref. 7]:

$$S(r) = S_0 \exp(-2r^2 / w^2)$$

Where S (w/cm^2) is the beam intensity at a distance r, S_0 is the beam intensity at the beginning of lasing and w is the beam radius. Such a beam can be characterized through a thermal distortion factor N_t which is given by:

$$N_t = \frac{\frac{-dn}{dT}}{n\rho c_p} x \frac{KSZ^2}{vw}$$

Where (dn/dT) is the slope of a curve of index of refraction n as a function of temperature T, C_P is the heat capacity of the air in (J/gm K^0) and ρ is the density of air (gm/cm^3). The product of $\rho\ C_P$ is the number of Joules of energy which must be absorbed to heat a cubic centimeter of air by one degree. K is the absorption coefficient of the air (cm^{-1}) and the product of KS is the number of Joules being deposited in a cubic centimeter of air in each second. z is the range to target and v is the velocity of the wind. As N_t increases, the beam becomes more and more distorted and its intensity falls off, as shown in Figure 15. Also N_t is proportional to intensity S, *and therefore* it is not possible at large distortion numbers to overcome the thermal blooming effects [Ref. 7].

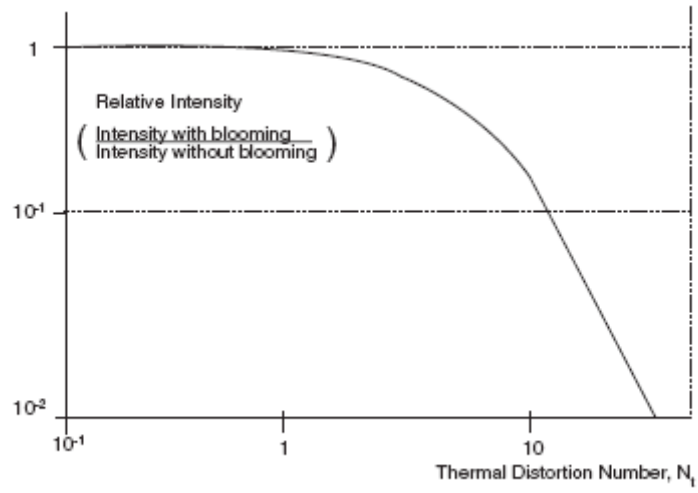

Figure 15. Relative Intensity versus Distortion Number (From Ref. [7])

5. Diffraction

Diffraction affects propagation over large distances and therefore has to be taken into account in the atmospheric losses. It refers to spreading, or divergence of light which emerges from an aperture of a given diameter.

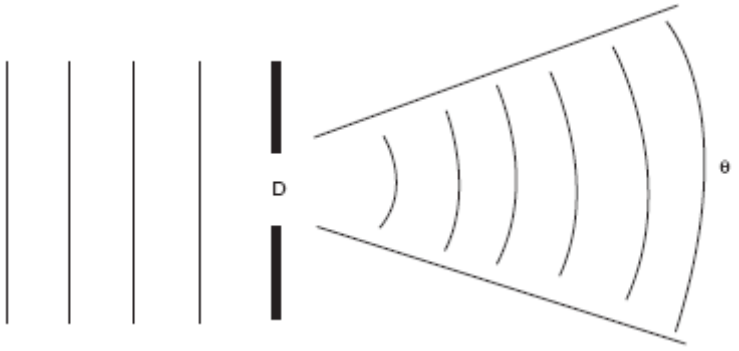

Figure 16. Diffraction of Light Passing through an Aperture (From Ref. [7])

In Figure 16 we see a beam of light which is passing through an aperture D. and results in the beam with diverged angle θ. This angle is related to the wavelength λ and in order to minimize the effect of diffraction, we use the Rayleigh criterion (the beam remains collimated for the larger distance):

$$\theta = \frac{\lambda}{D} \text{ (Approximately)}$$

The exact relationship depends on the shape of the aperture (for example, circular or square).

For circular apertures the above formula reduces to [Ref. 8],

$$\theta = 1.22\frac{\lambda}{D}$$

In short, the shorter wavelengths and larger apertures result in longer propagation distances without spreading [Ref. 7].

C. SATELLITE ORBITS REVIEW

In contrast to the flight profiles of aircraft sorties, satellites follow considerably constrained and predetermined orbits. The duration of satellite missions is measured in years rather than the hours for the aircraft missions. In order to achieve a stable orbit, a satellite must maintain the orbital velocity required at its altitude. Each satellite carries a one time supply of fuel with which to adjust its orbit. When it is not adjusting its orbit, the satellite is in a weightless, free fall condition where its forward inertial velocity, combined with its radial free fall is precisely balanced to follow the desired orbit. Military space systems utilize a wide variety of satellite types in a variety of orbits. The type of orbit used depends on the satellite's mission and launch constraints. The main categories of orbits are illustrated on Figure 17 (From [Ref. 13]).

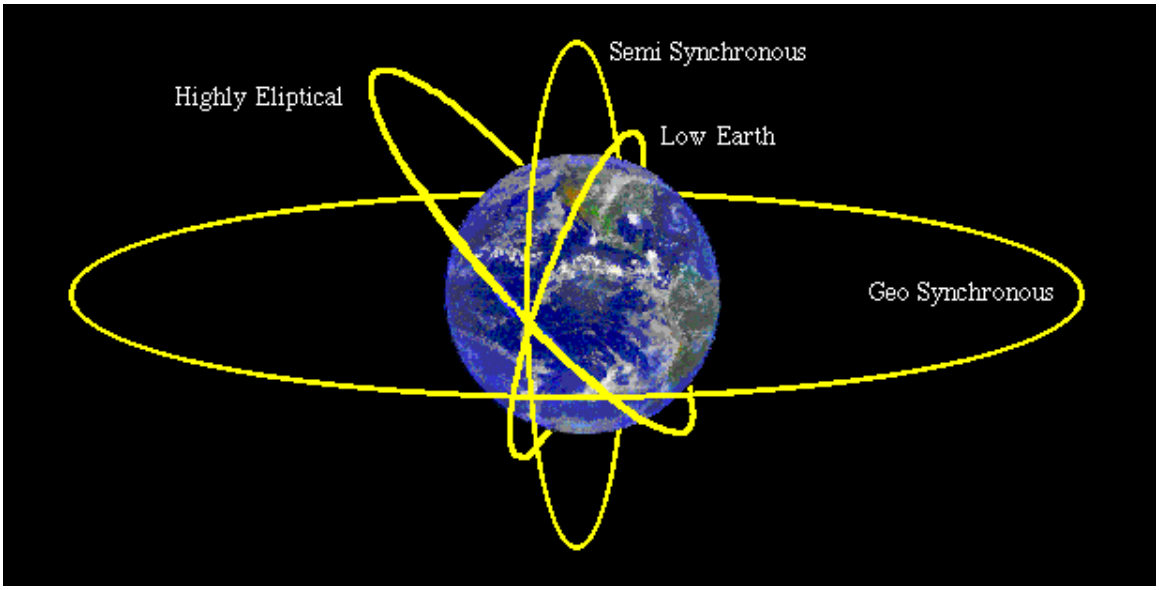

Figure 17. Typical Orbits (From Ref. [13])

1. Low Earth Orbit (LEO)

The range of this orbit is extended up to 500 km and is used mainly for remote sensing satellites, meteorological and reconnaissance satellite missions. Most military spy satellites are located in these altitudes as it is close to the earth and results in high image resolutions. Figure 18 shows the ground track of a LEO satellite for four different passes - orbits during one day.

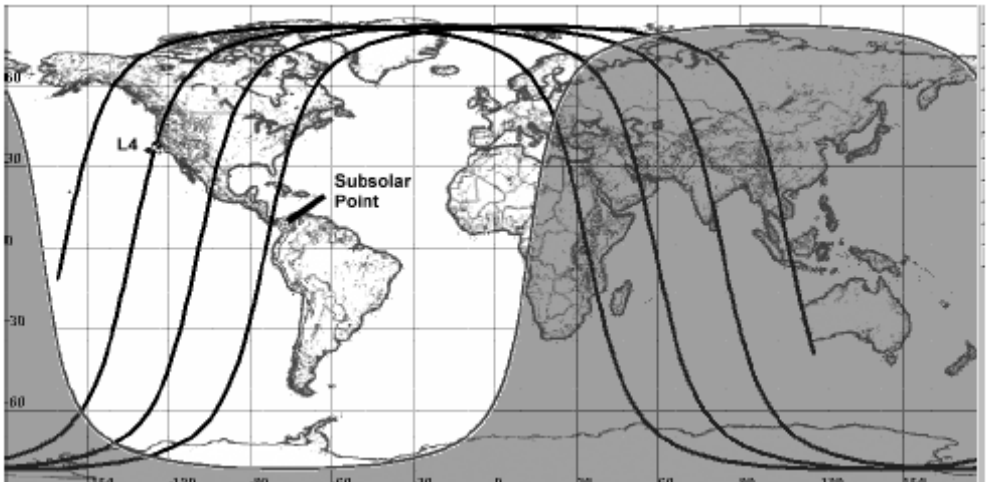

Figure 18. Low Earth Orbit Satellite Ground Track (From [Ref. 8])

2. Medium Earth Orbit (MEO)

This orbit is in a range of approximately 500 to 20000 km and is used primarily for earth mapping purposes. GPS satellites also are using this type of orbit to send signals to earth. Figure 19 shows the ground track of three different GPS satellites, currently on orbit.

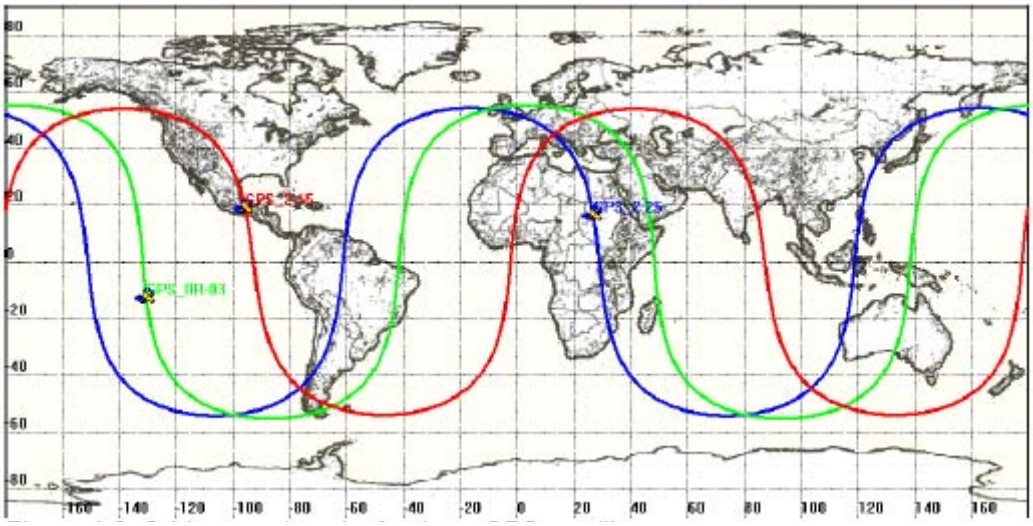

Figure 19. Ground Track of Three GPS Satellites (From [Ref. 8])

3. Geosynchronous and Geostationary Earth Orbits (GEO)

At an orbital altitude of more than 20000 km and specifically at around 35000 km above the earth's equator, these satellites orbit the earth once every twenty-four hours. Since they rotate at the same rate as the earth is rotating, their ground tracks appear to oscillate about a single point in the sky. This orbit is primarily used by communication satellites and is an area where the vast majority of commercial satellites take place. Figure 20 shows a typical ground track of a geosynchronous satellite.

On the other hand, when satellites are in GEO altitudes and exactly above the equator the name geostationary is used because the satellite appears as a fixed point in the sky.

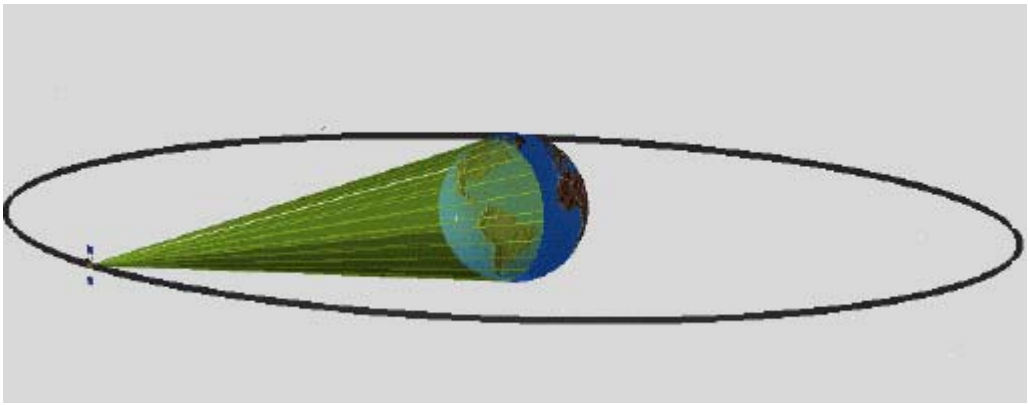

Figure 20. Ground Track of TDRS Geosynchronous Satellite (From [Ref. 8])

4. Semisynchronous Earth Orbit

At an orbital altitude of 20,273 km these satellites orbit the earth at a rate of 12 hours and repeat their trace every 24 hours ([Ref. 13]). This orbit is primarily used as navigation satellites since the position of the satellite is known as a function of the day and time.

5. Molniya or Highly Elliptical Earth Orbit (HEO).

Soviets have named this orbit as Molniya orbit after it was discovered by them. Without having the possibility to launch satellites from equatorial sites and being primarily interested in communication missions, they used this type of orbit in order to minimize the launch costs. With only four satellites continuous coverage of one hemisphere at all times is obtained using these orbits. Figure 21 shows a typical ground track of a Highly Elliptical Earth Orbit.

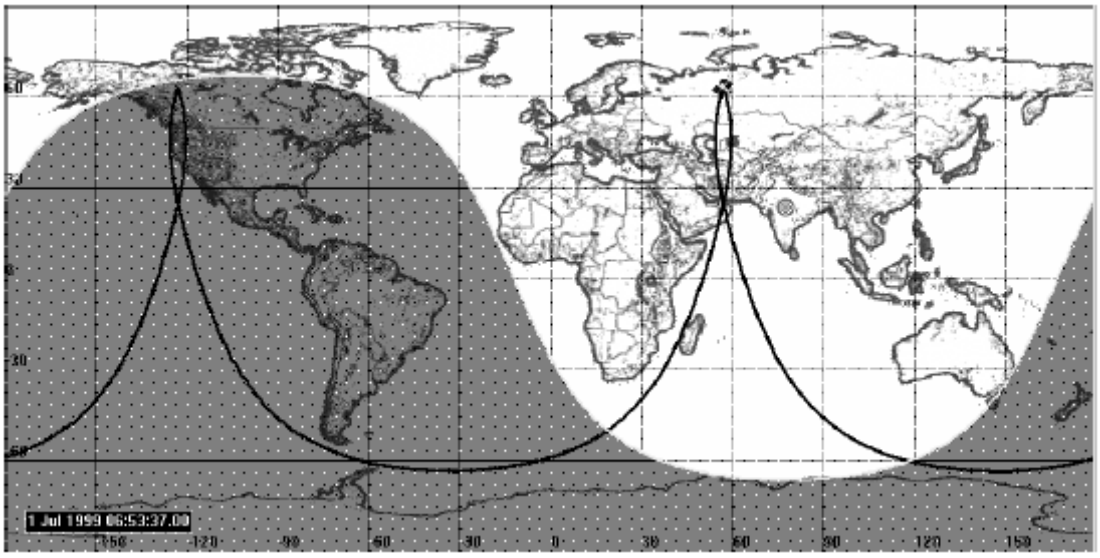

Figure 21. Ground Track of Molniya (HEO) Orbit (From [Ref. 8])

D. INTERCONTINENTAL BALLISTIC MISSILES FLIGHT PATH REVIEW

An intercontinental ballistic missile (ICBM) is a long range ballistic missile with ranges greater than 5500 km. They are having extreme capabilities in delivering warheads in large distances with fairly very large speeds.

They usually travel in three different phases along their flight paths which are specifically ([Ref. 14]):

- Boost phase: 3 to 5 minutes and up to 150 km
- Midcourse phase: 25 minutes and up to 1200 km
- Reentry phase: 2-3 minutes and starting at 100 km

The above specified timeframes and altitude ranges are strongly dependent on the type of the ICBMs and also varies with a number of other factors, as, for example, the type of propulsion used. In this study we are only interested in finding the approximate time frames and altitudes that an ICBM is usually flying in order to estimate the correct damage criterion with respect to anticipated target and engagement scenario range.

Taking into account the above information, we deduce that for hard – kill of an ICBM using ground-based lasers, midcourse phase is optimal, as the time frame is fairly big and the altitude is between LEO and MEO orbits. This allows the application of the

developed methodology to study the thermo mechanical behavior of ICBMs. Figure 22 shows a typical flight path of an ICBM.

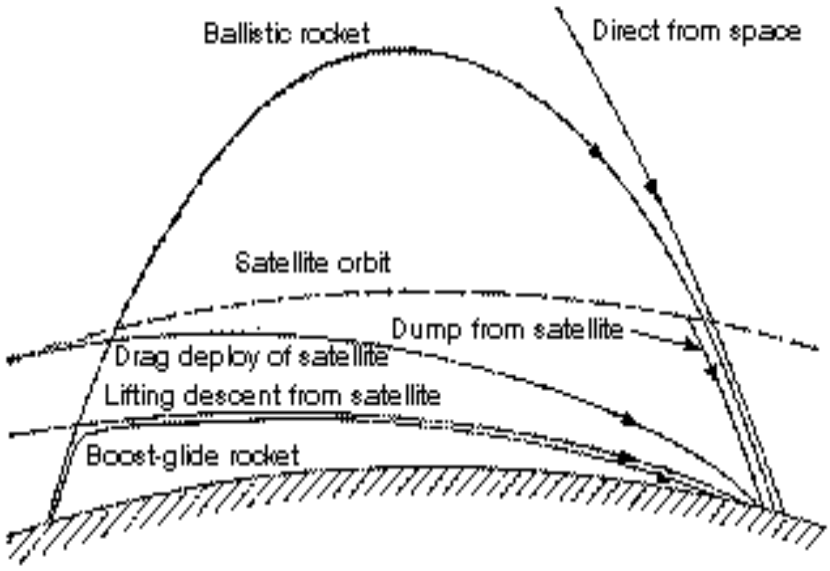

Figure 22. Flight Path of an ICBM with respect to space (From [Ref. 15])

E. CLASSIFICATION OF LASERS

Since space systems are typically unmanned satellites moving in well-established orbits, their positions and motions are known to potential adversaries. Moreover, information on their mission, importance and in many cases even their design will be available as well. As a result, a wide variety of potential anti-satellite threats can be expected against military space assets. These potential threats could be categorized in terms of their basing and their kill mechanisms. In general, anti-satellite basing concepts could include land, sea, and air or space platforms [Ref. 13]. This study is focused only on directed energy weapons, and specifically, in those weapons that can have the capabilities to work as ground-based laser weapons and jam or intercept satellites at selected orbits. A generic classification of Directed Energy Weapons is shown on Table 2.

Directed Energy Weapons	
High Power Microwave	Induce permanent damage to electronic circuits by over-stressing components with EM radiation, or thermally inducing structural damage.
High Energy Laser	Thermally induce structural, electronic, or sensor damage through irradiation.
Neutral Particle Beam	Thermally induce structural, electronic, or sensor damage through irradiation.

Table 2. Generic Classification of Directed Energy Weapons (From [Ref. 13])

During the past decades, different types of laser configurations have been tested and laser beams have been sent through atmosphere, in order to be able to reach satellite altitudes with adequate amounts of energy. The results are varying, each time, and are strongly dependent on mission requirements. The purpose of this analytical study is not to pinpoint specific laser machines that are currently on market, but to give a generic sense of what is needed in order to send laser energy through atmosphere successfully and satisfy the damage criterion we set in the analysis. For this purpose, we briefly refer those specific laser types that could serve our damage criterion and perhaps are able to deliver 10^4 Joules/ cm^2 on the desired orbits.

1. Chemical Oxygen Iodine Laser (COIL)

Chemical Oxygen Iodine Laser is capable of producing intense laser beam with a wavelength of about 1.3 microns [Ref 2]. Unlike other lasers, it is not strongly absorbed by atmosphere, as we can easily observe from Figure 10. It can also deliver beams of continuous wave energy in megawatt range. In this short operating wavelength there is a very definite interest by for the defense applications. Another significant advantage is that the shorter wavelength allows for smaller optics and results in lower manufacturing costs. Furthermore, it is also capable of getting acquisition ranges larger than 300 km and up to 1000 km. In recent years, numerous experiments have taken place in the United States using COIL laser.

2. Hydrogen Fluoride Laser (HF)

This type of laser works using wavelengths from 2.7 to 2.9 microns. At these regions atmospheric absorption is very high and hence its use is only limited to space

applications, even though it has the capability of delivering amounts of energy in the order of approximately 1 megawatt [Ref. 14].

3. Deuterium Fluoride Laser (DF)

With working wavelength regions from 3.4 to approximately 4 microns, it has a better transmission through atmosphere. However, the larger wavelength requires a larger optics. The mirror diameter has to be in the order of 4 meters, and renders it as a bad choice for a ground-based laser energy weapon. The typical output power is approximately 2 megawatts.

4. Solid State Laser (SSL)

Operating with only electrical energy, it produces a power output of 25 kilowatts and can reach a limit of 100 kilowatts under specific conditions. Although they create a fine beam quality, they are more suitable for terrestrial applications because of the low level of output power. They cannot be used as ground-based laser weapons against satellites [Ref. 14].

5. High Power Microwaves (HPM)

These produce hundreds of megawatts in a wavelength range of 0.1-0.01 microns. This very short wavelength makes them capable of being used as terrestrial and airborne laser weapons. The atmospheric losses are not appreciable due to extremely short wavelengths [Ref. 15]. The output power is in the range of tens of kilowatts up to hundreds of Megawatts. Nevertheless, the beam is highly diffractive and not preferred as ground-based laser weapons.

6. Free Electron Lasers (FEL)

Finally, another candidate ground-based laser weapon is the free electron laser. Several studies have been done lasting recent years in order to determine the capabilities of this promising laser machine. It is tunable over a wide range of wavelengths down to nanometers with optimum atmospheric propagation. Usually, manufactured systems are heavy but are not a factor for Ground-based laser systems. They have output power to kilowatts and high efficiency (up to 65%) [Ref. 16]. A free electron schematic is shown in Figure 23.

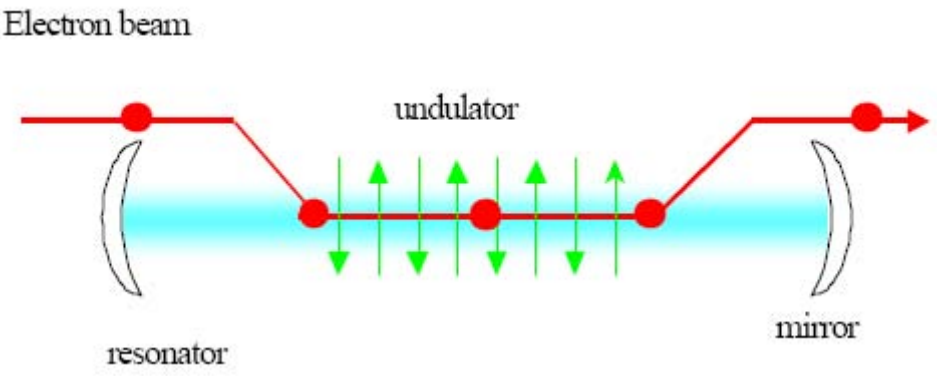

Figure 23. Free Electron Laser Schematic (From [Ref. 11])

Type of laser	Wavelength	Output Power Ranges	Atmospheric Losses	Optics	Area of application	Literature Review
COIL	1.3 μ	Megawatts	Large	Small	GBL ABL	Partially Classified
HF	2.7-2.9 μ	Megawatts	Large	Medium	SBL	Partially Classified
DF	3.4-4 μ	Megawatts	Small	Large	GBL	Partially Classified
SSL	Electrical Energy	Up to 100 kilowatts	N/A	Depends on the application	Terrestrial	Partially Classified
HPM	0.1-0.01 μ	Megawatts	Highly diffractive	Small	Terrestrial ABL, SBL	Partially Classified
FEL	Tunable	Kilowatts	Optimum	Depends	Possibly GBL, ABL, SBL	Partially Classified

Table 3. Summary and comparison of various laser machines and their capabilities.

IV. THEORITICAL BACKGROUND

A. HEAT TRANSFER ANALYSIS

An analogy between the thermodynamics and the mechanics of the structures is being exploited by the MSC Nastran software to extend the capability to heat transfer analysis. In this Chapter we will give the necessary theoretical background in order to understand thoroughly how the simulation program works underneath in order to provide us with the valuable and useful results.

As in the case of structural analysis, the analysis of heat transfer can be reduced by finite element techniques to the solution of a set of equilibrium equations in which the unknowns are defined at discrete set of points [Ref. 23]. Thus, the general equation that is solved when finite element methods are applied to heat transfer analysis may be written in the form

$$[K]\{u\} + [B]\{u\} = \{P\} + \{N\} \tag{4.1}$$

Where

$\{u\}$ is a vector of temperatures at grid points

$\{P\}$ is a vector of applied heat flux flows that are known functions of time

$\{N\}$ is a vector of nonlinear heat flows that depend on temperature

$[K]$ is a symmetric matrix of constant heat conduction coefficients

$[B]$ is a symmetric matrix of constant heat capacity coefficients.

Grid points are used to locate temperatures similar to the way they are used to locate displacements in structural analysis. However, one of the major differences between heat transfer and structural mechanics is that the temperature is a scalar function of position, whereas displacement is a vector which MSC Nastran assumes may have as many as six components. Thus, in heat transfer analysis the program provides one degree of freedom at each grid point.

The heat conduction matrix, $[K]$, and the heat capacity matrix, $[B]$, are formed from "element" properties, just as in structural analysis. In addition, a part of heat conduction matrix may be associated with surface heat convection and radiation. The components of the applied heat flow vector $\{P\}$ are associated with surface heat transfer. The vector of nonlinear heat flow $\{N\}$ results from surface radiation, from temperature dependent surface convection and from temperature dependent heat conductivity.

In the case of linear static analysis, which is used in the steady state analysis to obtain the temperature distribution on the surfaces of the models, $[B]$ and $\{N\}$ are null matrices. The users have the option to employ both single and multipoint constraints and many other specialized features normally associated with structural analysis. New solution techniques are used in nonlinear static analysis and in transient analysis.

The output of the heat transfer analysis includes the temperature at grid points, the temperature gradients and heat fluxes on surface and conduction elements. The heat flow into surface elements is further separated into components due to user prescribed flux, radiation and convective heat flux.

The Table 4 is a simplified flow chart for nonlinear steady thermal analysis and Table 5 shows a flow chart for thermal transient analysis used by the program.

Input File Processor
Geometry Processor
Conduction Matrix Assembler
Generate Radiation Matrix Combine with Conduction Matrix
Apply Constraints, Partition Matrix, Decompose
Generate Load Vector
Iterate Solution to Nonlinear Equations
Recover Element Fluxes
Deformed Structure Plotter / Post Processing

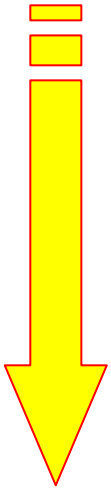

Table 4. Simplified Flow Chart for Thermal Nonlinear Static Analysis (From [Ref.17])

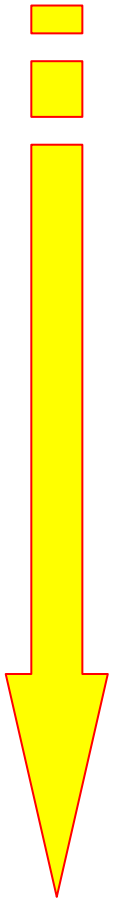

Input File Processor
Geometry Processor
Conduction and Capacity Matrix Assembly
Generate Radiation Matrix, Combine with Conduction Matrix
Apply Constraints, Partition Matrices
Dynamic Pool Distributor
Direct Matrix Input
Assemble Dynamic Matrices
Transient Load Generator
Integration of Equations with Nonlinear Loads and Radiation
Output Solution Points
Recover Dependent Temperatures and Element Fluxes
Deformed Structure Plotter / Post Processing

Table 5. Simplified Flow Chart for Thermal Transient Analysis (From [Ref.17])

B. SURFACE HEAT TRANSFER

Four types of surface heat transfer are provided for both steady state and transient analysis. These types are a prescribed heat flux, a convective heat flux due to difference between the surface temperature and the local ambient temperature, radiation heat exchange and a prescribed directed heat flux from a distant radiating source. In all cases the heat flux is applied to a surface element defined by grid points. The user specifies the area by points and the surface area is calculated automatically in all cases.

The user defines a distributed heat flux, Q, and the program calculates the vector of heat flows $\{\rho^e\}$ to be applied to the grid points connected to an element. The general form of the calculation of the j[th] component of $\{\rho^e\}$ is

$$\{\rho_j^e\} = \{A_j^e\}\{Q_j^e\} \tag{4.2}$$

where $\{A_j^e\}$,the sub area of the element, is associated with its j[th] vertex and $\{Q_j^e\}$ is the heat flux at the j[th] vertex.

In transient analysis, the time dependence of the flux is specified by specific application cards that program uses in order to calculate the sub areas in the different time frames. The procedure used is exactly the same, but the number of iterations is extremely large in comparison to the linear analysis.

C. STEADY STATE ANALYSIS

After the mesh is generated, equivalence and verification of the geometry and finite element model are performed, the program starts the analysis, taking into account the specified parameters from the user. The form of the thermal equilibrium equations after the multipoint dependent temperatures elimination is given by

$$[K_{nn}]\{u_n\} + [R_{nn}]\{u_n + T_a\}^4 = \{q_n\} + \{P_n\} \tag{4.3}$$

If $\{u_n\}$ is partitioned into $\{u_f\}$ (free points) and $\{u_s\}$ (single point constraints), the equilibrium equation can be written in partitioned form as follows:

$$\begin{bmatrix} K_{ff} & K_{fs} \\ K_{sf} & K_{ss} \end{bmatrix} \begin{Bmatrix} u_f \\ u_s \end{Bmatrix} + \begin{bmatrix} R_{ff} & R_{fs} \\ R_{sf} & R_{ss} \end{bmatrix} \begin{Bmatrix} u_f + T_a \\ u_s + T_a \end{Bmatrix}^4 = \begin{Bmatrix} 0 \\ q_s \end{Bmatrix} + \begin{Bmatrix} P_f \\ P_s \end{Bmatrix} \tag{4.4}$$

The components of $\{u_s\}$ have values prescribed by the user and the lower half of the above partitioned equation are used to evaluate the single point forces of constraints $\{q_s\}$ during data recovery. On rearranging the top half of the partitioned equation we obtain the equation (4.5)

$$\left[K_{ff}\right]\left\{u_f\right\}+\left[R_{ff}\right]\left\{u_f+T_a\right\}^4=\left\{P_f\right\}-\left[K_{fs}\right]\left\{u_s\right\}-\left[R_{fs}\right]\left\{u_s+T_a\right\}^4 \qquad (4.5)$$

The equation (4.5) is solved by an iterative method. The technique used is to expand $\left\{u_f\right\}$ into constant, linear and higher order terms with respect to an initial estimate, $\left\{u^1{}_f\right\}$, supplied by the user. The linear terms are kept on the left hand side of equation (4.5) and all the other terms are placed on the right hand side, where they are evaluated precisely for the current estimate of $\left\{u_f\right\}$. If we define $\left\{L\right\}$ to be the left hand side of the equation (4.5) and rewrite the equation (4.5), we obtain

$$\left[K_{ff}{}^*\right]=\left[K_{ff}{}^1\right]+4\left[R_{ff}\right]\left[u_f^1+T_a\right]^3 \qquad (4.6)$$

Using a suitable iteration algorithm the MSC Nastran program obtains satisfactory convergence (if indeed convergence can be achieved). Nastran provides an estimate of the lowest eigenvalue and of the error in the solution after each iteration. Thus, the solution converges finally if there is a result within 80% of the correct temperature, measured on an absolute scale. The user can force convergence, at the expense of extra iterations, by overestimating the temperature.

D. TRANSIENT ANALYSIS

The nonlinear terms permitted in transient heat transfer analysis include radiation and the general purpose nonlinear elements of the program. However nonlinear heat conduction and heat capacity is not supported. The reason is that the computational effort to recalculate the heat conduction and heat capacity matrices at each time step by the finite element method used by NASTRAN is seen to be numerically intensive. The general purpose nonlinear elements can, however, be used to represent nonlinear surface film conduction and other relatively simple nonlinear relationships. The general equation solved in transient analysis has the form

$$\left[K\right]\left\{u\right\}+\left[B\right]\left\{u'\right\}=\left\{P\right\}+\left\{N\right\} \qquad (4.7)$$

The conduction matrix includes linearized radiation terms. It is identical to $\left[K_{ff}^{*}\right]$ given in equation (4.6). The load vector $\{P\}$ may be formed in the same manner as for the steady heat transfer analysis with certain parameters permitted to be functions of time. Also, both the direction and the magnitude of the heat flux are permitted to be functions of time. The user has also available the methods used to prescribe transient loads in structural dynamic analysis. The prescribed temperatures at grid points and the ambient temperature used for film heat transfer are treated in the same manner as prescribed displacements in dynamic analysis.

The program uses an algorithm that has the ability of successfully conducting the following criteria.

- Unconditional stability for linear problems, regardless of the size of time step
- Ability to handle a singular heat capacity matrix
- Good stability for nonlinear problems
- Good efficiency
- High accuracy

THIS PAGE INTENTIONALLY LEFT BLANK

V. MODELING

A. SIMULATION OF A SATELLITE MODEL

1. Quickbird Characteristics

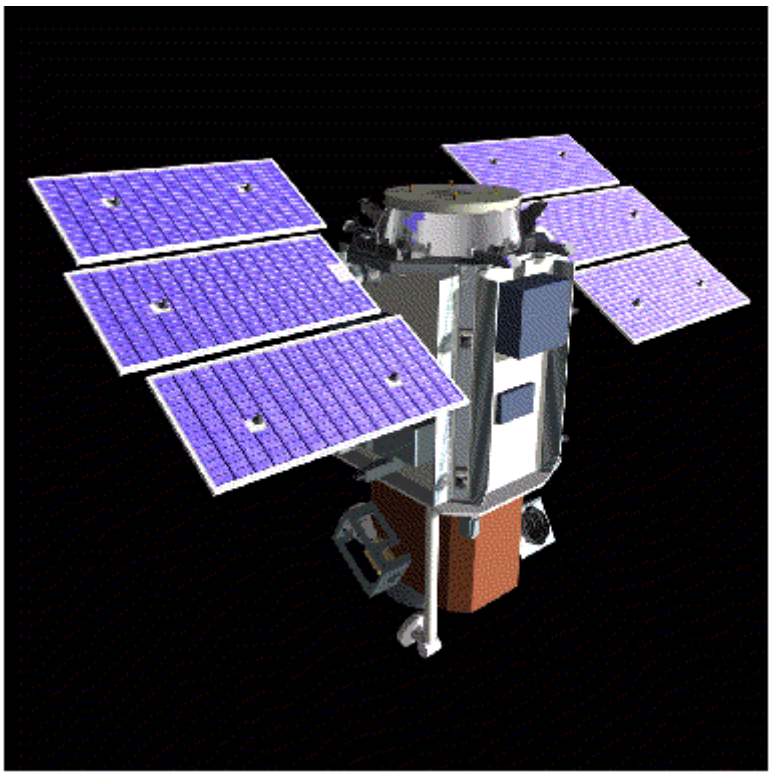

Figure 24. Quickbird Spacecraft [Ref. 1]

The Quickbird [Ref. 1] satellite is the candidate satellite that has been chosen as the prototype, in order to create a realistic satellite model and investigate the behavior. Also applying the methodology to such space assets as this satellite is of value to the international community involved in security and safety. It is a LEO satellite stationed at an altitude of about 460 km. The prime contract for this satellite is Ball Aerospace Corporation. As shown in Figure 24, it has the following characteristics:

- Mass at Launch: 1028 kg
- Payload Mass: 300 kg

- Dimensions: 3 x 1.6 x 1.6 m
- Solar Arrays: 5.2 m
- Solar Array Area: 3.7 m^2
- S/C bus height: 3.04 m

The satellite is divided into two main parts, the satellite bus and the payload. It also has two cameras for reconnaissance purposes and antennas for telemetry and tracking, as well as, communication purposes. It may be observed from Figure 24 that solar arrays are divided into three different parts on each side allowing the spacecraft to orient itself for optimum sun coverage. Finally, it is to be mentioned that the Quickbird satellite was chosen to be the prototype model, functioning as a reconnaissance satellite fling in LEO and are candidate targets for DEW lasers, both for offense and defense applications.

2. Idealized Satellite Model Characteristics

As mentioned earlier, we created a satellite model similar to Quickbird satellite and this is going to be the one that will be studied and analyzed. The model satellite matches on overall dimensions, major components, and overall weight characteristics. The thesis research is focused only on the thermo-mechanical behavior of the external surfaces and propellant tanks. These are the locations we use to assess the survivability and vulnerabilities from a potential laser weapon system. It is assumed that if the external surfaces of a mechanical structure failed under a hard kill mechanism, then the structural integrity of the satellite is compromised and disabled. Also, we consider the possibility that the propellant tanks may be hit and the fuel will explode under specific circumstances which are described later. In Figure 25, we see a depiction of the idealized satellite model created using MSC Patran, which is a part of the MSC Software suite of programs. Patran is a industry popular graphical interface to generate complex structural and geometrical entities and is used widely in the aerospace industry.

The author has named the satellite model “RENIA,” after his wife’s name.

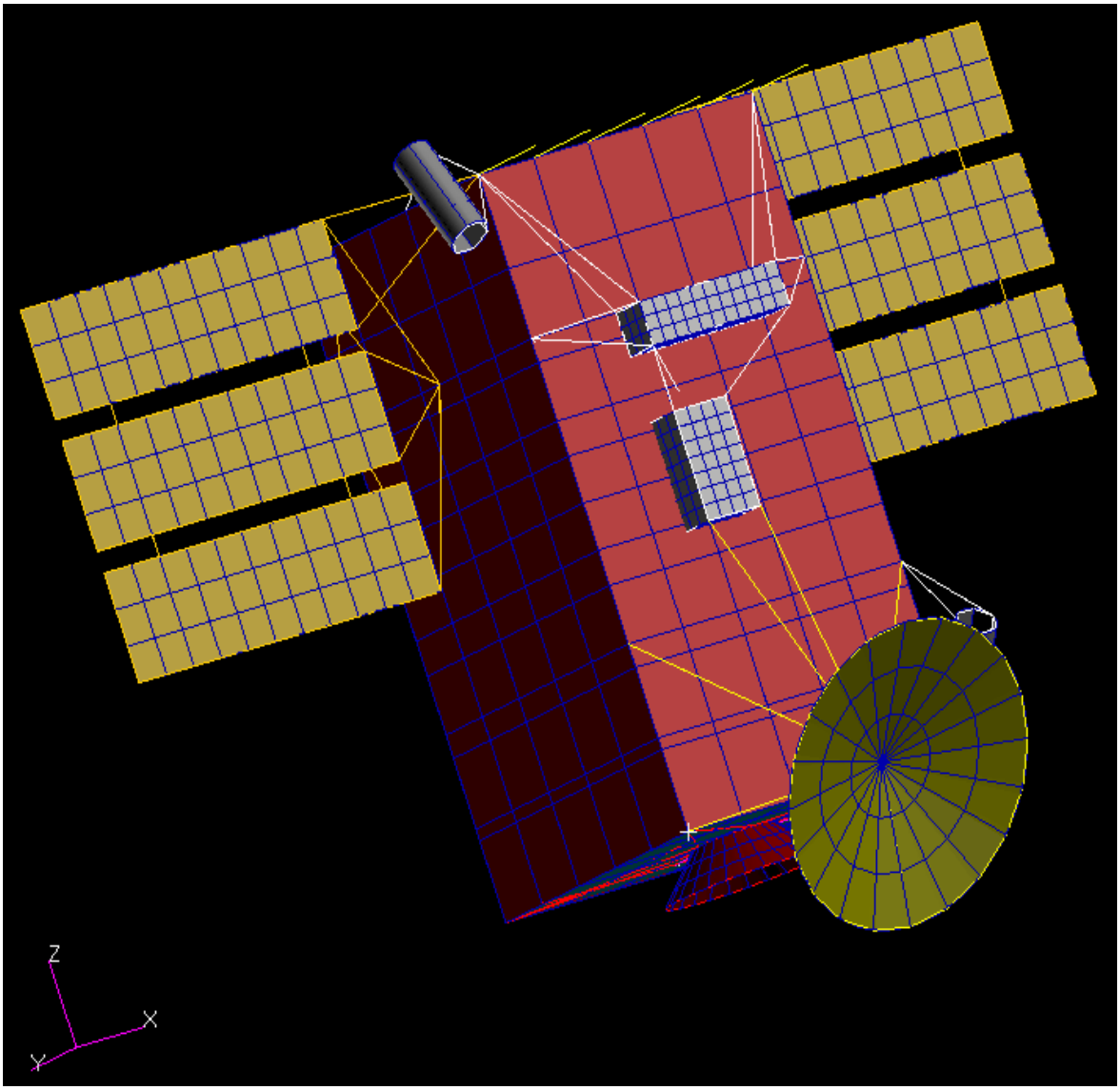

Figure 25. Exact Illustration of the Idealized Satellite Model

The exact characteristics of the model are given as follows:

- Mass at Launch: 1170 kg
- Dimension: 3 x 1.6 x 1.6 m
- Solar Arrays: 5.2 m
- Solar Array Area: 3.7 m^2
- S/C bus height: 3.0 m

Comparing the above model characteristics with the actual Quickbird we can conclude that our model is a good candidate for the space asset risk studies under DEW attack. The small difference in the overall mass does not affect analysis substantially.

Our satellite model consists of the following components as shown in Figure 26:

- Solar Arrays (2)
- Upper Platform, Side Panels, Lower Platform
- Propellant Tanks (4)
- Antenna
- Cameras (2)
- Telemetry Boxes (2)
- Adapter

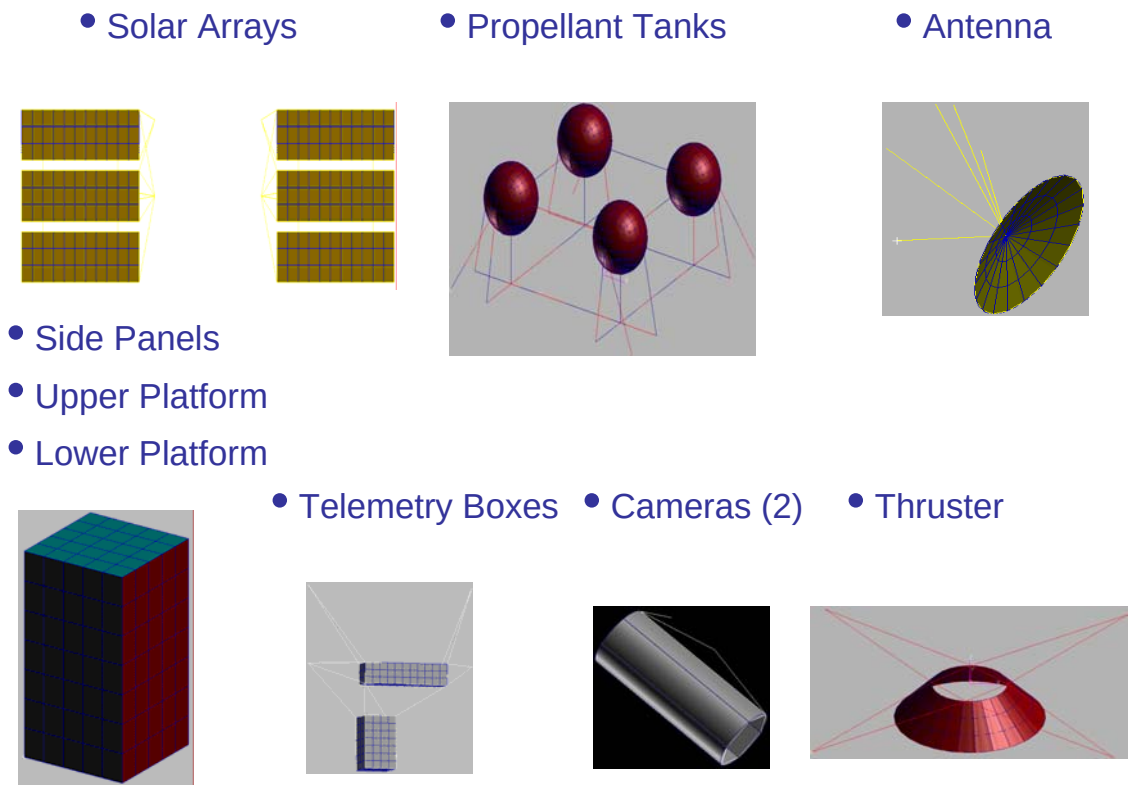

Figure 26. Idealized Satellite Model Components

The solar arrays have been designed to be in six pieces, similar to the configuration of Quickbird satellite. They are attached with the side panels and upper platform with a number of circular hollow bars in such a way that the model is statically viable.

The side panels model the satellite bus and payload and are connected to lower and upper platforms. Also, attached to the lower platform and in the bottom surface there is an attached adapter structure which is connected to the lower platform, the main bus and the propellant tanks. The four propellant tanks are selected to be spherically shaped. We consider them to be located just on top of the adapter and at the bottom part of the spacecraft, keeping the necessary propellant of the satellite mainly for maneuvering purposes.

Additionally, we have designed an antenna, two simple cameras and telemetry boxes located in the places that are shown in Figure 26, giving our satellite the communication, telemetry and tracking capabilities.

In our satellite model we created the components that most typical reconnaissance satellites have in common in order to accomplish their stated missions. We assumed in this research that to disable a satellite on orbit, it is enough to disable or destroy critical components that keep the satellite operational and active through its lifetime. For example, by deforming or destructing the solar arrays, satellite life is rendered non operational due to the inability of power loss and eventual lack of communication with ground receivers.

In Figure 27, we give a wireframe depiction of the satellite model, where propellant tank locations are shown as well as bar elements and joints, and other components may be seen.

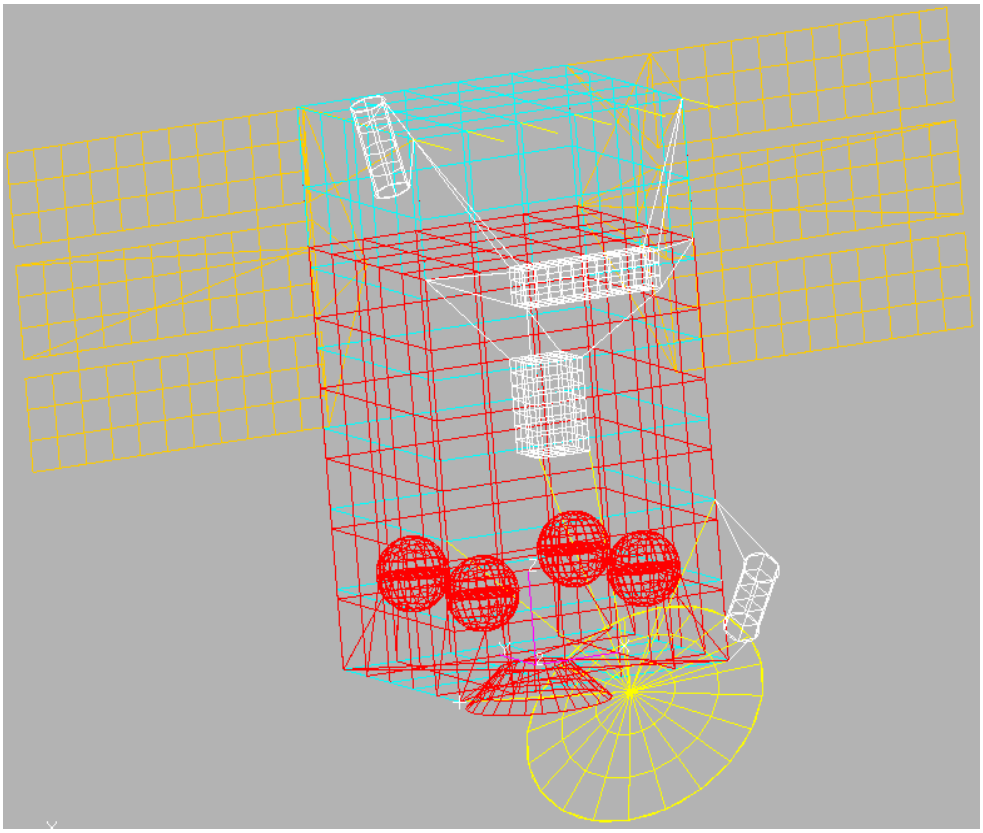

Figure 27. Idealized Satellite Model Wireframe Depiction

B. SIMULATION OF AN ICBM MODEL

1. Taepondong Characteristics

The Intercontinental Ballistic Missile (ICBM) we selected to model is a North Korean Ballistic Missile named Taepondong. This missile is interesting in that it is in production and has very good potential to strike peaceful nations. It is a two stage ICBM with total mass of 33,406 kg and with the following dimensions:

- Stage 1 dimensions: Diameter: 1.80 m. Length 12 m
- Stage 2 dimensions: Diameter: 0.96 m. Length 12m

It consists of stage 1 and stage 2 cylindrical structures, an adapter cone connecting the two stages together, a nose cone with the payload, and two propellant tanks for each stage. Figure 28 depicts the Taepondong characteristics [Ref. 17].

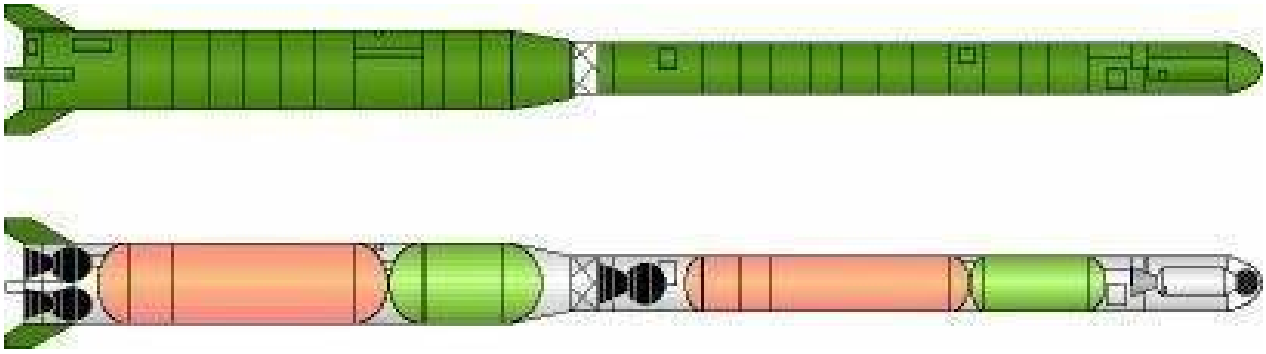

Figure 28. ICBM Taepondong [Ref. 17].

We selected Taepondong ICBM for modeling and simulation analysis as it is a recently designed ballistic missile and also exhibits characteristics of a potential threat to United States and allies. Its typical flight path is shown in Figure 29.

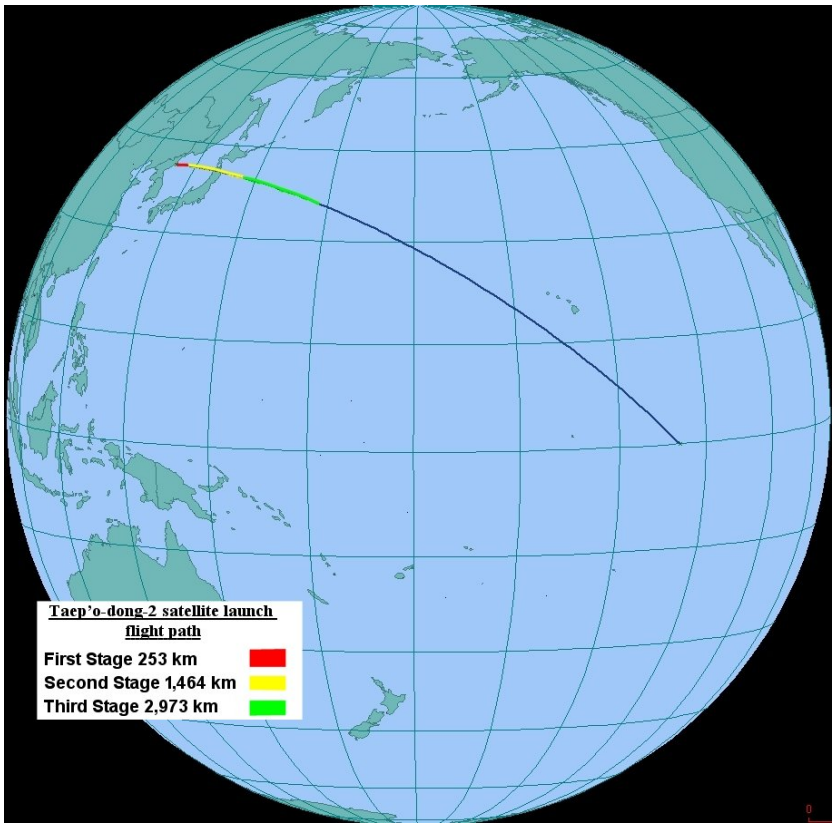

Figure 29. Taepondong Ground Track for Three Different Stages (From [Ref. 16])

2. Idealized ICBM Model Characteristics

The design, modeling and simulation analyses of our model of Taepondong missile is accomplished using MSC software, Patran and Nastran. The resulting model matches closely with the openly available literature of Taepondong missile with a total mass of 32,100 kg. It contains the following components:

- Stage 1 External Cylinder
- Stage 1 Bottom Fuel Tank
- Stage 1 Top Fuel Tank
- Stage 2 External Cylinder
- Stage 2 Bottom Fuel Tank
- Stage 2 Top Fuel Tank
- Adapter
- Nose Cone

In Figure 30, we can see in detail the picture of the above missile components with dimensions and relevant characteristics. The figure shown is not drawn to scale.

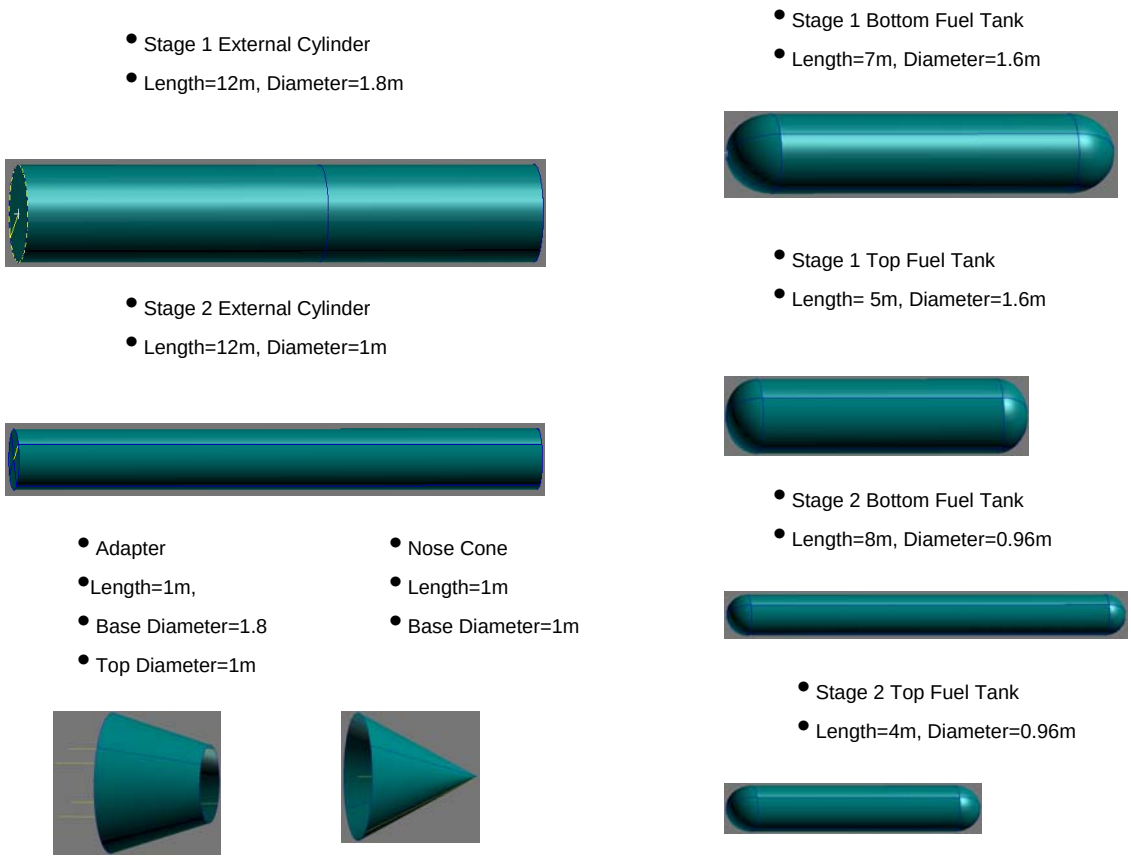

Figure 30. Idealized ICBM Model Components

In Figure 31, we can see the model containing all the above referenced components. The attachments between the different components have been designed using hollow bar elements of approximately one inch (1”) thickness and the model has been validated through modal and static analysis.

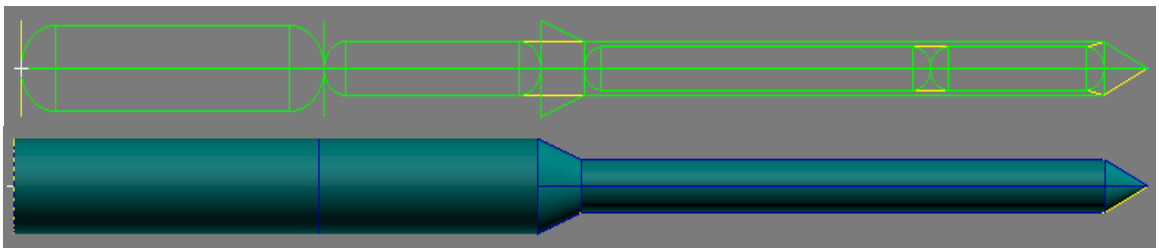

Figure 31. Idealized ICBM Model

THIS PAGE INTENTIONALLY LEFT BLANK

VI. SATELLITE THERMOMECHANICAL ANALYSIS AND RESULTS

A. MODEL DEFINITION

Suitable assumptions should be developed in order to define the parametric design space and obtain reasonable results. It is essential to know the limitations imposed to draw meaningful conclusions from the simulation results.

The problem is considered as a multi-physics thermal and structural problem dealing with thermo-mechanical effects on satellite and ICBM structures. Satellite model contains three different materials, aluminum, titanium and steel used for different components. We simulate the laser thermal energy as heat flux load using conduction and radiation modes of heat transfer but no convective processes is considered.

We performed static and modal analysis of the model in order to verify that it can survive in a real environment using the following constraints:

- X axis: 1 g
- Y axis: 1 g
- Z axis: 10 g

The displacement constraints have been applied in the four corners of the lower and upper platforms, imitating loads encountered in a real launch. Having performed the modal and static analysis, the model adequacy and other initial design parameters were validated.

The finite element model of the satellite which was shown earlier was modeled using different mesh sizes, densities, and element types. A reasonable model satisfying both accuracy and efficiency was selected resulting in the following data for elements and degrees of freedom of the whole model:

- Number of nodes ~ 5,502
- Number of elements ~ 6,420 (Plate/shell elements, beam elements)
- Degrees of freedom ~ 31,419

In the Table 6, we list the components of the satellite and the different materials and thicknesses we have used in our design. Firstly, we have assigned materials to satellite components in accordance with what is currently used and seemed practical. Secondly, two different cases of thicknesses have been selected for the whole satellite model for our study and these are the 1/4" and 1/2" inch panel design, respectively. These two thicknesses selected results in a total mass of satellite model as approximately 1000 kg and 1,300 kg respectively. Our design is observed to be close to the Quickbird characteristics. If we increase the thickness to 1/2", the total mass of the satellite increases to 1,800 kg, which is more than 30 percent of the original Quickbird mass. This design was discarded as being not acceptable. It may also be mentioned that thicknesses up to one half inch is a realistic assumption for satellite design and realistic for our vulnerability and survivability analysis.

Component	Material	Case 1 Thickness (m)	Case 2 Thickness (m)
Antenna	Aluminum	0.01 (1/2")	0.007 (1/4")
Thruster	Titanium	0.01 (1/2")	0.007 (1/4")
Telemetry Boxes	Aluminum	0.01 (1/2")	0.007 (1/4")
Satellite Bus	Aluminum – Steel	0.01 (1/2")	0.007 (1/4")
Cameras	Aluminum	0.01 (1/2")	0.007 (1/4")
Propellant Tanks	Steel - Titanium	0.01 (1/2")	0.007 (1/4")

Table 6. Satellite Component and Assigned Properties

B. MATERIAL CHARACTERISTICS

As we mentioned above, the materials that we used are the most common materials that have been used for years in the aerospace industry for the construction of satellites and space vehicles. These are the aluminum 6061-T6, titanium B120 VCA and steel C-1020. In our model we may incorporate other types of materials in the design simply by specifying their characteristics in model generation. We selected to use the above three materials as they are most commonly used and specifying initial design space.

In the Table 7, we have presented all the required characteristics of the selected design of the satellite components. For each material, there are two columns with characteristics in international units as well as in English units. The most important characteristics which play a major role in the analysis and results are the thermal expansion coefficient, thermal conductivity, minimum yield strength and melting point. The first two parameters influence thermal analysis in our satellite model. The yield strength is utilized in the thermal stress analysis evaluation and failure determination. The melting points will determine the failure modes for the temperature distribution analysis. The rest of the material characteristics are well known and available in materials data hand book and MIL specs handbook.

Material	ALUMINUM 6061-T6		STEEL C-1020		TITANIUM B120 VCA	
Units	SI	EU	SI	EU	SI	EU
Elastic Modulus (E)	7.31e10 Pa	10.5e6 psi	2.03e11 Pa	29e6 psi	1.02e11 Pa	16e6 psi
Poisson Ratio(ν)	0.33		0.313		0.27	
Density (ρ)	2700 kg/m^3	0.101 lbm/in^3	7850 kg/ m^3	0.283 lbm/in^3	4850 kg/ m^3	0.16 lbm/in^3
Thermal Expansion Coefficient, (α)	24.3e-6 m/m ºC		11.34e-6 m/m ºC		9.36e-6 m/m ºC	
Thermal Conductivity (k)	155.8 W/mºC		46.73 W/mºC		7.442 W/mºC	
Minimum Yield Strength	275 MPa	40000 psi	520 MPa	36000 psi	830 MPa	120000 psi
Melting Point	660 °C	1220 ºF	1375 ºC	2507 ºF	1675 ºC	3047 ºF

Table 7. Material Characteristics

C. LOADS / BOUNDARY CONDITIONS

In this section, we describe specified loads and boundary conditions, which are the imposed constraint factors to our problem. It is an essential part of the pre-processing segment where in realistic operating environmental conditions are imposed.

An important factor that drives our analysis is heat flux, the laser thermal energy impacting the satellite. We have selected the following cases where heat flux is specified as absolute input to the satellite model:

- 100 W/m²
- 1000 W/m²
- 10e4 W/m²
- 10e6 W/m²
- 10e9 W/m²
- 10e11 W/m²

These different amounts of heat flux will be applied to specific selected areas on our satellite and allow both radiation and conduction modes of heat dissipation. The heat flux is applied as directional heat load, and in particular, it is applied to the whole surface as a normal vector. In Figure 32, we show the heat flux applied to solar arrays (top surface). Also, in Figure 33, the heat flux is applied on the satellite bus (left side), but only in the left side panel. These two areas are only representative application areas we selected to apply heat flux to assess the survivability and vulnerability analysis.

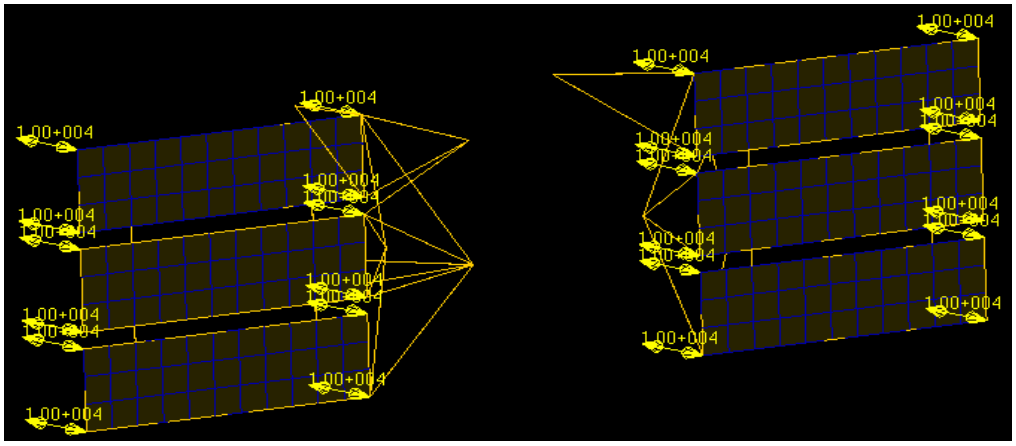

Figure 32. Application of Heat Flux in Solar Arrays (Top Surface)

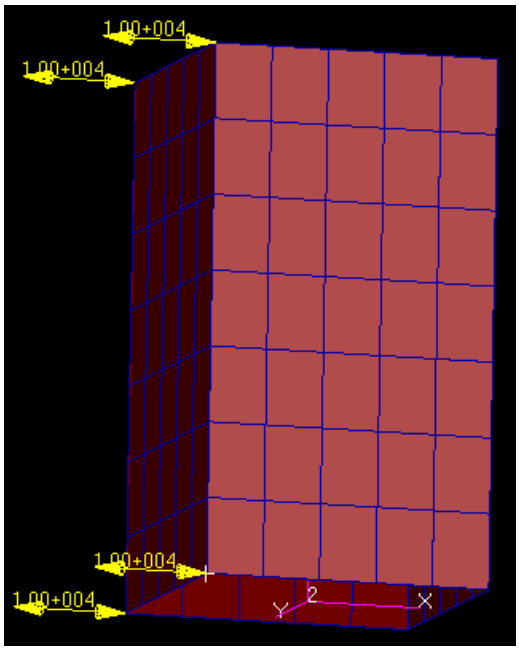

Figure 33. Application of Heat Flux in Satellite Bus (Left Side)

To accommodate radiation heat transfer, the following parameters are prescribed:

- Absorptivity: 0.5
- Emmisivity: 0.5
- Ambient Temperature: 20 °C
- View Factor: 1

We have chosen absorptivity and emissivity of 0.5, assuming that in a general case scenario in space, this value is a mean value for a typical satellite. Moreover, ambient temperature in space is between -70°C and 70 °C. For that reason we selected a mean ambient temperature of 20°C. The effect of the ambient temperature on our analysis was observed to be minimal for a range of 70 and -40 degrees Celsius ambient temperature. For example, the differences were in the order of 7 degrees Celsius for the temperature distribution analysis. It is assumed that this temperature does not influence appreciably the thermo-mechanical deformation and stress analysis. Finally, the view factor has been selected to be 1 resulting in a worst case scenario for the exchange of

radiation between satellite surfaces. Figure 34 shows the radiation vector (in cyan color) applied normal to the surface of the whole satellite bus.

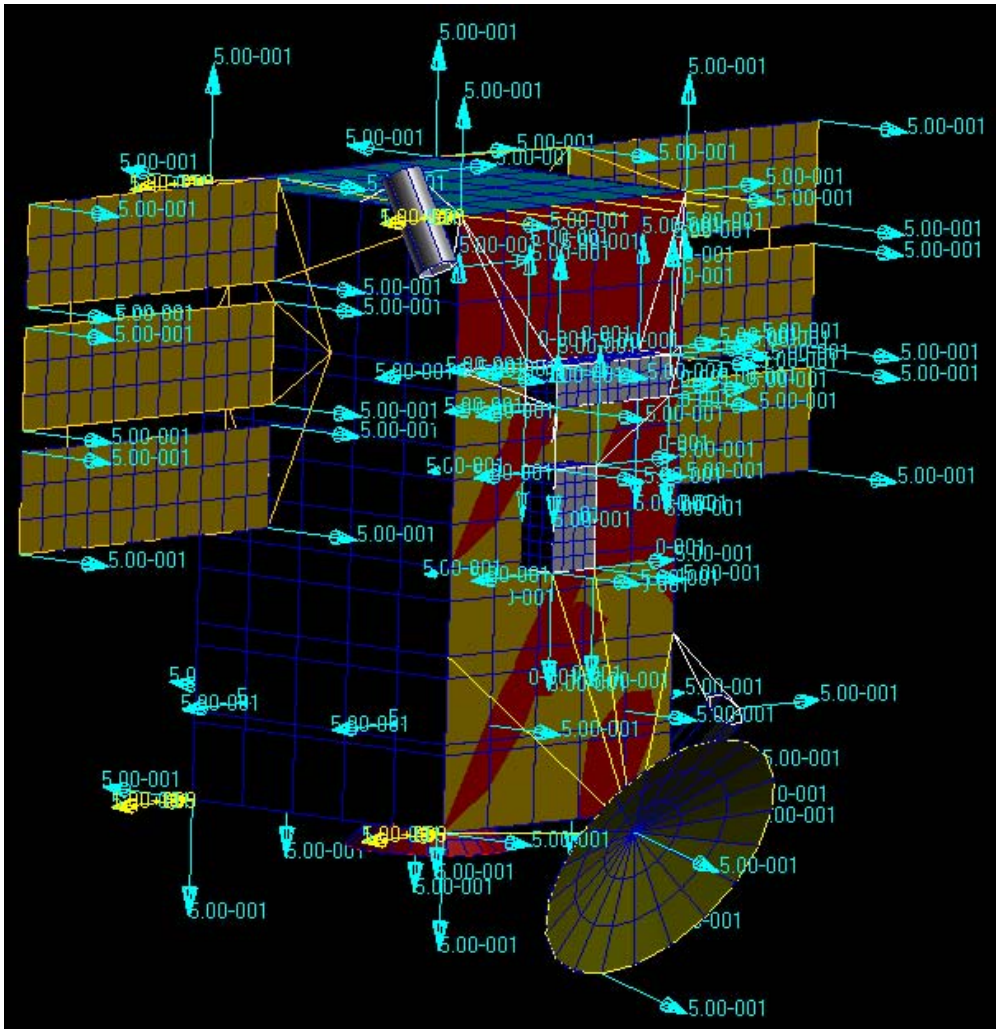

Figure 34. Radiation Parameters for the Whole Satellite Bus

D. FAILURE MODES / CRITERIA

In this section, we define failure modes and related criteria for our satellite model failure. These criteria help in assessing the survivability and vulnerabilities and estimate of the hard/soft kill. Specifically, these failure modes are as follows:

- **deformations** greater than the original thickness
- **temperatures** greater than the melting point of the materials

- **stresses** greater than the yield stress of the materials
- **deformations, temperatures, stresses and other specified requirements** greater than desired mission critical parameters

Our satellite model is considered failed or disabled when the above criteria is satisfied and conclude that satellite is sufficiently damaged and incapacitated. Even if the satellite survives it will not be able to be used for critical missions and download valuable data to ground stations.

Additional failure modes and criteria can be formulated to extend the analysis and risk mitigation studies to include difference scenarios and mission objectives.

E. STEADY STATE ANALYSIS AND RESULTS

1. Thermal Analysis and Results

After we expose the satellite with different energy levels, we run the simulation by analysis and compute initial temperature distributions over the surfaces of the satellite model. This is essentially the first step and basically it gives us the foundation for the rest of the analysis. Applied heat flux and radiation parameters are translated into temperatures through the selected materials, as it was discussed extensively in Chapter IV, and shows temperature increase due to the incoming laser energy. Results for two different cases are presented, one for solar arrays and the other for the side panels of the satellite model. The thicknesses selected for these cases are 0.01 m (1/2") and 0.007 m (1/4") respectively. The selected material for these two surfaces is aluminum. There are three parameters to model in each case- thicknesses, representative area of exposure and input laser thermal energy. The total number of cases that we simulate in this study is twenty four (24). In Table 8 we give a summary of the 24 different problems we solved in order to study the thermo mechanical behavior of our satellite model.

Representative Areas	Solar Arrays	Solar Arrays	Side Panels	Side Panels	
Thicknesses	0.007 (1/4")	0.01 (1/2")	0.007 (1/4")	0.01 (1/2")	
Heat Fluxes	100 W/m²	100 W/m²	100 W/m²	100 W/m²	
	1000 W/m²	1000 W/m²	1000 W/m²	1000 W/m²	
	10e4 W/m²	10e4 W/m²	10e4 W/m²	10e4 W/m²	
	10e6 W/m²	10e6 W/m²	10e6 W/m²	10e6 W/m²	
	10e9 W/m²	10e9 W/m²	10e9 W/m²	10e9 W/m²	
	10e11 W/m²	10e11 W/m²	10e11 W/m²	10e11 W/m²	
Total Simulation Cases	6	6	6	6	24

Table 8. Summary of Simulation Cases on Satellite Model

In Table 7 we give the results of case 1_1 in which solar arrays are hit with six different levels of heat flux, the material being aluminum and with the thicknesses 0.007m (1/4") and 0.01m (1/2") respectively. For each heat flux level, we obtain a temperature distribution over the satellite model. As mentioned earlier, in accordance with our failure modes and criteria, if temperature is higher than the melting point temperature of the material, in this case aluminum, then the satellite component is said to have failed and we can say safely that our goal to hard kill the satellite has been accomplished completely. Cells that have been marked red indicate that the computed temperature is higher than the melting point temperature of the material resulting in a failed satellite part. In case 1_1 (Table 9), when the heat flux reaches 10e6 W/m² the temperature rises to 3370 degrees Celsius, which indicates that solar arrays have failed. If we increase the heat flux level up to 10e9 W/m², which is approximately the estimated published damaged criterion of 10e4 W/cm², we observe that all the satellite components

have failed and the resulting temperatures are extremely high. The temperatures reach magnitudes of 10e5 degrees Celsius resulting in the satellite melt down and mission for hard kill accomplished totally.

Heat Flux Parts	1000 W/m²	10e4 W/m²	10e6 W/m²	10e9 W/m² (3.125% load)	10e11 W/m² (3.125% load)
Antenna	22	27.3	86.3	249	1.19e5
Camera	21.9	26.9	83.3	223	1.13e5
Lower Platform	20	20.1	20.5	42.9	1.38e3
Propellant Tanks	20	20.1	20.5	18.1	1.38e3
Side Panels	23.9	34	142	735	2.38e5
Solar Arrays	125	382	3370	2.56e4	5.92e6
Telemetry Boxes	22	27.3	86.3	249	1.19e5
Thruster	20	20.1	20.5	20	1.38e3
Upper Platform	23.9	34	142	735	2.3e5

Table 9. Satellite Components Temperature Distribution (°C) for Case 1_1: Solar Arrays Heat Flux Application, Aluminum material and Thickness 0.007 m

In Table 10, the thickness is increased to one inch and the results shows that even though the solar arrays have failed when we applied the same amount of heat flux (10e6 W/m²) as before, the temperature is not as high as the previous case. It is almost three times less if we compare the resulting peak temperatures dropping to 1,230 degrees from 3,370 degrees Celsius. This is reasonable as the satellite is two times thicker than before and more capacity to absorb and dissipate incoming laser energy. Similar results were obtained for every applied heat flux level greater than 10e6 W/m^2 resulting in the failure of the satellite components.

Heat Flux Parts	1000 W/m²	10e4 W/m²	10e6 W/m²	10e9 W/m² (3.125% load)	10e11 W/m² (3.125 % load)
Antenna	23.1	31.3	518	518	1.81e5
Camera	22.9	30.6	470	470	1.7e5
Lower Platform	20.1	20.2	208	208	5.18e3
Propellant Tanks	20.1	20.1	129	129	5.18e3
Side Panels	26	41.4	1230	1230	3.43e5
Solar Arrays	124	382	2530	2530	5.86e6
Telemetry Boxes	23.1	31.3	518	518	1.81e5
Thruster	20.1	20.2	20	20	5.18e3
Upper Platform	26	41.4	1230	1230	3.43e5

Table 10. Satellite Parts Temperature Distribution (°C) for Case 1_2: Solar Arrays Heat Flux Application, Aluminum and Thickness 0.01 m

In the next case, we apply different heat flux levels to the left side panel of the satellite bus instead of the solar arrays. The results are follow the same pattern as above for cases 2_1 and 2_2, as shown in Tables 9 and 10 respectively. The temperatures rise above the melting points and reach critical points when we apply heat flux of 10e6 W/m². Although the temperatures are a little bit lower here, in comparison with solar arrays, it is obvious though that satellite parts have failed and the satellite model has been degraded seriously.

Heat Flux Parts	100 W/m²	1000 W/m²	10e4 W/m²	10e6 W/m²	10e9 W/m² (12.5 % load)	10e11 W/m² (3.125 % load)
Antenna	26.8	74.5	262	1440	6020	6.01e6
Camera	26.4	72.5	267	1500	6260	5.63e6
Lower Platform	25.7	66.4	236	1330	5630	5.02e6
Propellant Tanks	25.7	62.8	225	1333	2590	4.64e6
Side Panels	31.3	108	375	1780	7220	9.75e6
Solar Arrays	25.1	61.2	215	1330	6960	4.53e6
Telemetry Boxes	24.8	59.3	209	1290	5580	4.31e6
Thruster	24.2	55.6	188	1120	4890	3.95e6
Upper Platform	26.5	73.1	268	1500	6260	5.7e6

Table 11. Satellite Parts Temperature Distribution (°C) for Case 2_1: Side Panels Heat Flux Application, Aluminum and Thickness 0.007 m

Heat Flux Parts	100 W/m²	1000 W/m²	10e4 W/m²	10e6 W/m²	10e9 W/m² (18.75 % load)
Antenna	26.3	72.1	259	1430	6980
Camera	25.9	69.3	259	1490	7220
Lower Platform	25.4	64.8	234	1330	6510
Propellant Tanks	25	61.7	223	1320	6500
Side Panels	30	102	370	1780	8360
Solar Arrays	24.8	59.6	211	1290	6400
Telemetry Boxes	24.5	57.3	202	1280	6400
Thruster	24.3	55.7	190	1120	5640
Upper Platform	26	70	262	1490	7220

Table 12. Satellite Components Temperature Distribution (°C) for Case 2_2: Side Panels Heat Flux Application, Material Aluminum, and Thickness 0.01 m

The results presented in the Tables 8 through 12 are condensed in a graphical form using the Excel software in Figure 35. This graph reveals more intuitively that temperatures are very high on the surfaces where the incoming heat flux is applied resulting from the nonlinear analysis that program has performed. Another observation is that the temperature distribution is very high as we reach the heat flux level of 10e6 W/m². In Figure 35 we have plotted all the satellite component surfaces without the solar arrays, in order to show that the temperature difference between all other satellite parts except the solar arrays is very small. In Figure 36 we show the solar arrays temperature distribution and the huge temperature difference is observed. It has to be noted that heat flux higher than 10e6 W/m² does not result in failure of all the satellite components. It

simply means that even though everything has failed above this heat flux level, the temperature distribution differences are huge between the representative application areas and the surrounding areas of the satellite model. This is logical and gives us the understanding that if a satellite fails when exposed to an energy level higher that the critical level of 10e6 W/m² and the satellite is disabled and useless through the rest of its lifetime.

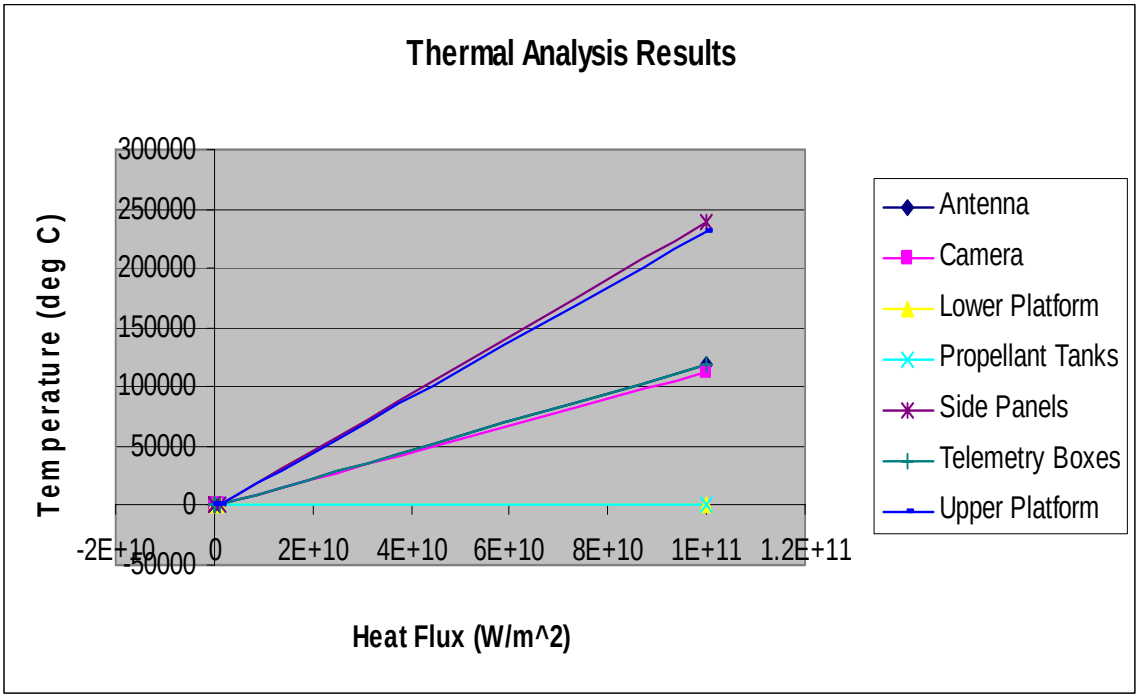

Figure 35. Temperature Distribution vs. Heat Flux in Satellite Parts for Case 1_1 (Without Solar Arrays Representation)

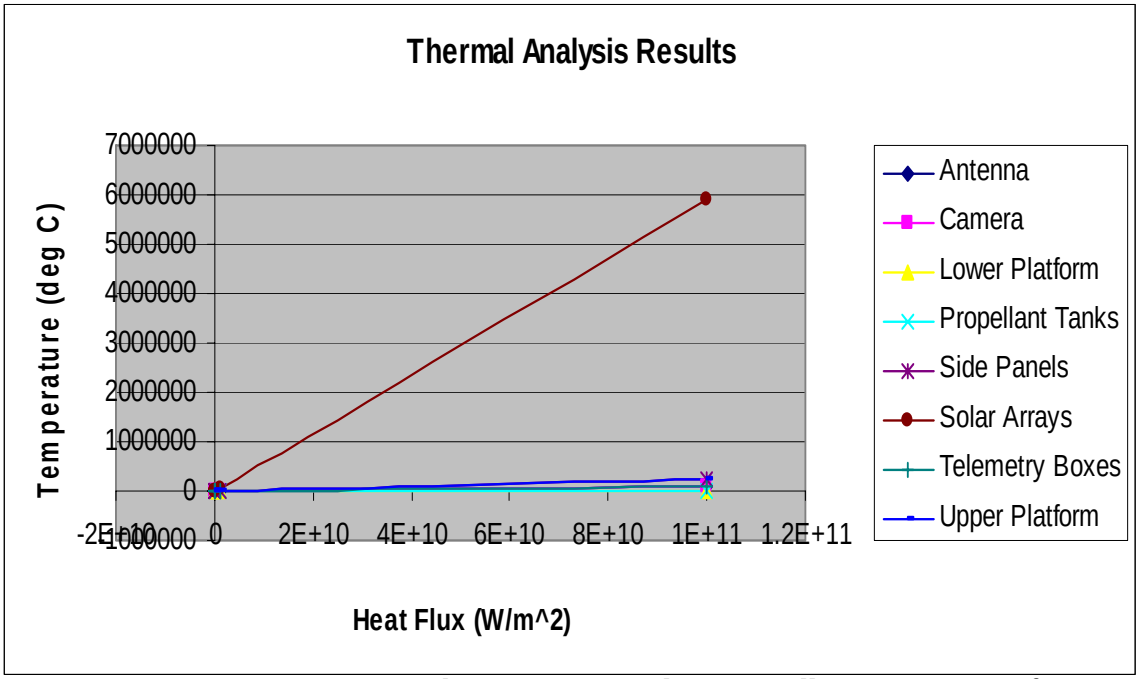

Figure 36. Temperature Distribution vs. Heat Flux in Satellite Components for Case 1_1 (With Solar Arrays Representation)

In Figures 37 and 38 we show the contour plots of the temperature distribution on the satellite with applied heat flux on the representative areas (side panels and solar arrays). As may be observed, the locations that have been hit with the laser energy are red in color and the temperatures are low (blue and white areas) at locations away from the points of heat flux application due to the design of material conduction and radiation parameters. The locations that are depicted as red are indicates satellite component failure.

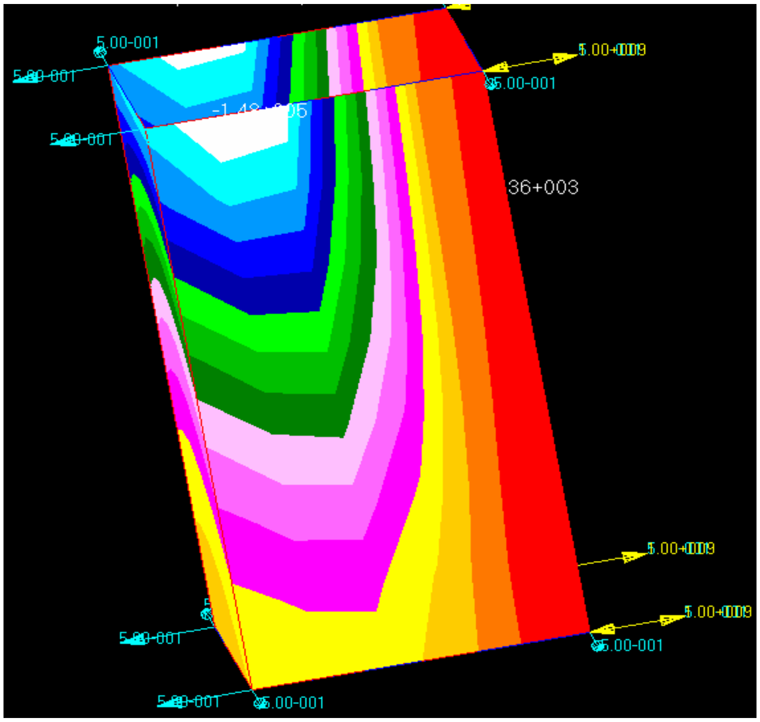

Figure 37. Temperature Distribution in Satellite Side Bus (Thickness 0.01 m, Heat Flux 10e9 W/m²)

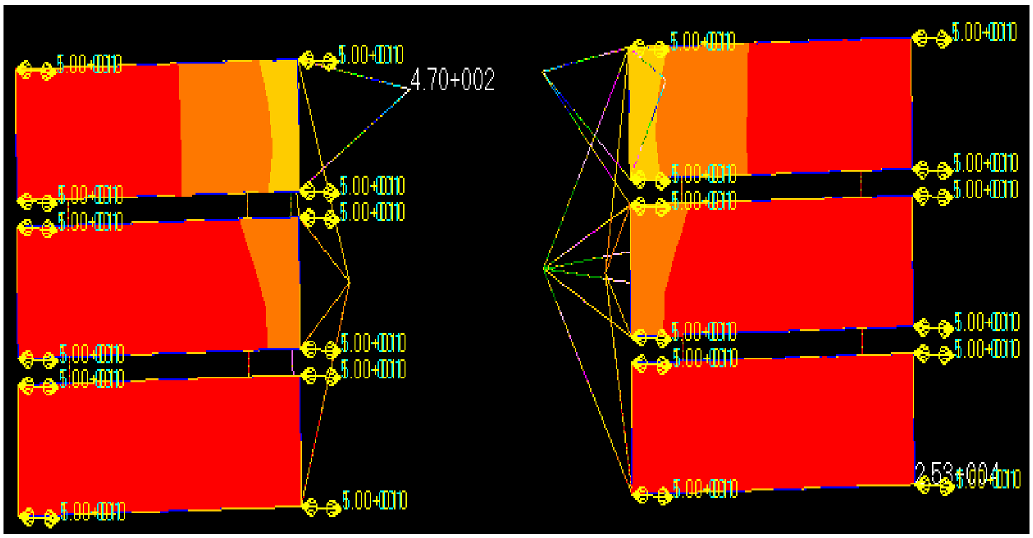

Figure 38. Temperature Distribution in Satellite Solar Arrays (Thickness 0.01 m, Heat Flux 10e9 W/m²)

2. Structural Analysis and Results

In order to study the structural deformation and thermal stress computation, the first step is to compute the temperature distribution on the surface for the given thermal impact. After computing the temperature distribution on the whole satellite model, we use these temperatures as inputs and study temperatures effects on the satellite components from a structural point of view. That is, deformations of the satellite model and their effect on the criticality of the associated structural stiffness. The results of the thermo-mechanical analysis are presented in the following Tables cases 1_1 through 2_2 and provide some very interesting information.

Table 13 shows that for applied heat flux of 1000 W/m², the antenna, solar arrays, and telemetry boxes have a deformation nearly two times the original thickness. Based on the failure mode established, the satellite has failed structurally on application of 1000 W/m² incoming laser thermal energy. This result shows that with this very small amount of energy a satellite on orbit is subject to critical design failure a loss of space asset/infrastructure.

Heat Flux Parts	1000 W/m²	10e4 W/m²	10e6 W/m²	10e9 W/m² (3.125 % load)	10e11 W/m² (3.125 % load)
Antenna	8.66e-3	9.09e-3	1.46e-2	5.81e-2	1.56
Camera	1.42e-3	1.47e-3	2.46e-3	1.19e-2	3.58
Lower Platform	8.64e-4	9.23e-4	1.7e-3	2.48e-3	2.07
Propellant Tanks	2.27e-3	2.48e-3	4.66e-3	2.12e-3	5.17
Side Panels	8.64e-4	9.23e-4	2.22e-3	1.3e-2	3.75
Solar Arrays	2.99e-2	8.84e-2	7.84e-1	5.21	1210
Telemetry Boxes	8.93e-3	9.28e-3	1.46e-2	7.57e-2	16.2
Thruster	7.47e-4	9.22e-4	2.81e-3	4.22e-3	4.28
Upper Platform	8.68e-4	8.45e-4	1.46e-3	1.28e-2	2.3

Table 13. Satellite Parts Deformations for Case 1_1: Solar Arrays Heat Flux Application, Material-Aluminum and Thickness-0.007 m

In Table 14, we show deformations for the components of the satellite model, with the thickness being one inch. The failure point here also starts at 1000 W/m², but the results are an order of magnitude less. This result leads us to into the same deduction, that 1000 W/m² adequate energy to produce lethal effects on a real satellite.

Heat Flux Parts	100 W/m²	1000 W/m²	10e4 W/m²	10e6 W/m²	10e9 W/m² (3.125 % load)	10e11 W/m² (3.125 % load)
Antenna	7.72e-3	8e-3	8.8e-3	1.91e-2	6.42e-2	31.3
Camera	1.7e-3	1.73e-3	1.85e-3	3.45e-3	1.93e-2	4.16
Lower Platform	8.46e-4	8.78e-4	9.82e-4	2.27e-3	9.93e-3	1.55
Propellant Tanks	2.13e-3	2.24e-3	2.56e-3	5.91e-3	1.13e-2	3.8
Side Panels	8.63e-4	8.78e-4	9.82e-4	3.25e-3	2.28e-2	3.59
Solar Arrays	7.17e-3	2.2e-2	7.07e-2	6.83e-1	3.88	899
Telemetry Boxes	8e-3	8.23e-3	8.91e-3	1.91e-2	1.2e-1	31.3
Thruster	8.33e-4	9.31e-4	1.23e-3	4.34e-3	2.01e-2	3.38
Upper Platform	8.64e-4	8.65e-4	8.88e-4	2.07e-3	1.84e-2	2.58

Table 14. Deformations of Satellite Components for Case 1_2: Solar Arrays Heat Flux Application, Material-Aluminum and Thickness-0.01 m

Tables 15 and 16 present results of the heat flux applied to areas on the side panel. The results show that the satellite model has failed on application of 100 W/m². It is very interesting that with this small amount of energy substantial satellite damage is accomplished. This result assumes importance considering that commercial lasers are available to deliver this amount of energy on a low earth orbit satellite and even for satellites in higher altitudes. There is no need to refer in higher amounts of applied heat flux. The results shown in the following tables give deformations in the order of meters, implying that the satellite undergoes large deformations on orbit. Another noteworthy point is that the above referenced temperatures and deformations would result in total failure of propellant tanks and associated disability.

Heat Flux / Parts	100 W/m²	1000 W/m²	10e4 W/m²	10e6 W/m²	10e9 W/m² (3.125 % load)
Antenna	8.57e-3	1.08e-2	2.32e-2	1.11e-1	4.51e-1
Camera	1.51e-3	2.92e-3	1.07e-2	6.16e-2	2.58e-1
Lower Platform	1.01e-3	2.73e-3	9.59e-3	4.82e-2	1.97e-1
Propellant Tanks	2.46e-3	4.56e-3	1.31e-2	5.94e-2	2.55e-1
Side Panels	1.02e-3	2.79e-3	9.59e-3	4.82e-2	1.97e-1
Solar Arrays	7.47e-3	9.08e-3	2.41e-2	1.5e-1	1.49
Telemetry Boxes	8.85e-3	9.49e-3	1.42e-2	5.75e-2	2.06e-1
Thruster	8.53e-4	2.13e-3	6.88e-3	3.17e-2	1.23e-1
Upper Platform	1.06e-3	2.68e-3	9.25e-3	4.55e-2	1.84e-1

Table 15. Satellite Components Deformations for Case 2_1: Side Panels Heat Flux Application, Material-Aluminum and Thickness-0.007 m

Heat Flux Parts	100 W/m²	1000 W/m²	10e4 W/m²	10e6 W/m²	10e9 W/m² (3.125 % load)
Antenna	7.8e-3	1.06e-2	2.34e-2	1.1e-1	7.93
Camera	1.83e-3	2.97e-3	1.04e-2	6.08e-2	3.32
Lower Platform	9.97e-4	2.61e-3	9.42e-3	4.83e-2	2.33
Propellant Tanks	2.36e-3	4.39e-3	1.29e-2	5.85e-2	4.51
Side Panels	1e-3	2.68e-3	9.42e-3	4.83e-2	4.51
Solar Arrays	4.96e-3	7.73e-3	2.45e-2	1.54e-1	13.9
Telemetry Boxes	8.08e-3	8.99e-3	1.37e-2	5.19e-2	2.24
Thruster	1e-3	2.41e-3	7.91e-3	3.7e-2	2.89
Upper Platform	1.01e-3	2.58e-3	9.17e-3	4.57e-2	4.51

Table 16. Satellite Components Deformations for Case 2_2: Side Panels Heat Flux Application, Material-Aluminum and Thickness-0.01 m

In the Figures 39 and 40 we give a graphical representation of the deformation results with and without solar arrays surfaces, due to the huge difference in the amount of deformations produced on solar arrays and on the other surfaces of the satellite model. The results are similar for the side panels and are not included in this report.

The deformation differences between solar arrays and all the other parts of the satellite model are seen to be very large. The failures in the satellite are two to three times larger in the representative areas where the heat flux is applied.

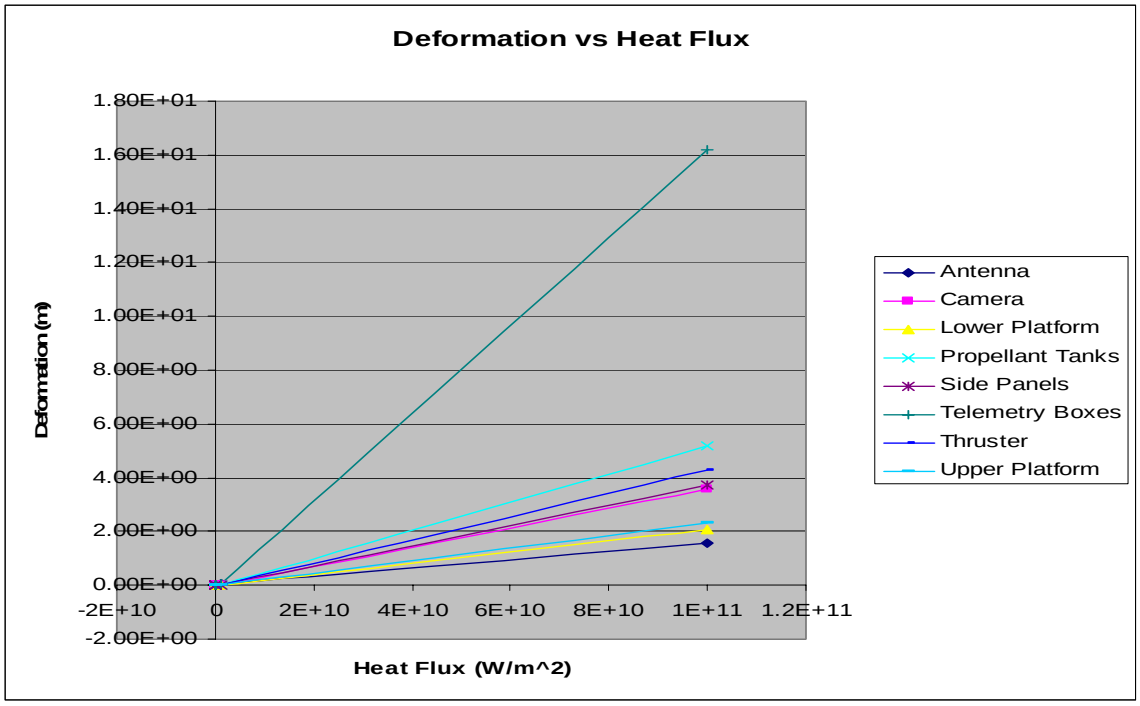

Figure 39. Deformation vs. Heat Flux in Satellite Parts for Case 1_1 (Without Solar Arrays Representation)

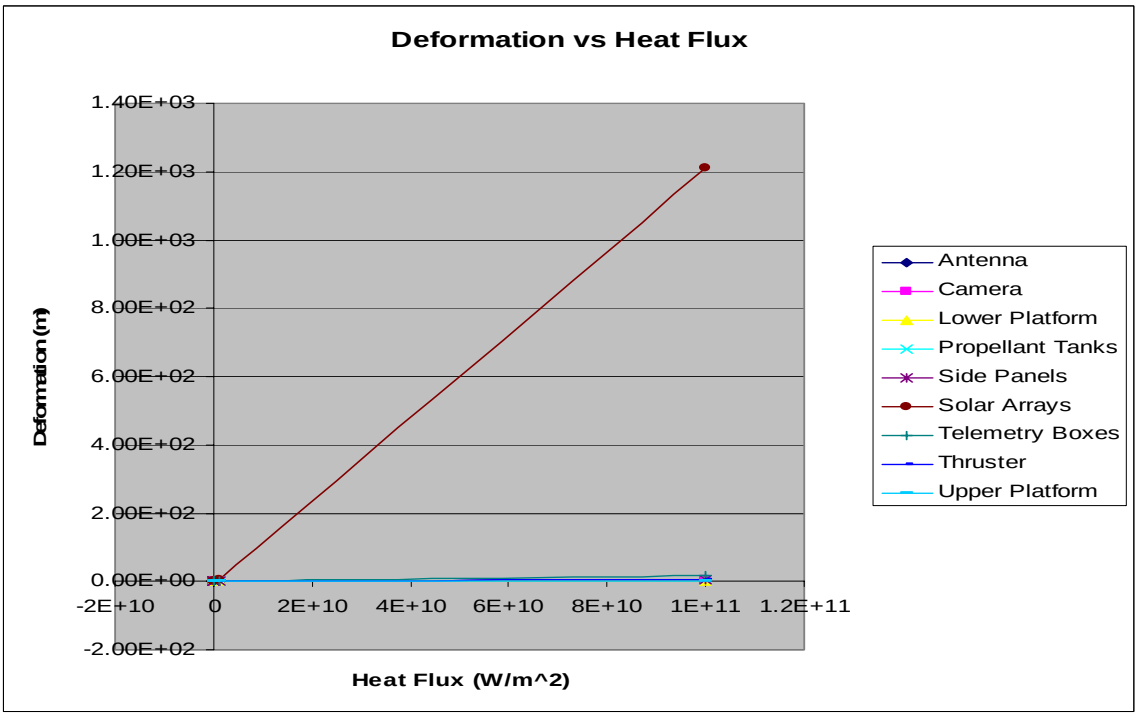

Figure 40. Deformation vs. Heat Flux in Satellite Parts for Case 1_1 (With Solar Arrays Representation)

In Figures 41 and 42 we show representations of the deformations on satellite side panels and solar arrays. We can note the change in the shape of the satellite bus and the solar arrays which is very damaging for the functionality of typical satellites on orbit. The deformations reveal typical outcomes of applying the indicated amount of laser heat flux to satellites on orbit.

Figure 41. Deformation of 7.47e-3 m (FAILURE) in Satellite Side Panels (Thickness 0.007 m, Applied Heat Flux 1000 W/ m^2)

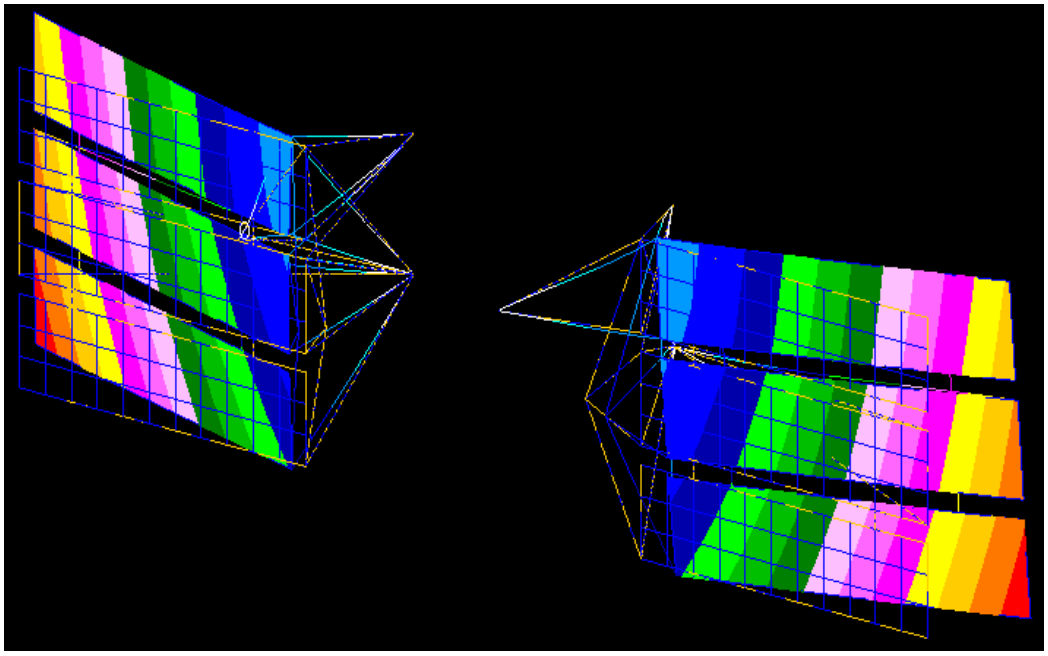

Figure 42. Deformation of 2.99e-2 m (FAILURE) in Satellite Solar Arrays (Thickness 0.007 m, Applied Heat Flux 1000 W/ m²)

3. Stress Analysis and Results

In conjunction with the structural analysis, we obtain the corresponding thermal stresses on satellite surfaces due to the incoming laser energy. Stresses are the third defined parameter in our failure modes and criteria hypothesis. We consider that the satellite structure has failed functionally when stresses are greater than the yield strength of the selected material, as plastic deformation ensues thereafter.

In the Tables 17 through 20 the values of stresses for the different case scenarios, on the satellite parts, have been shown. The red areas on the figures indicate failure areas. We notice that for applied heat fluxes greater than 10e9 W/m², the components have stresses greater than the yield stress of the materials. It is to be noted that in these areas the satellite cannot withstand the applied thermal loads resulting in larger plastic deformations or disintegrate entirely. This result of producing stresses higher than the yield stress of the material is yet another important failure mode rendering the satellite useless.

Heat Flux Parts	1000 W/m²	10e4 W/m²	10e6 W/m²	10e9 W/m² (3.125 % load)	10e11 W/m² (3.125 % load)
Antenna	2.38e8	2.71e8	7.07e8	1.54e9	9.23e11
Camera	2.38e8	2.71e8	7.07e8	1.54e9	9.23e11
Lower Platform	2.38e8	2.43e8	3.15e8	1.07e9	3.49e11
Propellant Tanks	2.38e8	2.43e8	3.15e8	1.07e9	3.49e11
Side Panels	2.38e8	2.71e8	7.07e8	2.25e9	9.37e11
Solar Arrays	2.33e8	2.71e8	7.27e8	1.41e10	3.28e12
Telemetry Boxes	2.38e8	2.71e8	3.15e8	1.54e9	9.23e11
Thruster	2.38e8	2.43e8	3.15e8	1.07e9	3.49e11
Upper Platform	2.33e8	2.71e8	7.07e8	2.25e9	9.37e11

Table 17. Satellite Parts Stresses for Case 1_1: Solar Arrays Heat Flux Application, Material-Aluminum and Thickness-0.007 m

Heat Flux Parts	100 W/m²	1000 W/m²	10e4 W/m²	10e6 W/m²	10e9 W/m² (3.125 % load)	10e11 W/m² (3.125 % load)
Antenna	2.38e8	2.41e8	3.01e8	9.74e8	3.6e9	1.12e12
Camera	2.38e8	2.41e8	3.01e8	9.74e8	3.6e9	1.12e12
Lower Platform	2.38e8	2.41e8	2.49e8	4.23e8	2.84e9	4.38e11
Propellant Tanks	2.38e8	2.41e8	2.49e8	4.23e8	2.84e9	4.38e11
Side Panels	2.38e8	2.41e8	3.01e8	9.74e8	4.31e9	1.12e12
Solar Arrays	2.21e8	2.40e8	3.01e8	1.06e9	2.16e10	5.08e12
Telemetry Boxes	2.21e8	2.40e8	3.01e8	9.74e8	3.6e9	1.12e12
Thruster	2.38e8	2.41e8	2.49e8	4.23e8	2.84e9	4.38e12
Upper Platform	2.21e8	2.40e8	3.01e8	9.74e8	4.31e9	1.12e12

Table 18. Satellite Parts Stresses for Case 1_2: Solar Arrays Heat Flux Application, Material-Aluminum and Thickness-0.01 m

The results shown in the Tables 17, 18 and 19, 20 are for different representative areas of heat application. In the first group of tables, the solar arrays have been hit with the heat flux, whereas in the second group of tables the representative application area of the heat flux is side panels of the satellite bus. The results are quite similar and a flux input value of 10e9 W/m² cause the critical failure for both of the cases.

Heat Flux Parts	100 W/m²	1000 W/m²	10e4 W/m²	10e6 W/m²	10e9 W/m² (3.125 % load)
Antenna	2.67e8	6.29e8	2.15e9	1.22e10	5.12e10
Camera	2.67e8	6.29e8	2.15e9	1.22e10	5.12e10
Lower Platform	2.56e8	5.70e8	1.90e9	1.07e10	4.59e10
Propellant Tanks	2.56e8	5.70e8	1.90e9	1.07e10	4.59e10
Side Panels	2.67e8	6.29e8	2.15e9	1.22e10	5.12e10
Solar Arrays	2.67e8	6.29e8	2.15e9	1.22e10	5.12e10
Telemetry Boxes	2.67e8	6.29e8	2.15e9	1.22e10	5.12e10
Thruster	2.56e8	5.70e8	1.90e9	1.07e10	4.59e10
Upper Platform	2.67e8	6.29e8	2.15e9	1.22e10	5.12e10

Table 19. Satellite Parts Stresses for Case 2_1: Side Panels Heat Flux Application, Material-Aluminum and Thickness-0.007 m

Heat Flux Parts	100 W/m²	1000 W/m²	10e4 W/m²	10e6 W/m²	10e9 W/m² (3.125 % load)
Antenna	2.64e8	6.10e8	2.10e9	1.21e10	9.36e11
Camera	2.64e8	6.10e8	2.10e9	1.21e10	9.36e11
Lower Platform	2.55e8	5.65e8	1.90e9	1.06e10	2.92e11
Propellant Tanks	2.55e8	5.65e8	1.90e9	1.06e10	2.92e11
Side Panels	2.64e8	6.10e8	2.10e9	1.21e10	9.36e11
Solar Arrays	2.64e8	6.10e8	2.10e9	1.21e10	9.36e11
Telemetry Boxes	2.64e8	6.10e8	2.10e9	1.21e10	9.36e11
Thruster	2.55e8	5.65e8	1.90e9	1.06e10	2.92e11
Upper Platform	2.64e8	6.10e8	2.10e9	1.21e10	9.36e11

Table 20. Satellite Parts Stresses for Case 2_2: Side Panels Heat Flux Application, Material-Aluminum and Thickness-0.01 m

Similar to the graphs for thermal and structural deformation analysis presented earlier, we developed the graph (Figure 43) which gives the stress distribution due to the incoming heat flux for the case 1_1. We can clearly see that the stresses are higher in the area that is being hit with laser energy and all the other parts have fairly lower values of stresses. It is reasonable to expect such a result, as the higher stress values are found in solar arrays, one of the representative areas that have been hit with laser energy.

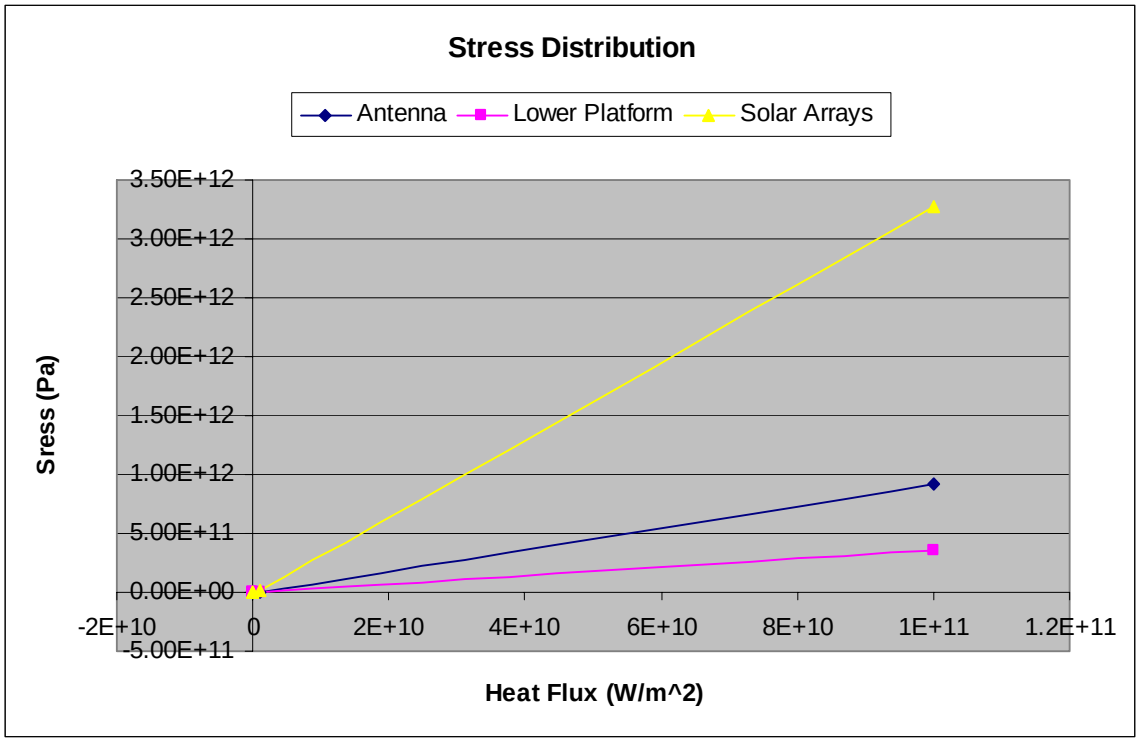

Figure 43. Stress vs. Heat Flux in Satellite Parts for Case 1_1

Figures 44 and 45 shows the stress distribution on satellite side panels and solar arrays. The red and yellow areas indicate high stress distribution and the blue and white areas indicate lower values. In Figure 45 the stress distribution on the solar arrays is higher on the beams resulting in the main panels being white in color. However, the solar arrays failed when we applied 10e9 W/m² heat flux.

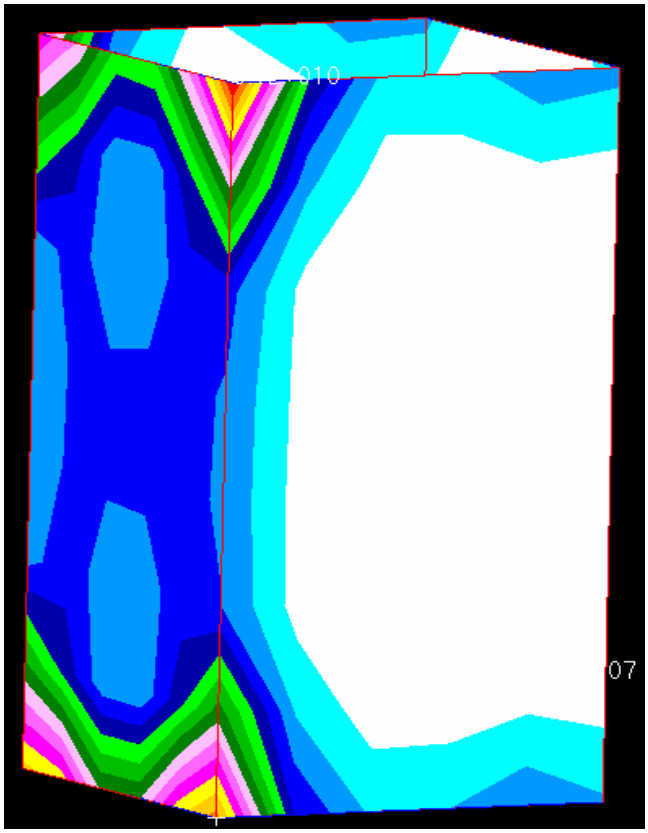

Figure 44. Stress of 5.12e10 Pa (FAILURE) in Satellite Side Panels (Thickness 0.007 m, Applied Heat Flux 10e9 W/ m²)

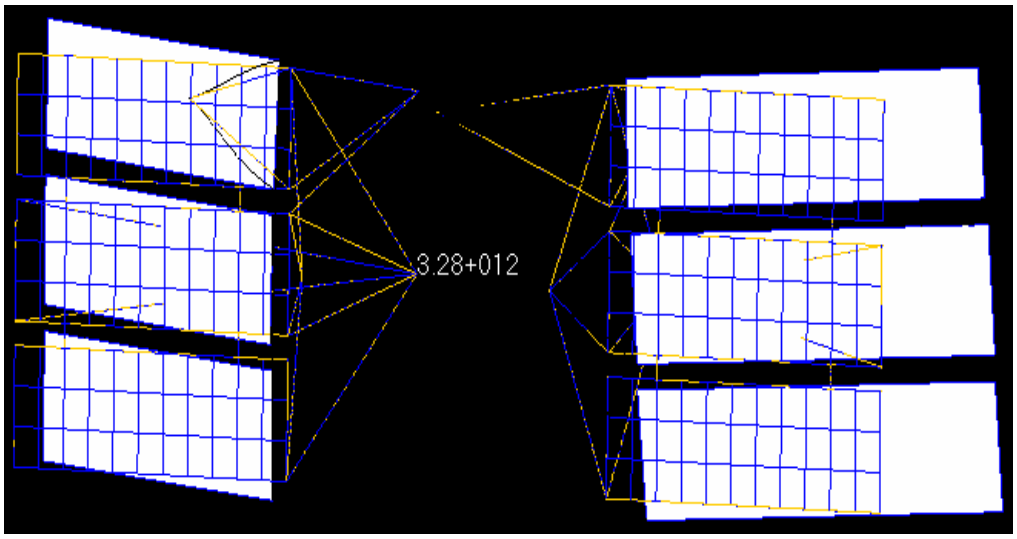

Figure 45. Stress of 1.41e10 Pa (FAILURE) in Satellite Solar Arrays (Thickness 0.007 m, Applied Heat Flux 10e9 W/ m²)

F. TRANSIENT ANALYSIS AND RESULTS

In this section, we depart from steady state analysis and we force the heat flux to be applied as a transient thermal load. We investigate the behavior from the transient point of view and present a short comparison with steady state analysis results. This helps in assessing effective modes of laser thermal energy application on to a satellite surface.

In using the term transient, we mean that the applied heat flux on to the satellite surface by a ground-based laser is for a finite amount of time. The process helps in assessing the effects of the duration of the pulse width of the laser exposure as well as the resulting extent of the damage caused to the satellite.

1. Thermal Analysis and Results

Heat Flux Parts	100 W/m²	1000 W/m²
Side Panels	57.5 at 30 sec	1100 at 30 sec

Table 21. Temperature Distribution for Case 2_2: Side Panels Heat Flux Application, Material-Aluminum and Thickness-0.01 m

The basic notion here is the same as in steady state analysis. We will apply the heat flux for some finite amount of time. Transient temperature distributions will be created as a consequence and these temperatures form as inputs for the subsequent structural and stress analysis.

We perform a limited number of transient thermo-mechanical analysis to show us the difference and extract important deductions. As depicted in detail in Table 21, only 100 W/m² and 1000 W/m² are adequate to show us that the temperatures have exceed the melting point of aluminum at 30 sec. The 30 sec period is observed to yield us the maximum temperature and thereafter a steady state temperature is reached. This is based on an exposure time of up to 100 seconds.

In Figure 46, transient temperature distribution is depicted for 100 different nodes of the satellite side panels that have been hit with laser energy. The maximum

temperature is seen to be 57.5 degrees Celsius at 30 sec and thereafter the temperature remains constant. Based on this observation, using ground-based laser for 30 sec can result in the maximum damage to a satellite. In this scenario, the temperature is very low due to the low applied heat flux of only 100 W/m². On the contrary, in Figure 47 maximum temperature is 1100 degrees Celsius for the same amount of time (30 sec) with the applied heat flux being 1000 W/m². This temperature results in a total failure of the satellite as the melting point of aluminum is 660 degrees Celsius.

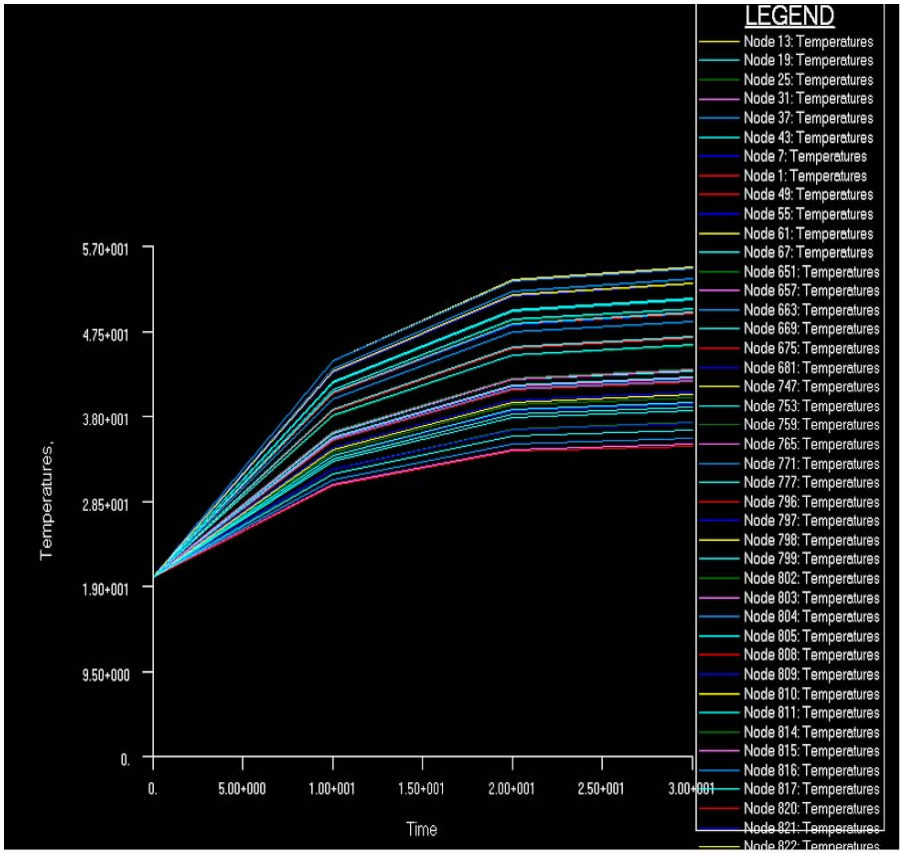

Figure 46. Transient Temperature Distribution in Satellite Side Panels (Thickness-0.007 m, Applied Heat Flux 100 W/ m²)

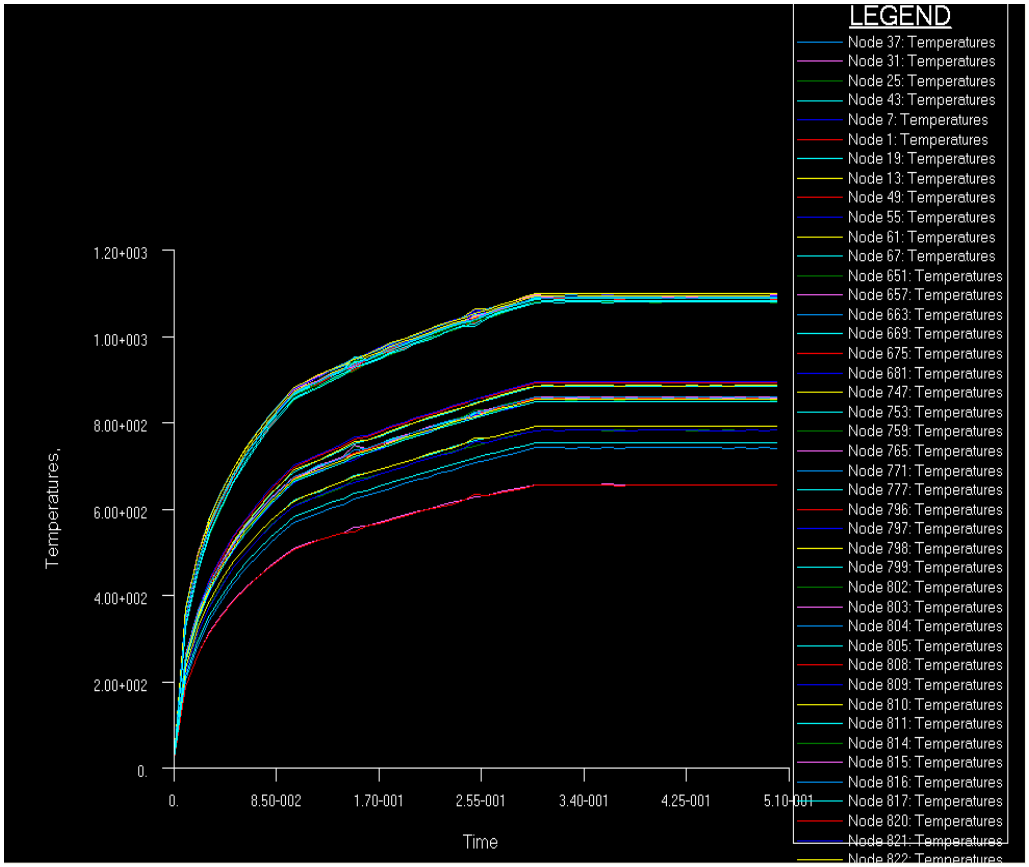

Figure 47. Transient Temperature Distribution (FAILURE) in Satellite Side Panels (Thickness 0.007 m, Applied Heat Flux 1000 W/ m²)

2. Deformation—Stress Analysis and Results

The next and final step to the transient analysis is the computation of deformations and stresses, using as inputs the temperatures from thermal analysis. Table 22 shows that for a value of 1000 W/m² of applied heat flux, and for a duration time of 30 seconds, we obtain a deformation failure but not a stress failure.

Deformations are nearly two times greater than the original thickness of the material but the corresponding stresses are one order of magnitude less than the yield stress. We can conclude that with only 1000 W/m² the desired mission to disable the model satellite is accomplished, by means of excessive deformation of the satellite surface. Figures 48 and 49 show the transient deformation and stress results on the satellite side panels. It is again to be noted that places with red and yellow colors have the greatest deformation and stress distributions and locations with white and blue colors

have the minimum values. Observing the deformed shapes, we can say that the satellite is disabled and cannot provide valuable information to the ground stations for any kind of operation.

Heat Flux	100 W/m²	1000 W/m²
Deformation	1.32e-3	2.96E-2
Stress	3.29e8	7.17e9

Table 22. Deformation and Stresses for Case 2_2: Side Panels Heat Flux Application, Material-Aluminum and Thickness-0.01 m

Figure 48. Deformation of 2.96e-2 m (FAILURE) in Satellite Side Panels (Thickness 0.01 m, Applied Heat Flux 1000 W/ m²)

Figure 49. Stresses of 7.17e9 Pa (Partial FAILURE) in Satellite Side Panels (Thickness 0.01 m, Applied Heat Flux 1000 W/ m²)

THIS PAGE INTENTIONALLY LEFT BLANK

VII. BALLISTIC MISSILE THERMOMECHANICAL ANALYSIS AND RESULTS

A. MODEL DEFINITION

We apply our methodology for the analysis of ballistic missiles and we need to define the parametric space for the problem in order to establish the initial parameters and finally deduce results consistent with the requirements and assumptions.

In this study, we use titanium, steel and aluminum for building the components of the ballistic missile model. In order to be consistent, the thicknesses will be fixed for all components to be 0.0254 m (1 inch). The material properties are as defined earlier and are shown in Table 7.

We selected to score a hit on the external cylinder of the 1st stage of the ballistic missile with laser thermal energy. This selection is based on the decision that all ballistic missile components are structurally similar and the mission and objectives of defending against the ballistic missiles are different. Symmetric construction is used for the missile body for convenience. The directional heat flux load used for our simulation are:

- 100 W/m²
- 10e4 W/m²
- 10e5 W/m²
- 10e6 W/m²

The external cylinder of the 1st stage as the load application area is only representative and present approach may easily be applied for other areas of the ballistic missile model. The radiation parameters are the same as for the satellite model. We also make the assumption that the ballistic missile is hit in the midcourse flight phase, in which it is assumed to spend most amount of flight time. This phase is usually in low earth orbit, as mentioned earlier in Chapter IV. The radiation parameters are as follows:

- Absorptivity: 0.5
- Emmisivity: 0.5
- Ambient Temperature: 20 °C
- View Factor: 1

We do not consider convection mode of thermal dissipation, but only thermal conduction and radiation modes are assumed active. Figure 50 shows the distribution and application of the directional heat load and the radiation parameters on the ballistic missile model.

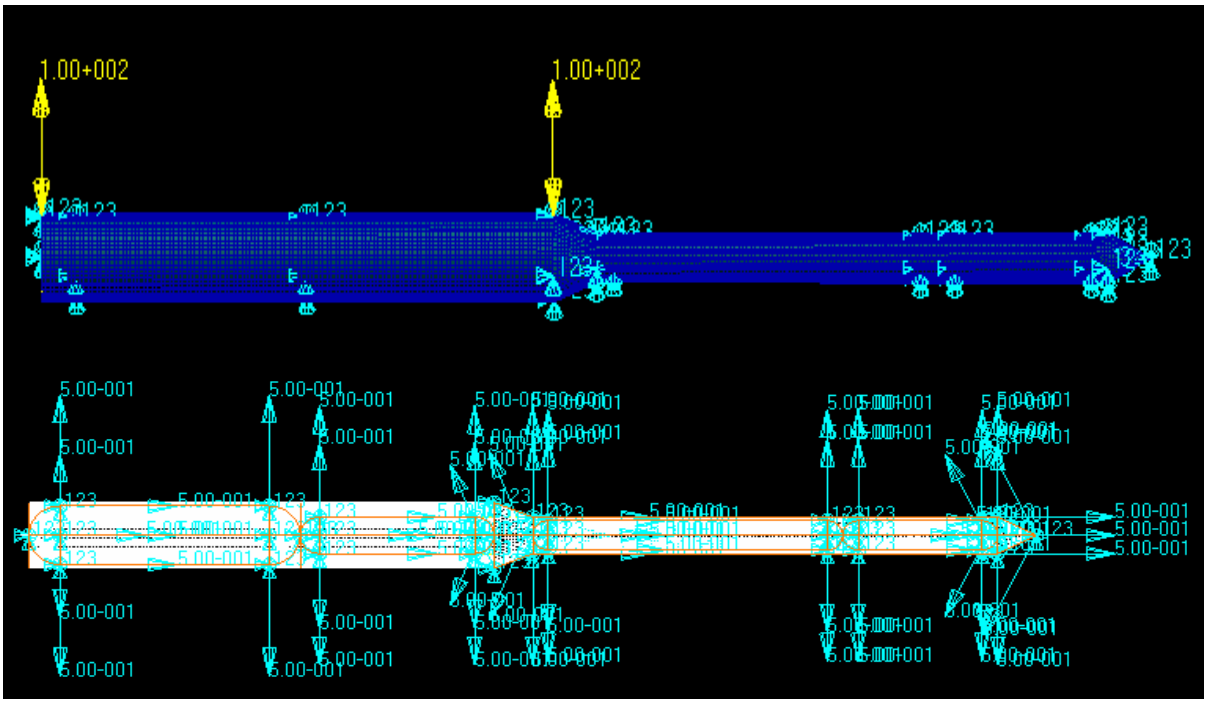

Figure 50. Heat Flux and Radiation Parameters of the Ballistic Missile Model

We make the assumptions on failure modes consistent with the satellite model and specify the following criteria:

- **deformations** greater than the original thickness.
- **temperatures** greater than the melting point of the materials.
- **stresses** greater than the yield stress of the materials.
- **deformations, temperatures** and **stresses** greater than other mission critical parameters.

We use the established failure modes and criteria to assess the survivability and vulnerabilities of the ballistic missile model.

The finite element model for the ballistic missile was generated for different mesh sizes and elements. The final design selected, considering the size, accuracy, cost and

schedule for the ensuing thermo-mechanical analysis resulted in the following number of nodes, elements and degrees of freedom.

- Nodes ~ 25,342
- Elements ~ 25,533 (Plate/Shell elements and Beams)
- Degrees of Freedom: 76,026

B. STEADY STATE ANALYSIS AND RESULTS

1. Thermal Analysis and Results

Thermal analysis was performed on the ballistic missile model, and the results are presented in the Table 23:

Heat Fluxes / Parts	100 W/m²	10e4 W/m²	10e5W/m²	10e6W/m²
Stage 1 External Cylinder	35.1 °C	380 °C	880 °C	3370 °C FAILURE
Stage 1 Bottom Fuel Tank	20.1 °C	21.7 °C	23.3 °C	101 °C
Stage 1 Top Fuel Tank	20.1 °C	21.7 °C	23.3 °C	101 °C
Adapter	25.5 °C	212 °C	569 °C	2500 °C FAILURE

Table 23. Ballistic Missile's Thermal Analysis Results

The table gives temperatures for different components with increasing thermal energy input on the 1st stage surface. We can observe that with 10^6 W/ m^2 applied heat flux to the titanium stage 1 external cylinder, temperatures rises up to 3370 °C, which exceeds the melting point temperature of the material, resulting in structural failure. We also have failure for the adapter structure, which is an adjacent part to the 1st stage external cylinder.

These results are shown summarized graphically in Figure 51, where the points on the curves are the parametric design and analysis points. These curves depict the highly nonlinear variation of the applied heat flux with resulting temperatures in the selected ballistic missile parts.

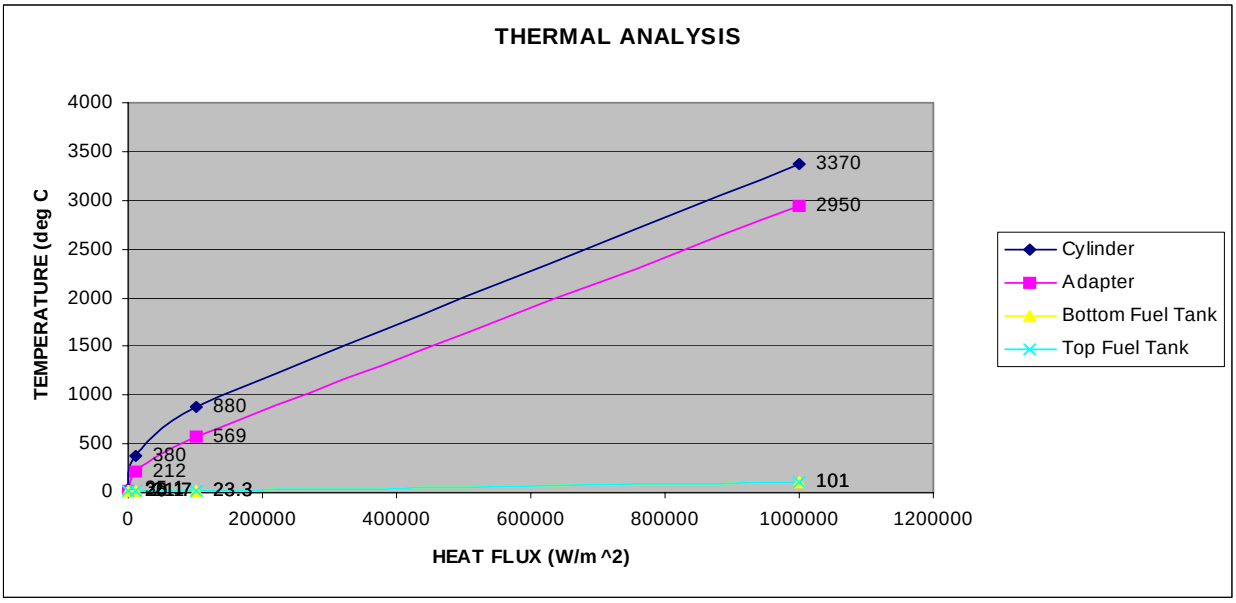

Figure 51. Temperatures versus Heat Flux

In Figure 51, the temperature distribution is shown where heat flux of 10^6 W/ m^2 was applied to the 1st stage external cylinder.

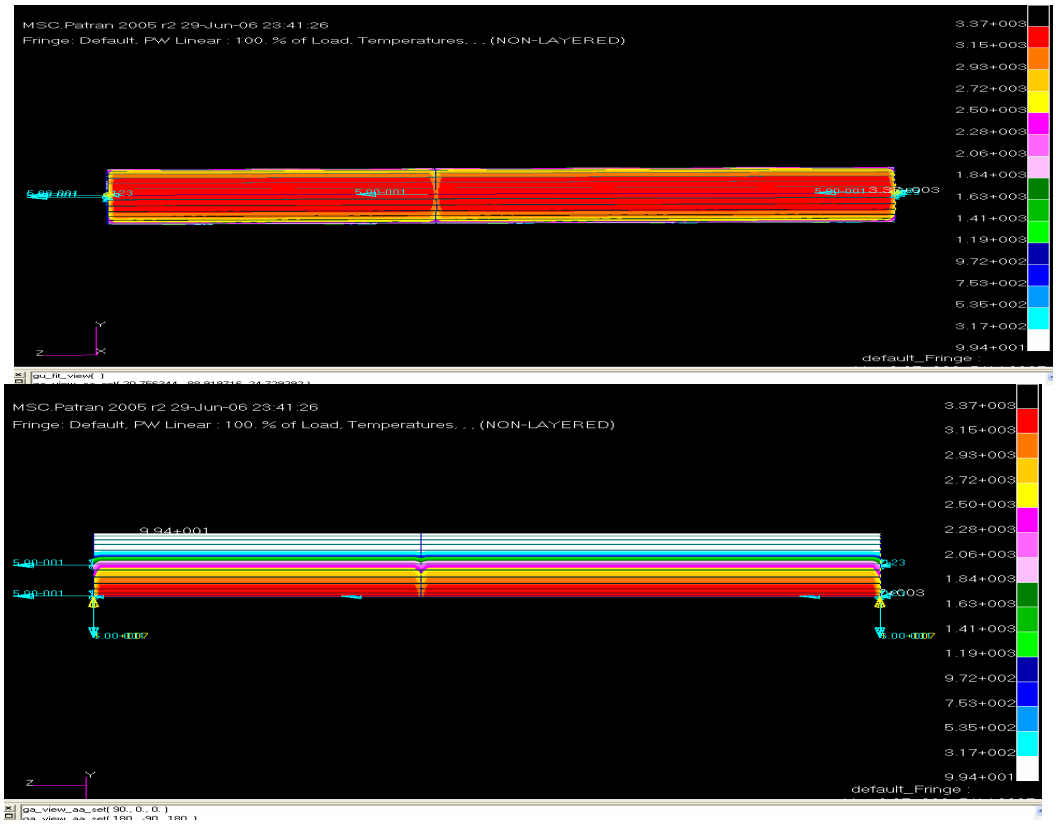

Figure 52. Temperature Distribution Pictures for Heat Flux of 10^6 W/ m^2

2. Structural Analysis and Results

The next step was to perform the structural analysis in which we apply as inputs the temperature distributions computed from the thermal analysis. The results from the analysis are presented in Table 24 and Figures 53 and 54 respectively. Table 24 shows that the maximum deformation for an applied heat flux of 10^6 W/ m^2 is 0.0472 m, where the initial thickness of the cylinder was 0.0254m. In accordance with our established failure modes criteria, the cylinder deformation is greater than the original thickness and the ballistic missile is deemed incapacitated or structurally failed.

Heat Fluxes Parts	100 W/m²	10e4 W/m²	10e5W/m²	10e6W/m²
Stage 1 External Cylinder	4.87e -4	5.12e -3	1.22e -2	4.72e -2 FAILURE
Stage 1 Bottom Fuel Tank	5.5e -4	5.52e -4	5.53e -4	2.72e -3
Stage 1 Top Fuel Tank	2.92e -4	2.94e -4	2.96e -4	1.45e -3
Adapter	2.57e -4	7.44e -4	1.5e -3	4.4e -3

Table 24. Ballistic Missile's Deformation Results

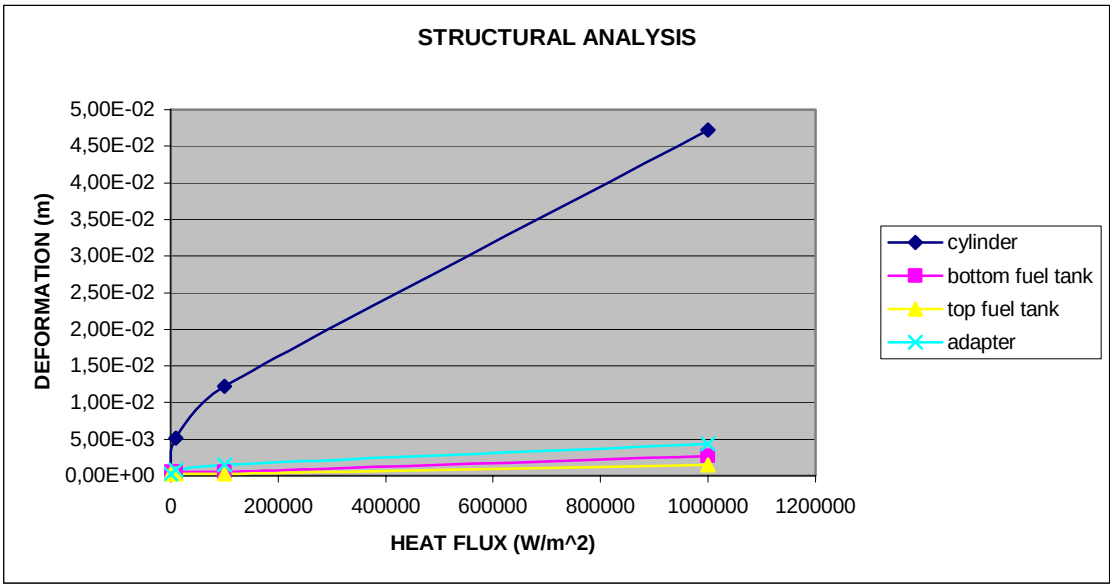

Figure 53. Deformation versus Applied Heat Flux Results

HEAT FLUX = 10e6 W/m²

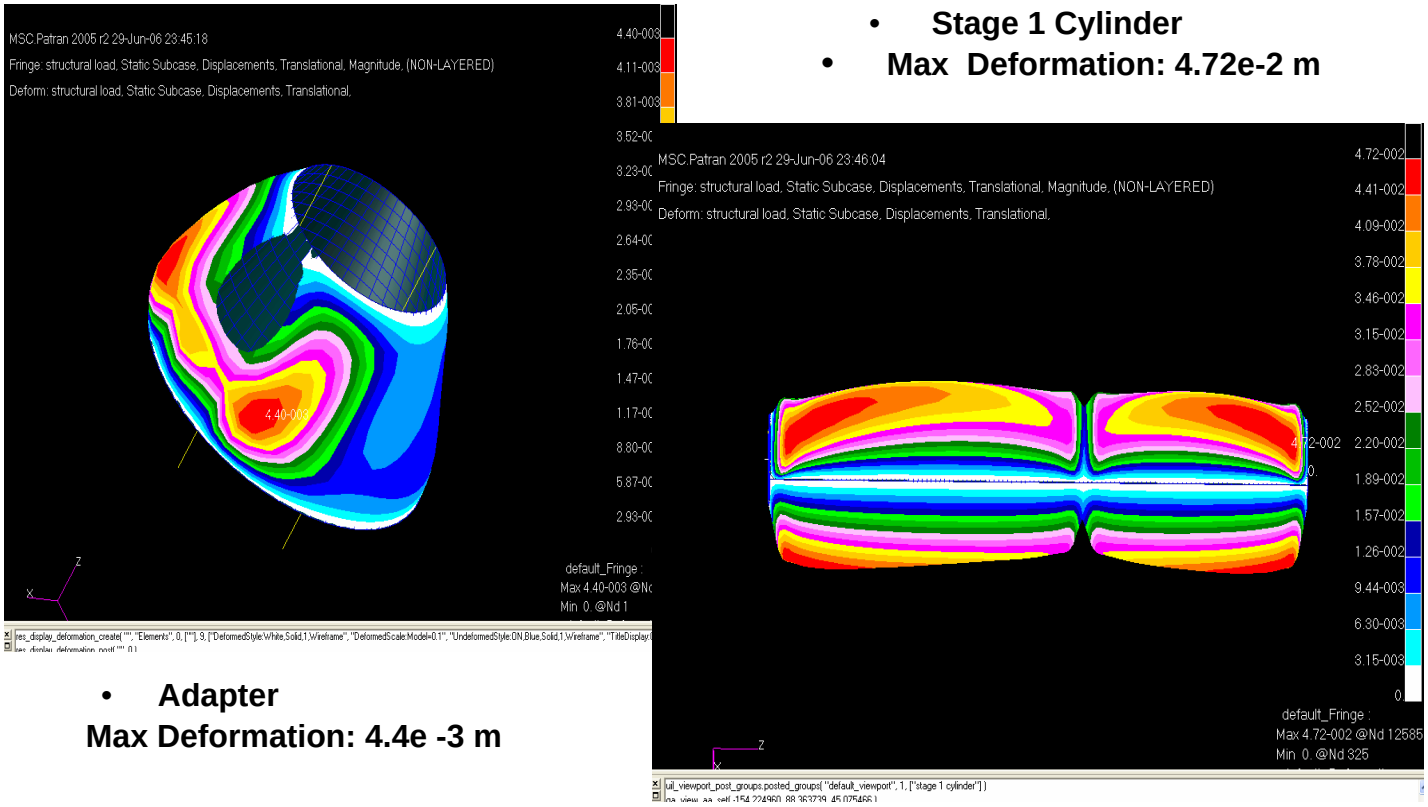

- **Stage 1 Cylinder**
- **Max Deformation: 4.72e-2 m**

- **Adapter**

Max Deformation: 4.4e -3 m

Figure 54. Thermal Deformation Results

3. Stress Analysis and Results

We evaluated thermal stresses of our missile model based on the deformation due to thermal loads. The results are shown in Table 25 and in Figure 55. As mentioned earlier in our criteria, the yield strength of the material was determining factor for the assessment of the stress distributions. This failure is observed for applied heat flux greater than 10^5 W/ m^2.

Heat Fluxes Parts	100 W/m²	10e4 W/m²	10e5W/m²	10e6W/m²
Stage 1 External Cylinder	5.48e 7	4.8e 8	1.2e 9 FAILURE	5.19e 9 FAILURE
Stage 1 Bottom Fuel Tank	1.67e 8	1.55e 8	3.06e 8	1.01e 9 FAILURE
Stage 1 Top Fuel Tank	1.16e 8	1.55e 8	3.06e 8	1.01e 9 FAILURE
Adapter	5.47e 8	4.52e 8	1.2e 9 FAILURE	5.19e 9 FAILURE

Table 25. Ballistic Missile Stress Analysis Results

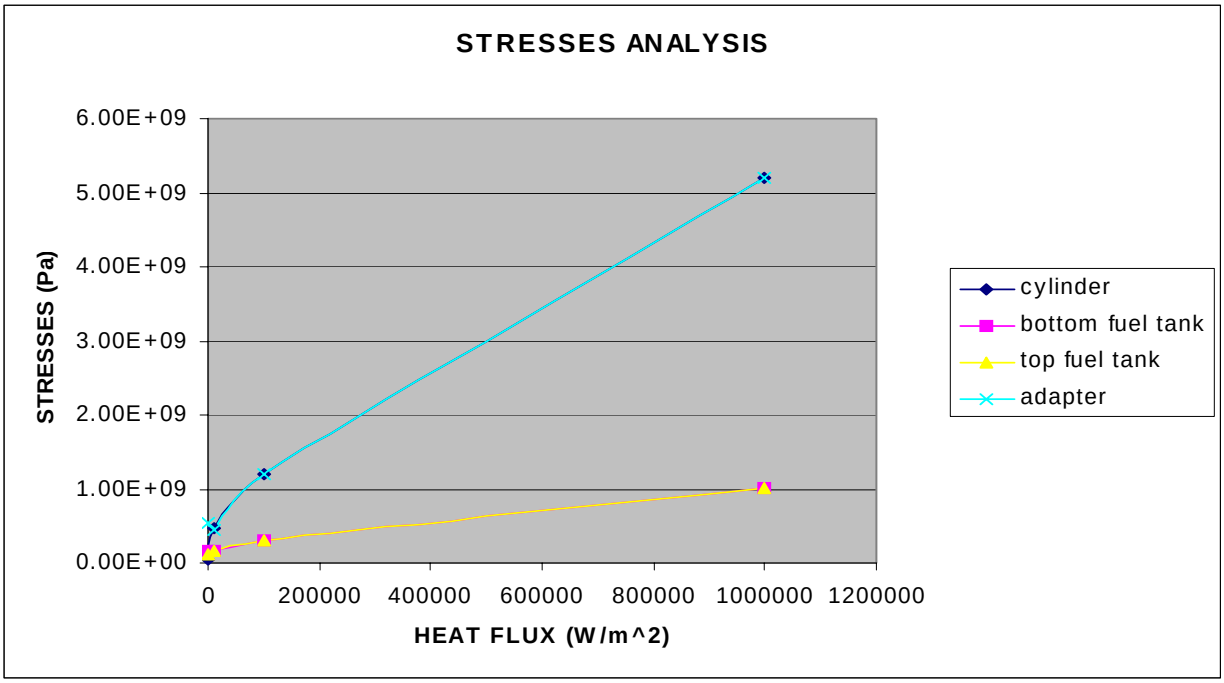

Figure 55. Stress versus Applied Heat Flux Results

C. TRANSIENT ANALYSIS AND RESULTS

The transient analysis of the effects of the incoming laser energy on to external surfaces of the ballistic missile is investigated. The results obtained here are compared as was done in the satellite analysis, with the steady thermo-mechanical analysis to assess the survivability issues.

1. Thermal Analysis and Results

After performing the transient thermal analysis, as we did for the satellite model, we obtain the converged solution as shown in Table 26. We can deduct that for applied heat flux of 1000 W/m² for time duration of 30 sec, the temperature rises to near melting point of the titanium construction areas. It is observed that with an application of heat flux larger than 1000 W/m², sufficient damage is done to the ballistic missile to conclude that the disintegration of the missile is imminent. Figure 56 shows that for directional heat load of 100 W/m², on 1st stage external cylinder surface, the temperature rises up to 510 degrees Celsius, which is not high for titanium. On the contrary, observing the Figure 57, the temperature rises up to 1200 degrees Celsius, which is very close to the melting point of titanium. Using the transient application of heat flux we can observe that the results are similar to those we obtained in the transient analysis of the satellite model. A finite amount of time (up to 30 sec) is enough for our ballistic missile to fail and not continue to stay in its original flight path.

Heat Flux Parts	100 W/m²	1000 W/m²
Side Panels	510 at 30 sec	1200 at 30 sec

Table 26. Stage 1 External Cylinder Transient Thermal Analysis Results

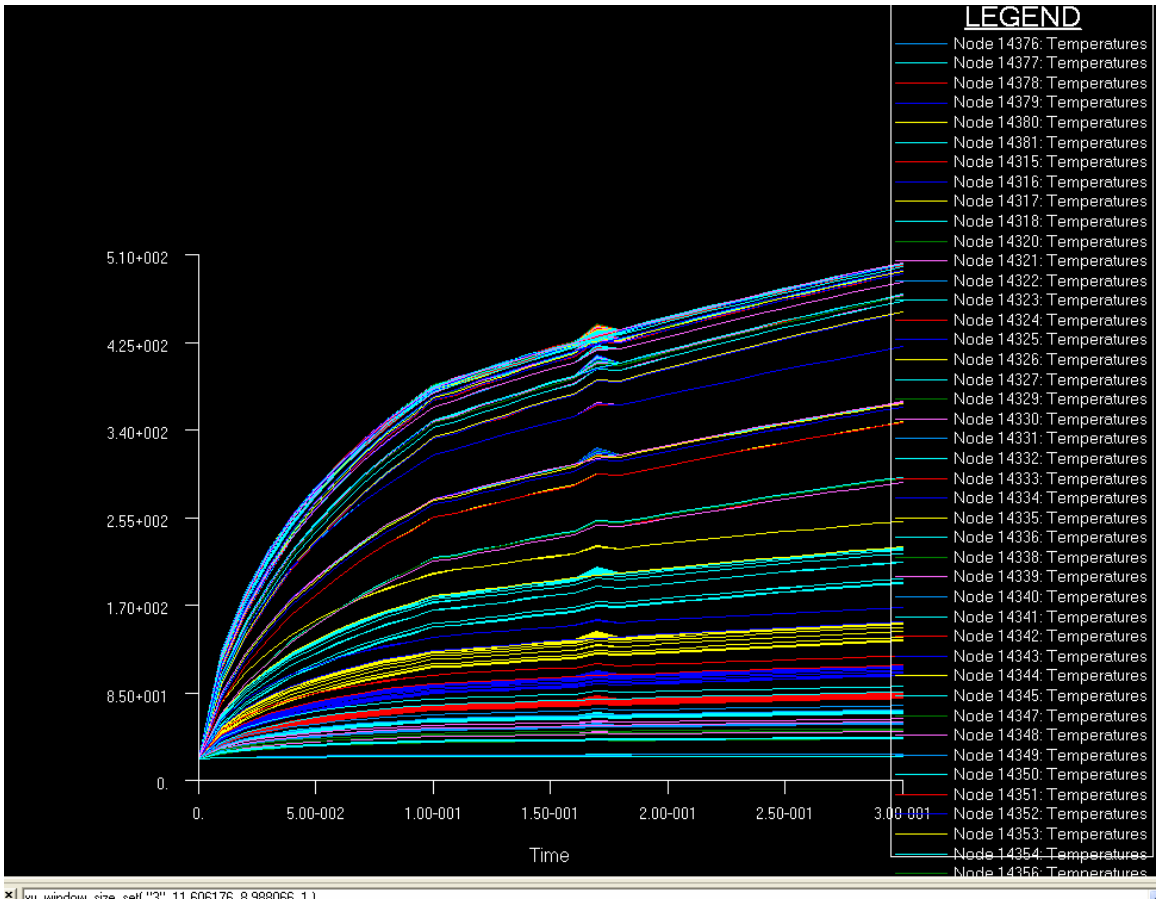

Figure 56. Transient Temperature Distribution (^{0}C) in Ballistic Missile External Cylinder Stage 1 (Thickness 0.0254 m, Material Titanium, Applied Heat Flux 100 W/ m^{2})

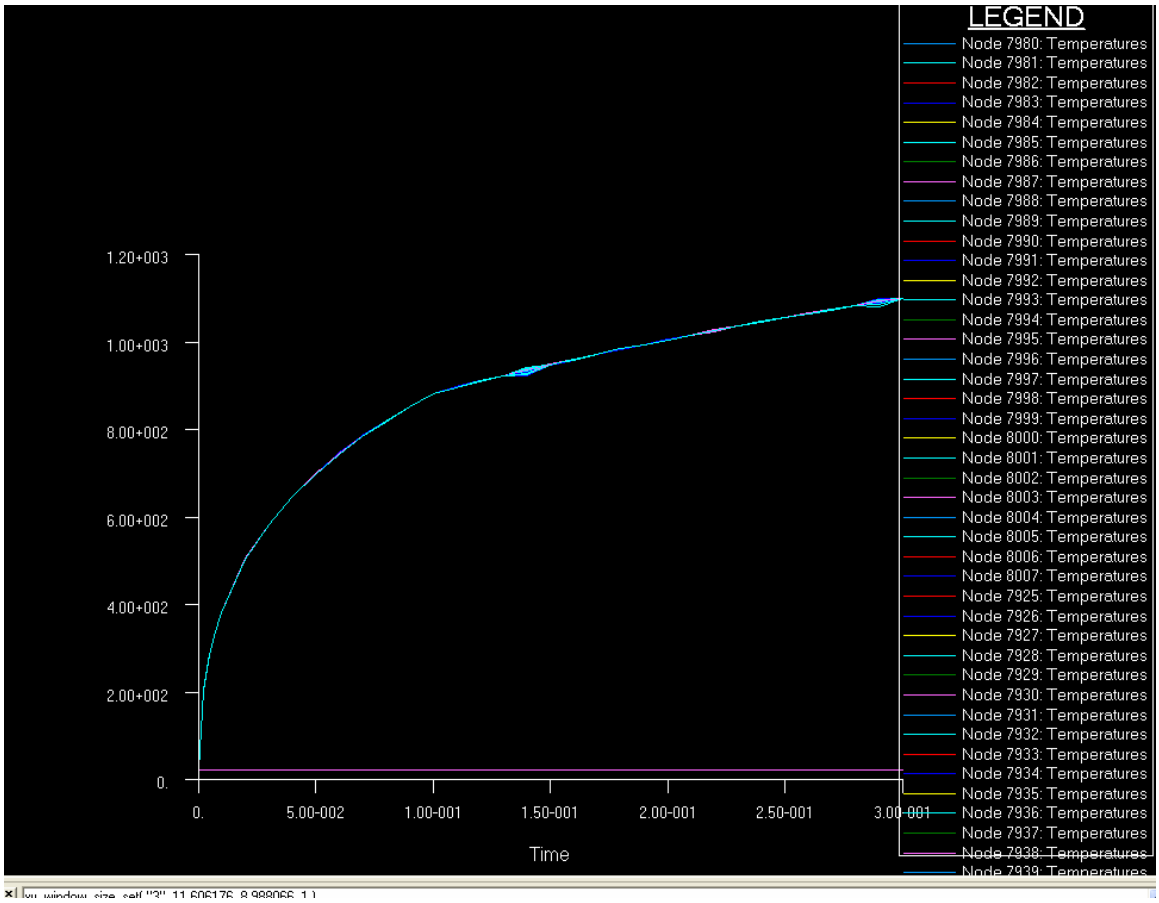

Figure 57. Transient Temperature Distribution (^{0}C) in Ballistic Missile's External Cylinder Stage 1 (Thickness 0.0254 m, Applied Heat Flux 1000 W/ m², Titanium)

2. Structural—Stress Analysis and Results

The computed temperatures that are shown in Table 26 are applied to the structural model and we perform thermal deformation and thermal stress analysis. Table 27 shows the results where for heat fluxes up to 1000 W/m², the deformation has exceeded the limits resulting in the failure of the ballistic missile. The corresponding stresses are quite large, approaching the yield strength of titanium. This leads us to conclude that the stress failure modes occur for heat fluxes larger than 1000 W/m², which is within the range of ground-based laser weapons as published in the open literature.

Heat Flux	100 W/m²	1000 W/m²
Deformation	1.84e-3	3.02e-2
Stress	4.22e8	8.12e9

Table 27. Stage 1 External Cylinder Transient Deformation - Stress Analysis Results

VIII. CONCLUSIONS AND RECOMMENDATIONS

To hit an unhardened satellite and intercontinental ballistic missile is a dynamic possibility today. Nations all over the world are trying to make their systems strong enough in order to withstand incoming laser energy and avoid hard or soft kill of their systems, caused by enemy laser attacks. The use of future laser weapons is only a matter of time to be part of the world's weapons arsenal. Quiet ground-based directed energy weapons would have adequate power to terminate a satellite's or intercontinental ballistic missiles within short time spans.

Based on the open literature studies and results from our modeling and simulation of the laser induced thermo-mechanical modeling and simulations, important deductions are made that can be used by concerned military agencies. The simulations show that incoming laser energy attack on a satellite or intercontinental ballistic missile can have lethal effects.

The published open literature damage criteria seem to be very conservative. It is observed from our simulations that laser energy of 1000 W/m^2, delivered on to the satellite in orbit, can cause total deformation of satellite external surface. An application of 10e4 W/m^2 of laser energy on to a satellite or ballistic missile can cause them to fail thermo-mechanically. Temperatures rise above melting points or thermal deterioration of selected materials precedes failure due to stresses exceeding the yield stresses. Based on the models we created and the simulations we performed, we estimate laser thermal energies needed to disable and/or destroy enemy space assets that may be generated by Kilowatt or Megawatt range ground-based lasers capable of delivering the energies only for a very short amount of time.

The results were even more surprising when we compare the steady state and transient analysis. The sustained time of laser exposure of the needed thermal energies are seen to be of the order of 30 seconds for our models, adequate to produce the desired outcome to totally disable or destroy the satellites or intercontinental ballistic missiles.

The modeling and simulation leading to the risk assessment of the survivability and vulnerability of the space assets, a multidisciplinary methodology based on MSC

Software computer aided engineering tools was developed for thermo-mechanical analysis of satellites and ballistic missiles exposed to directed energy weapons.

Thermal analysis of the models is presented based on the open literature estimates of the energy levels deliverable onto the space assets. The published literature estimates critical energies of the order of 10e8 W/m², but we observe from our analysis that only 10e4 W/m² or even 1000 W/m² can cause irreversible damages to a satellite or a ballistic missile structure. Some of our results also point out that even 100 W/m² is adequate energy level to produce partial failures on the structures and have desirable catastrophic results. The above referenced numbers are identified as the critical energy levels for the mechanical failure modes of the satellite and the ballistic missile models based on the failure modes established in this report.

The low thermal energies needed to disable the space assets are especially useful and is to be considered for low earth orbit altitudes. The difficulty that may be encountered at LEO can be one of pointing accuracy, whereas in geostationary orbits the pointing accuracy is not a problem as the target position remains constant. The developed methodology could be used to determine the laser energy requirements to reach those altitudes and accomplish hard kill missions.

Further research can be done in estimating the energy levels that are needed to be used from a ground based laser weapon in order for 1000 W/m² to be delivered and maintained on satellite surface. Atmospheric propagation losses play a major role and will determine the amount of laser energy that a ground laser must produce in order to cause catastrophic effects on a satellite, as discussed in the thesis. Other areas of potential payoffs will be to simulate composite materials for satellite design, mission oriented failure modes, analytical modeling of solar arrays treating it as an isotropic and/or anisotropic plate and simulating thermo-mechanical behavior.

Modeling and simulation methodology proposed in this report may be used in two different ways either defensively or offensively. In a defensive approach, one can harden our satellites and ballistic missiles with designs that can withstand, or have the ability to reradiate into space the amounts of incoming laser energy to survive an offensive attack.

In an offensive approach, the enemy space assets, such as satellites and ballistic missiles, may be disabled using a ground-based laser with optimal amounts of heat flux as simulated in our analysis.

THIS PAGE INTENTIONALLY LEFT BLANK

LIST OF REFERENCES

[1] Quickbird Satellite Characteristics, January 2006, www.directory.eoportal.org/pres_QUICKBIRD2.html, last accessed March 2006.

[2] Hans Mark, "The Airborne Laser from Theory to Reality: An Insider's Account," *Defense Horizons*, Number 12, April 2002.

[3] Landis Geoffrey, "Space Power by Ground-Based Laser Illumination," *IEEE AES Systems Magazine*, Vol. 6, No. 6, pp.3–7, 1991.

[4] Hitchens Theresa, "USAF Transformation Flight Plan Highlights Space Weapons," *Space Security, Center for Defense Information*, February 2004.

[5] Donelly John, "*Laser of 30 Watts Blinded Satellite 300 miles High*," Defense Week, p.1, 8 December 1997.

[6] Ghostroy Subrata, *"Space Weapons,"* Institute of Peace and Conflict Studies, Article No 1875, 27 October 2005.

[7] Nielsen E. Philip, *Effects of Directed Energy Weapons*, 1997.

[8] Olsen Richard, "*Remote Sensing from Air and Space,"* Naval Postgraduate School, November 2005.

[9] Possel H. William, "Lasers and Missile Defense. New Concepts for Space-Based and Ground-Based Laser Weapons," Occasional Paper No. 5, Center for Strategy and Technology, Air War College, 1998.

[10] Niles P. Sean, "High Energy Laser Applications in a Surface Combatant: Terminal Phase Theater Ballistic Missile Defense, Low Atmosphere Propagation and Free Electron Laser Gain," Master's Thesis, Naval Postgraduate School, Monterey, California, 2005.

[11] Polykandriotis Konstantinos, "Simulations of the Proposed TJNAF 100KW Free Electron Laser and Comparison with TJNAF Low Power Experiments," Master's Thesis, Naval Postgraduate School, Monterey, California, 2001.

[12] Thomson W. Robert Jr., "Experimental Damage Studies for a Free Electron Laser Weapon," Master's Thesis, Naval Postgraduate School, Monterey, California,1999.

[13] ICBMs, January 2006, http://www.wias.net/Papers/space_ew1.html, last accessed March 2006.

[14] Taepondong ICBM, January 2006, http://en.wikipedia.org/wiki/Intercontinental_ballistic_missile#Flight_phases, last accessed March 2006.

[15] Atmospheric Propagation, January 2006, www.hq.nasa.gov/office/pao/History/conghand/atmosphe.htm, last accessed March 2006.

[16] Global Security, January 2006, www.globalsecurity.org/wmd/library/news/dprk/2006/060705-nkir2623.htm, last accessed March 2006.

[17] MSC Nastran, *Quick Reference Guide*, Vols. 1 and 2, 2004

[18] Taepondong, January 2006, http://www.astronautix.com/stages/taeong11.htm, last accessed March 2006.

[19] Wood, Gary L, Pellegrino, M. John, "High Energy Laser Weapons: Technology overview by Perram. Marciniak and Goda," SPIE, Vol. 5414, pp.51–56, 2004

[20] Keuren E. Van, Hill Cherry, Dr. J. Knighten, "Use of High Power Microwave Weapons," IEEE, 1994.

[21] Geoffrey Landis, "Satellite Eclipse Power by Laser Illumination," Acta Astronautica, Vol.25, No 4, pp. 229–233, 1991.

[22] Satellite Security, January 2006, http://www.armscontrol.org/act/1997_10/miracloct.asp, last accessed March 2006.

[23] Klaus – Jurgen Bathe, "Finite Elements Analysis," 2002.

INITIAL DISTRIBUTION LIST

1. Defense Technical Information Center
   Ft. Belvoir, Virginia

2. Dudley Knox Library
   Naval Postgraduate School
   Monterey, California

3. Professor Ramesh Kolar, Code ME/Kj
   Department of Mechanical and Astronautical Engineering
   Monterey, California

4. Distinguished Professor Brij Agrawal, Code ME/Kj
   Department of Mechanical and Astronautical Engineering
   Monterey, California

5. Professor Phillip Pace, Code EC/PC
   Department of Electrical and Computer Engineering
   Monterey, California

6. Chairman Information Sciences Department
   Naval Postgraduate School
   Monterey, California

7. Chairman Mechanical and Astronautical Engineering
   Naval Postgraduate School
   Monterey, California

8. Professor Bill Colson
   Department of Applied Physics
   Monterey, California

9. Professor Bret Michael
   Department of Computer Science
   Monterey, California

10. Distinguished Professor Emeritus John Powers
    Department of Electrical Engineering
    Monterey, California

11. Lecturer Joe Welch,
    Information Sciences
    Monterey, California

12. LtJG Georgios Mantzouris
Hellenic Navy
Athens, Greece